UNIVERSITY OF MINNESOTA
ST. ANTHONY FALLS HYDRAULIC LABORATORY

Project Report No. 354

Hydraulic Transient Study of Passaic River Flood Protection Tunnel

by

Jianming He, Charles C.S. Song

and

Ying Liu

Prepared for

PASSAIC RIVER DIVISION
U.S. ARMY CORPS OF ENGINEERS
New York District
Hoboken, NJ 07030

September, 1994

Minneapolis, Minnesota

UNIVERSITY OF MINNESOTA
St. Anthony Falls Hydraulic Laboratory

Project Report No. 354

Hydraulic Transient Study of Passaic River Flood Protection Tunnel

by

Jianming He, Charles C. S. Song

and Ying Liu

Prepared for

PASSAIC RIVER DIVISION
US ARMY CORPS OF ENGINEERS
NEW YORK DISTRICT
Hoboken, NJ 07030

September 1994

TABLE OF CONTENTS

LIST OF FIGURES

I. INTRODUCTION

1.1 Problem Description

The purpose of this study is to evaluate the hydraulic transient status in the proposed Passaic River Flood Protection Tunnel. The tunnel system is designed to convey flood waters from the upstream areas of Passaic River directly into Newark Bay. The tunnel consists of two upstream inlets, the Pompton Inlet and the Spur Inlet, and a 42 ft diameter main tunnel. The main tunnel length is about 20.1 miles (from the Pompton inlet to the downstream end). The distance between the Spur inlet and the main tunnel is about 1.2 miles. The tunnel system will be excavated from 150 to more than 400 ft under ground. From the hydraulic transient point of view, there are the following possible safety concerns in this tunnel system, which need to be evaluated using hydraulic transient computer simulation program.

(1) Surge phenomena induced during the initial filling stage.

(2) Water hammer phenomena due to a sudden pressure change.

(3) The effects of the surge and water hammer on the inlets, workshafts, and downstream outlet.

The fully dynamic transient mixed flow mathematical model (MXTRANS) developed at the University of Minnesota was used for this study. The modeling configuration is based on the current design data. Any modification of the tunnel system, including the parameters related to the workshafts, inlets, and outlet, may affect the results.

A total of three typical storm events (2yr, 100yr and 500yr), provided by the Passaic River Division of the New York District, US Army Corps of Engineers, were used in the numerical simulations.

1.2 Study Progress

This study was initiated after Prof. Charles C. S. Song visited the Passaic River Division of the New York District, US Army Corps of Engineers, on April 11, 1994. Based on the original design information provided by the Passaic River Division during Prof. Song's visit, there are two alternative designs of the downstream outlet, one being a free weir with the top elevation of 10 ft, and the other being an arc–gate–control structure.

The first Progress Report of the study was sent to the Passaic River Division on June 21, 1994. The results include the simulation with the fixed

weir at the downstream end. Later, on June 25, 1994, the Passaic River Division faxed the latest downstream outlet design, which has three 22x25 ft sluice gates with a bottom elevation at –20 ft. There is also an overflow weir with a crest elevation at 10 ft.

Initially, seven(7) simulation runs were made with the three storm events, two sea level elevations (0.0 and 6.2 ft), and two upstream water surface elevations. On Aug. 1 and 2, 1994, the Passaic River Division stuff of the N.Y. District Corps of Engineers visited the University of Minnesota, and led a comprehensive discussion about the modeling results of the seven cases with Drs. Charles C. S. Song and Jianming He of the St. Anthony Falls Hydraulic Laboratory, the University of Minnesota. Following these discussions, five more simulation runs were made as the final modeling effort. The conditions of these five runs are as follows [1].

	Case A1	Case A2	Case A3	Case A4	Case A5
Flood event	2yr	100yr	100yr	500yr	500yr
Pompton Elevation	173.0	173.0	173.0	179.0	179.0
Spur Elevation	163.0	163.0	163.0	168.0	168.0
Pompton Tunnel "n"	0.0133	0.0133	0.0133	0.0133	0.0133
Spur Branch "n"	0.0133	0.0133	0.0133	0.0133	0.0133
Sea Level	6.2	6.2	6.2	6.2	6.2
Outlet Design	GC	GC	GC	GC	GC
Initial Condition	dry	dry	wet	dry	wet

In the table above, "n" is the Manning coefficient of the tunnel, and GC signifies gate–controlled. Also wet condition means that the tunnel system is filled to the downstream sea level. In addition to those changes, the proposed constructed heights of Workshafts Nos. 2B and 2C were raised to elevations 50 and 25 ft from original design height of 45 and 20 ft, respectively.

Since the first seven simulation runs yielded some valuable information, these results are attached as Appendix II in the this report.

II. THE MIXED TRANSIENT FLOW MODEL

2.1 Modeling Equations

The flow to be simulated is very unsteady and contains highly dynamic phenomena such as pressurization surge. The model used, then, must be able to simultaneously calculate unsteady open channel flows and unsteady pressurized flows, including the abrupt change that occurs at the shock or the surge front.

The well–known St. Venant equations:

$$\frac{\partial y}{\partial t} + v\frac{\partial y}{\partial x} + \frac{c^2}{g}\frac{\partial v}{\partial x} = 0 \tag{1}$$

$$g\frac{\partial y}{\partial x} + \frac{\partial v}{\partial t} + v\frac{\partial v}{\partial x} + g(S_f - S_o) = 0 \tag{2}$$

are used to represent the unsteady open channel flow. In the above equations, y is the flow depth, v is the flow velocity, c is the gravity wave speed, S_o is the channel slope, S_f is the energy slope, and g is the acceleration due to gravity, x is the distance along a tunnel, and t is time.

The corresponding equations for unsteady pressurized flow are:

$$\frac{\partial y}{\partial t} + V\frac{\partial y}{\partial x} + \frac{a^2}{g}\frac{\partial v}{\partial x} = 0 \tag{3}$$

$$g\frac{\partial y}{\partial x} + \frac{\partial v}{\partial t} + v\frac{\partial v}{\partial x} + g(S_f - S_o) = 0 \tag{4}$$

in which a is the pressure wave speed, while y takes the meaning of piezometric head measured from the tunnel invert. The systems of equations (1) ~ (4) are solved by the methods of characteristics [2].

Because the transition from the open channel flow condition to pressurized flow condition must be abrupt, as in the case of a hydraulic jump, the special shock boundary conditions must be applied. It was shown by Cardle and Song [2], for a pressurization surge or a positive surge, that three characteristic equations plus two shock boundary conditions can be used to calculate five unknowns at the interface. These five unknowns are v and y on both sides of the interface and the speed of the interface movement. The

model can also simulate the negative surge which occurs during the depressurization process. The detailed physical nature of the surging process has been discussed by Guo and Song [3].

A number of other boundary conditions representing junctions, dropshafts, upstream end, downstream end, reservoirs, and other accessories are also provided in the model. Inflow hydrographs, outflow conditions, and other active or passive flow control methods can also be included in the input data file. Velocity, depth, discharge, and other variables at any location and any time may be specified as outputs.

For more than twenty years, the above dynamic transient mixed flow mathematical model has been widely applied to a number of large sewer tunnel systems, such as Chicago TARP Phase I [4, 5] and TARP Phase II [6, 7], Milwaukee Inline Storage System [8, 9], and Rochester, New York, Genesee River Storage–Conveyance System [10].

2.2 Modeling Configuration

Fig. 2.1 shows the modeling schematic of the tunnel system. There are a total of 379 computation stations with the modeling configuration. The distance between two stations is 300 ft except the junction stations (Stations 98, 121, and 122) which represent the same location. The stationing of the main tunnel, excluding the Spur branch, is displayed in Fig. 2.2, which will be used to show the water elevation along the main tunnel.

2.3 Downstream Condition

As mentioned before, there are two alternative downstream outlet designs in the original design, one being a weir, and the other being an arc–gate–controlled structure. The final design of the outlet is shown in Figs. 2.3, 2.4, and 2.5, which has three sluice gates with a bottom sill elevation at –20 ft. to control the outflow. There is also an overflow weir with a crest elevation of 10 ft. The mean sea level is at elevation of 0.6, but the tide levels could be at elevation 6.2 ft. during flood conditions. For a dry tunnel (emptied tunnel) condition, all the gates are closed initially. The gates start to open when the water level in the tunnel is higher than the water level in Newark Bay. The gate opening rate is 1.0 ft per minute. The tunnel capacity design is based on the tide level of 6.2 ft. NGVD, which is higher than the maximum opening of the gates. Therefore, the outlet flow is gate–controlled.

At the downstream end, a C^+ characteristic equation from the governing equations (3) and (4) can be used. The other equation for the two unknowns (velocity v_n and water depth y_n) is the differential storage equation

$$v_n A_n - Q_o = A_r \frac{dy_n}{dt} \tag{5}$$

where A_n and A_r represent the cross–section area of the tunnel and the outlet structure, respectively; and $Q_o=Q_g+Q_w$ is the total outflow rate through the gates (Q_g) and the overflow opening (Q_w). The flow rate through the gates can be calculated by the following formula [11, 12],

$$Q_g = N_g \mu e B (2g\Delta H)^{\frac{1}{2}} \tag{6}$$

where

N_g = number of gates;
μ = 0.82 = flow rate coefficient of the gate–controlled flow;
e = gate opening;
B = gate width;
ΔH = the water level difference between the tunnel end and sea tide.

The flow rate over the weir can be simply expressed using a weir flow formula

$$Q_w = 3.0 W H_w^{\frac{3}{2}} \tag{7}$$

where W is the circumference length of the opening, and H_w is the downstream water head above the opening. If the water elevation at the downstream end is less than the crest, $Q_w = 0.0$.

2.4 Inflow Hydrographs

The hydrographs used in the simulations were provided by the Corps Engineers. There are three storm events (2yr, 100yr, and 500yr).

A. *2–Year Storm Event*

The provided hydrograph of this storm begins at 1:00 hour, Jan. 1, 1940, and ends at 23:00 hours, Jan. 12, 1940. But the significant inflow to the tunnel system starts at 9:00 hours, Jan. 3, 1940. Hence, the start time of the simulation is 9:00 hours, Jan. 3, 1940. The inflow before that time can be treated as initial flow in the tunnel system. The inflow hydrograph at the two inlets is shown in Fig. 2.6.

B. *100–Year Storm Event*

The duration of the original hydrograph of this storm is the same as above. For the same reason, the simulation with this storm event starts at 2:00 hours, Jan. 3, 1940. The inflow hydrograph at the two inlets is shown in Fig. 2.7.

C. *500–Year Storm Event*

Similarly, for the 500–year storm event the simulation starts at 23:00 hours, Jan. 2, 1940. The inflow hydrograph at the two inlets is shown in Fig. 2.8.

III. GENERAL HYDRAULIC TRANSIENT CHARACTERISTICS

Based on the geometry information and hydrographs described above, the final five simulation cases are reported in this chapter. They are

Case: A1 — 2–year storm and dry tunnel;
Case: A2 — 100–year storm and dry tunnel;
Case: A3 — 100–year storm and wet tunnel;
Case: A4 — 500–year storm and dry tunnel;
Case: A5 — 500–year storm and wet tunnel.

All the other design parameters in the above five cases are the same, such as

Sea tide level	= 6.2 ft;
Gate–controlled outlet;	
Manning coefficient'	= 0.0133;
Pompton inlet elevation	= 173.0 ft for 2yr and 100yr storms,
	= 179.0 ft for 500yr storm;
Spur inlet elevation	= 163.0 ft for 2yr and 100yr storms,
	= 168.0 ft for 500yr storm.

In addition, the proposed constructed heights of Workshafts Nos. 2B and 2C were set at elevations 50 ft and 25 ft.

3.1 Two–Year Storm with Dry Tunnel (Case: A1)

Fig. 3.1 shows the time variation of water elevations at the two upstream inlets and the downstream outlet during the 2–year storm event with an initially–empty (dry) tunnel. As stated before, the simulation starts with a significant inflow and ends after the high inflow period. Total simulation period is 55.5 hours. As the figure indicates, both upstream inlets are always free surface flow during this storm period.

Fig. 3.2 is the instantaneous hydraulic gradelines along the main tunnel (excluding Spur branch). The station number in this figure is referred to in Fig. 2.2. The vertical dashed lines represent the location of ventilation shafts or workshafts. As Fig. 3.2 shows, a hydraulic jump occurs near the point where the tunnel slope drops. The flow in the tunnel is apparently divided into open channel flow and closed conduit flow by the hydraulic jump. The water elevation almost remains unchanged after about 10 hours from the beginning of the storm.

The maximum water surface elevation along the main tunnel is displayed in Fig. 3.3. Note that the maximum elevation at different locations may occur at different times. The results also indicate that the maximum water surface elevation in the tunnel is much lower than the vertical shaft outlets, which means that this storm event under the current design condition is safe from overflow hydraulic transients.

3.2 100–Year Storm with Dry Tunnel (Case: A2)

Fig. 3.4 shows the time variation of water surface elevations at the two upstream end inlets and the downstream end outlet during the 100–year storm event with an initially–empty (dry) tunnel. In this case, the tunnel system is quickly pressurized, and the flow becomes a closed conduit flow. The pressurization starts from the downstream end about 4 hours after the beginning of the storm. As the tunnel continues to be filled and the pressurized portion expands, surge develops at the interface between the pressurized zone and the free surface zone. The magnitude of the surge increases as the inflow rate increases. When the surge migrates to the upstream ends, it produces a sudden water level rise, as shown in Fig. 3.4. A more detailed short period near the sharp peak is displayed in Fig. 3.5. Since the Spur inlet is somewhat closer to the downstream end than the Pompton inlet, the surge arrives at the Spur inlet a little earlier. When the surge arrives at the Pompton inlet, the water surface elevation rises from 30 ft. to 172 ft. in about 7 minutes, and then falls to 0.0 ft. in about 6 minutes. This is a severe surge but it doesn't result in backflow (spilling over the intake) at the inlet since the peak is still lower than the inlet water surface elevation.

Fig. 3.6 shows the time variation of water surface elevations at the two workshafts, Nos. 2B and 2C. Hydraulic characteristics very similar to that shown in Fig. 3.4 can be identified in this figure since the surge travels through the whole tunnel system. Fig. 3.7 displays the change in depth during the surge period in detail. Since workshaft No. 2C is very close to the downstream end, the surge there is very weak. But at workshaft No. 2B the peak surge is higher than the top elevation of the workshaft, which results in a large amount of overflow (backflow from the tunnel) from the workshaft, as shown in Fig. 3.8. The peak overflow rate is about 1050 cfs. The duration of the overflow is less than 3 minutes.

Fig. 3.9 gives the instantaneous hydraulic gradelines along the main tunnel (excluding the Spur branch) during this storm. As shown in this figure, the water level increases rapidly during the first 5 hours of this storm. Fig. 3.10 shows the maximum water surface elevation in the main tunnel stations. As shown in the figure, the maximum value at workshaft No. 2B is higher than the top of the shaft elevation.

The inflow and outflow of the tunnel system is shown in Fig. 3.11. The difference between the total inflow and downstream outflow is equal to the total overflow at the two inlets. The modeling results indicate that during the period of 20 to 40 hours after the beginning of the storm, a small amount of

the inflow, mostly at Spur inlet, cannot pass through the tunnel. The total maximum overflow rate at the two inlets is about 900 cfs. Here, overflow really represents flow which will not get into the tunnel and will be bypast down the Pompton or Passaic Rivers. The scale–up overflow is shown in Fig. 3.12

3.3 100–Year Storm with Wet Tunnel (Case: A3)

Fig. 3.13 shows the time variation of water surface elevations at the two upstream inlets and the downstream outlet during the 100–year storm event with an initially–filled (wet) tunnel. The initial water surface elevation in the tunnel system is the downstream tide level (6.2 ft).. At this water level only the low downstream section of the tunnel is pressurized, and the upstream section is still a free water surface. Therefore, as the inflow enters into the tunnel, the interface between pressurized zone and free surface zone moves very quickly to the upstream ends. As a result, the hydraulic characteristics in this case is almost identical to the case with a dry tunnel as described above. Similarly, a strong surge occurs at the both upstream inlets, as shown in Fig. 3.14.

As the surge travels in the tunnel, it also affects the water elevation at workshafts Nos. 2B and 2C, as shown in Figs. 3.15 and 3.16. The overflow problem at workshaft No. 2B appears to not have improved with the wet tunnel condition, as indicated in Fig. 3.17. It appears that the tunnel needs to be filled to somewhat higher level in order to reduce the surge.

Fig. 3.18 shows five instantaneous hydraulic gradelines along the main tunnel (excluding the Spur branch) during this storm. At time=3.5 hours, the interface occurs immediately at the break between the mild slope and the steep slope. The maximum water surface elevations along the main tunnel is shown in Fig. 3.19. Comparing this case with the dry tunnel case, the maximum value with the wet tunnel case appears to be much higher between two vertical shafts in the downstream section. Since the downstream section is initially filled, the high elevation peaks are apparently due to the water hammer phenomena. Since the dropshafts play a roll of releasing the high water hammer wave, the water surface elevation at the dropshaft location is not very high in Fig. 3.19. Nevertheless, the maximum water surface elevation at Workshaft 2C is higher than its outlet elevation, which may results in some overflow. This result is not identified in both Figs. 3.16 and 3.17 because the plotting data in the two figures are output every six seconds. The higher water hammer wave at Workshaft 2C apparently lasts less than six seconds.

The inflow and outflow hydrographs are about the same as that of the dry tunnel case, as shown in Figs. 3.20 and 3.21.

The modeling results in this case indicate that the wet tunnel filled to the sea level does not improve the overflow problem at workshaft No. 2B. Adversely, this wet tunnel condition leads to a strong water hammer problem at the downstream section. However, the water hammer may not be a serious problem since this section is more than 400 ft underground.

3.4 500–Year Storm with Dry Tunnel (Case: A4)

Fig. 3.22 shows the time variation of water surface elevations at the two upstream inlets and the downstream outlet during the 500–year storm event with an initially empty (dry) tunnel. The difference between this case and Case A2 is the different inflow hydrograph. The 500–year storm has a longer high flow rate period, but the peak flow rate in the two storms is almost the same. Since the increase in the small rate during the early part of the 500–year inflow hydrograph (shown in Fig. 2.8) is rather slow, the strength of the surge is much smaller when compared with Case A2. Details during the surging period are shown in Fig. 3.23. The water surface elevations at the Spur inlet is lower than its dropshaft height during t=9 up to 40 hours. This is because the flow at the Spur inlet during that period is cut off.

The water surface elevations at workshafts Nos. 2B and 2C are shown in Figs. 3.24 and 3.25. The surge peak at workshaft No. 2B is also smaller than that in Case A2, and most importantly the maximum elevation is lower than the workshaft outlet elevation. As a result, there is no more overflow from the workshafts during this hydrograph.

Fig. 3.26 shows five instantaneous hydraulic gradelines along the main tunnel (excluding the Spur branch) during this storm. The maximum water elevation along the main tunnel is shown in Fig. 3.27. The results also indicate that the maximum water elevation line is below the vertical shaft outlet line except at the upstream inlet.

Similar to Case A2, some overflow at the two inlets can be found, as shown in Fig. 3.28. Comparing with Case A2, the overflow duration in this case is longer, but the total maximum overflow rate is smaller due to the higher upstream water surface elevation at the two inlets. The maximum overflow is only about 752, as shown in Fig. 3.29 in detail.

The above modeling results show that hydraulic transient caused by the 500–year storm hydrograph is mild. The reason for this is explained below.

Fig. 3.30 shows a detailed comparison of the two inflow hydrographs (100–year and 500–year) during the first 8 hours of the storms. Their accumulative inflow volume is displayed in Fig. 3.31. As the figures indicate, the 100–year inflow hydrograph increases faster than the 500–year inflow hydrograph during the initial stage. Also interesting to note is a small drop at about t=5.5 hours, coinciding with the arrival of the surge, in the 500–year hydrograph. The most critical period determining the surge magnitude is between the initiation of the surge downstream and the arrival of surge upstream. Since the 100–year hydrograph is higher than the 500–year hydrograph during this period, the surge is greater for the 100–year inflow hydrograph than the 500–year inflow hydrograph.

3.5 500–Year Storm with Wet Tunnel (Case: A5)

As in Case A3, the tunnel is assumed to be initially filled to the high tide level of 6.2 ft. The simulated results of this case are shown in Figs. 3.32 to 3.39. These figures show almost the same hydraulic characteristics as in Case A4. However, as in Case A3, this case also features some water hammer phenomena in the downstream section.

IV. CONCLUSIONS AND RECOMMENDATIONS

Based on the modeling results and analyses, the following is a list of the important conclusions.

1. For the 2–year storm flood with an initially dry tunnel, the Passaic River Flood Protection Tunnel System does not have transient problems under the current design conditions.

2. For the 100–year storm flood with an initially dry tunnel, a strong surge is identified throughout the tunnel system due to rapid increase of the inflow at both upstream inlets during the initial 5 hour period. As a result of the surge, an overflow problem is found at workshaft No. 2B. It lasts about 13 minutes with a peak flow rate of 1050 cfs.

3. For the 500–year storm flood with an initially dry tunnel, a weaker surge is found in the tunnel system because inflows increase less rapidly than the 100–year storm during the initial 5 hour period. The weaker surge does not result in any overflow at the vertical shafts.

4. Under the tested wet tunnel condition (the tunnel is initially filled to the downstream sea tide level), the surge problem still exists since the tunnel is only partially filled at the beginning. In addition, a minor water hammer problem is induced at the downstream section, which may cause an extra overflow at workshaft No. 2C.

Some recommendations for improving the current design based on the modeling results are listed below:

1. There are two methods to improve the surge condition under the 100 year storm flood. One is to control the inflow rate at an early stage. The other is to modify the design of workshaft No. 2B, such as the diameter, outlet geometry, and location. Note that the above simulations are based on the new outlet elevation at workshafts Nos. 2B and 2C. The writers think that a feasible method to avoid the strong surge under the current design conditions of the tunnel system is to modify the inflow hydrograph during the first five hours. The rate of rise of the modified hydrograph should be slightly smaller than that of 500–year hydrograph furnished by The Corps of Engineers. This work is recommended for a future study.

2. The tested wet tunnel condition, with the tunnel initially filled to an elevation of 6.2 ft will make the hydraulic transient even somewhat worse. It is worthwhile to test other wet conditions with the initial water higher than 6.2 ft. To avoid hydraulic transients, a substantial portion of the mild slope portion of the tunnel should be filled.

3. The gate outlet at the downstream end results in a significant head loss under the current design, and may have negative effects on the surging problems. Improvement can be accomplished by changing the size of the gates.

4. Because the inflow rate and the rate of increase of inflow is the most important factor affecting hydraulic transients before the tunnel is completely filled, it is recommended that a detailed modeling of the intake control structures and their operations under various river flow conditions be conducted

REFERENCES

1. Facsimile Transmittal from Ray Schembri of the N.Y. District, Corps of Engineers, to Charles C.S. Song, "Tunnel Surging Analysis – In Progress Review Meeting," Aug. 18, 1994.

2. Cardle, J. A. and Song, C.C.S., "Mathematical Modeling of Unsteady Flow in Storm Sewers." *International Journal of Engineering Fluid Mechanics*, Vol. 1, No. 4, 1988.

3. Guo, Q. and Song, C.C.S., "Surging in Urban Storm Drainage Systems," ASCE, *Journal of Hydraulic Engineering*, Vol. 116, No. 12, June, 1989.

4. Song, C.C.S., Guo, Q., and Zheng, Y., "Hydraulic Transient Modeling of TARP Systems," St. Anthony Falls Hydraulic Laboratory, Project Report No. 270, March 1988.

5. Song, C.C.S., Lin, W., and Gong, C., "Hydraulic Transient Modeling of TARP Systems," St. Anthony Falls Hydraulic Laboratory, University of Minnesota, Project Report No. 332, March 1992.

6. Guo, Q., and Song, C.C.S., "Hydraulic Transient Analysis of TARP Phase II O'Hare System," St. Anthony Falls Hydraulic Laboratory, University of Minnesota, Project Report No. 276, July 1988.

7. Song, C.C.S., He, J., Liu, Y., and Gong, C., "Hydraulic Transient Study of Mainstream & Des Plaines TARP Phase II Systems," St. Anthony Falls Hydraulic Laboratory, University of Minnesota, Project Report No. 353, July 1994.

8. Song, C.C.S., and Lin, W., "Study of Potential Hydraulic Transient for Milwaukee Inline Storage System," St. Anthony Falls Hydraulic Laboratory, University of Minnesota, Project Report No. 297, July 1990.

9. Lin, W., and Song, C.C.S., "Hydraulic Transient Analysis of Tunnels and Dropshaft for Milwaukee Inline Storage System," St. Anthony Falls Hydraulic Laboratory, University of Minnesota, Project Report No. 340, July 1993.

10. Song, C.C.S., Cardle, J.A., and Gavali, S., "Mathematical Modeling of the Genesee River Storage–Conveyance System, Rochester, N.Y., St. Anthony Falls Hydraulic Laboratory, University of Minnesota, Project Report No. 215, July 1982.

11. King, H. W., *Handbook of Hydraulics*, McGraw–Hill Book Company, Inc., 1954.

12. Facsimile Transmittal from Ray Schembri of the N.Y. District, Corps of Engineers, to Jianming He, "Find Head Losses through the Gates," Aug. 18, 1994.

APPENDIX I

Figures 2.1 through 3.39

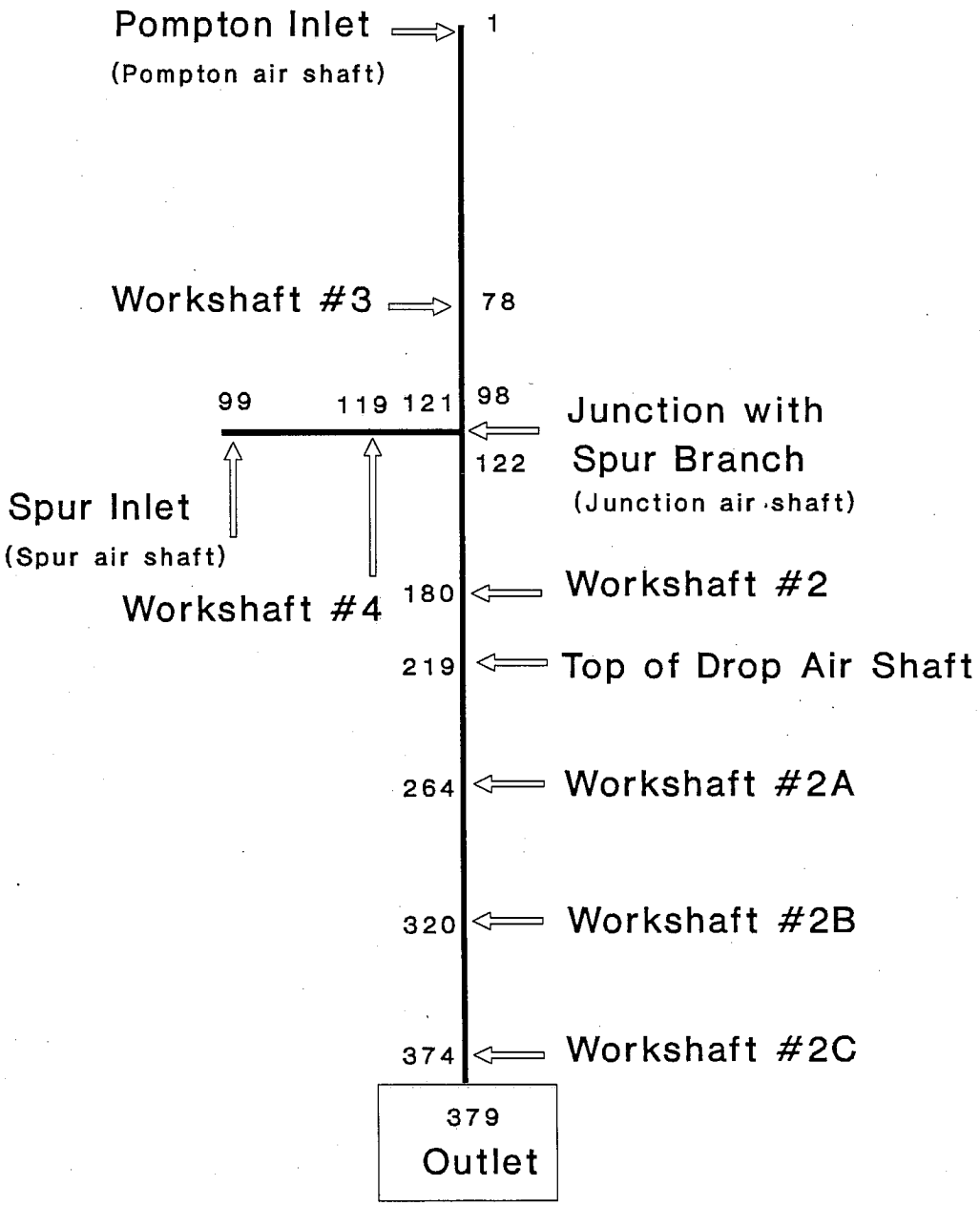

Fig. 2.1 Schematic of the Passaic River Flood Protection Tunnel System and the computation stations

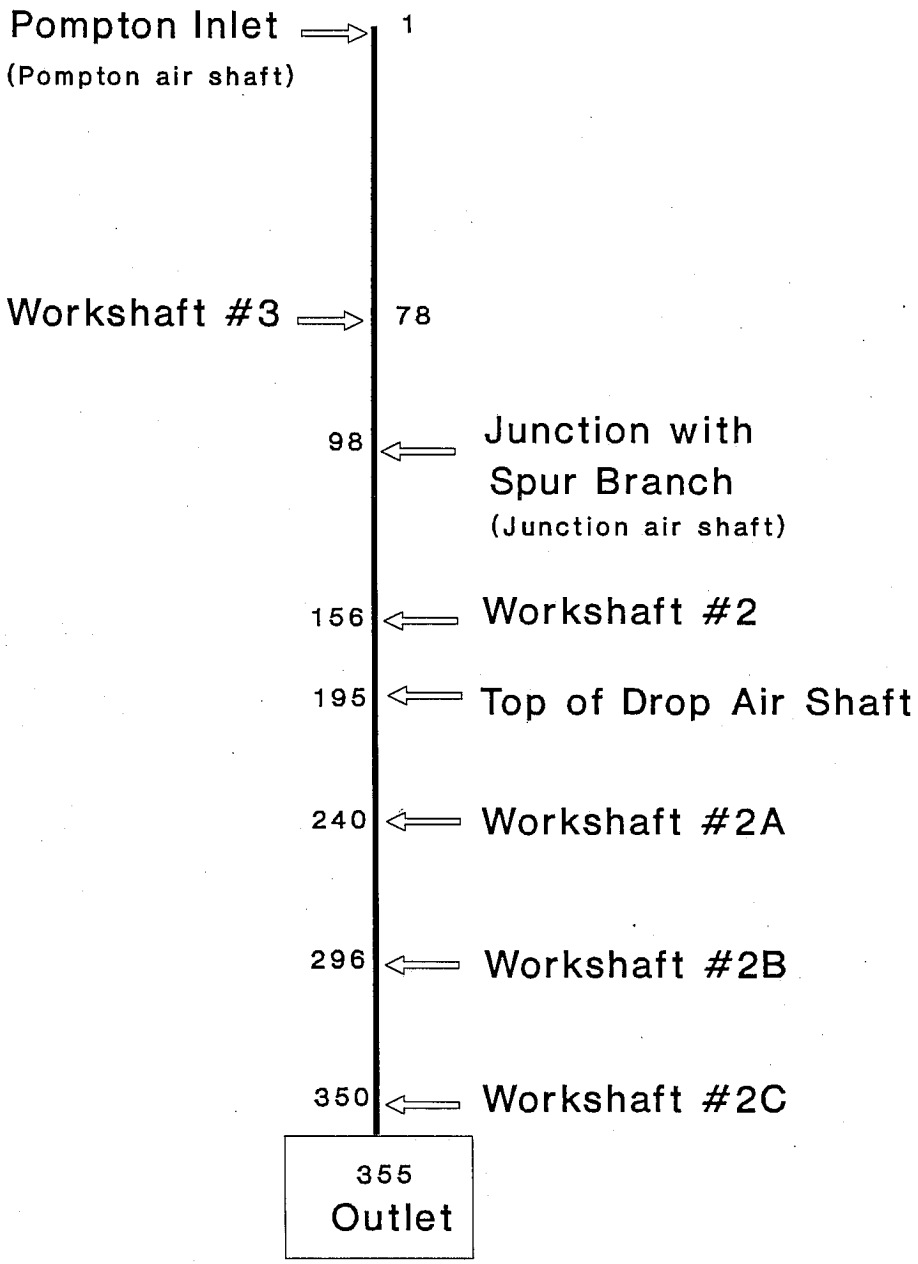

Fig. 2.2 Schematic of the main tunnel, excluding the Spur Branch, and the station numbers for showing the hydraulic grade line along the main tunnel

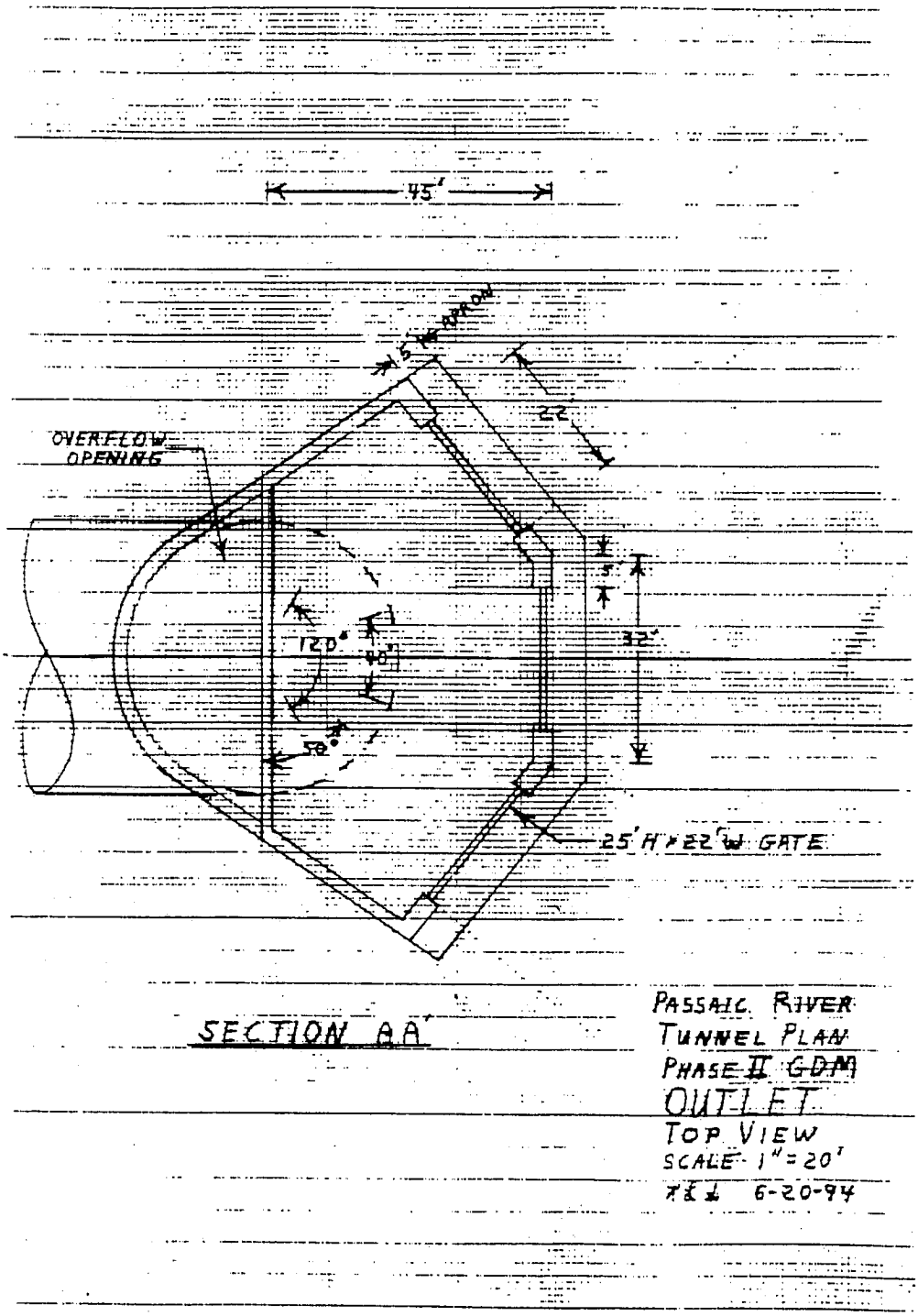

Fig. 2.3 Top–view of the downstream outlet

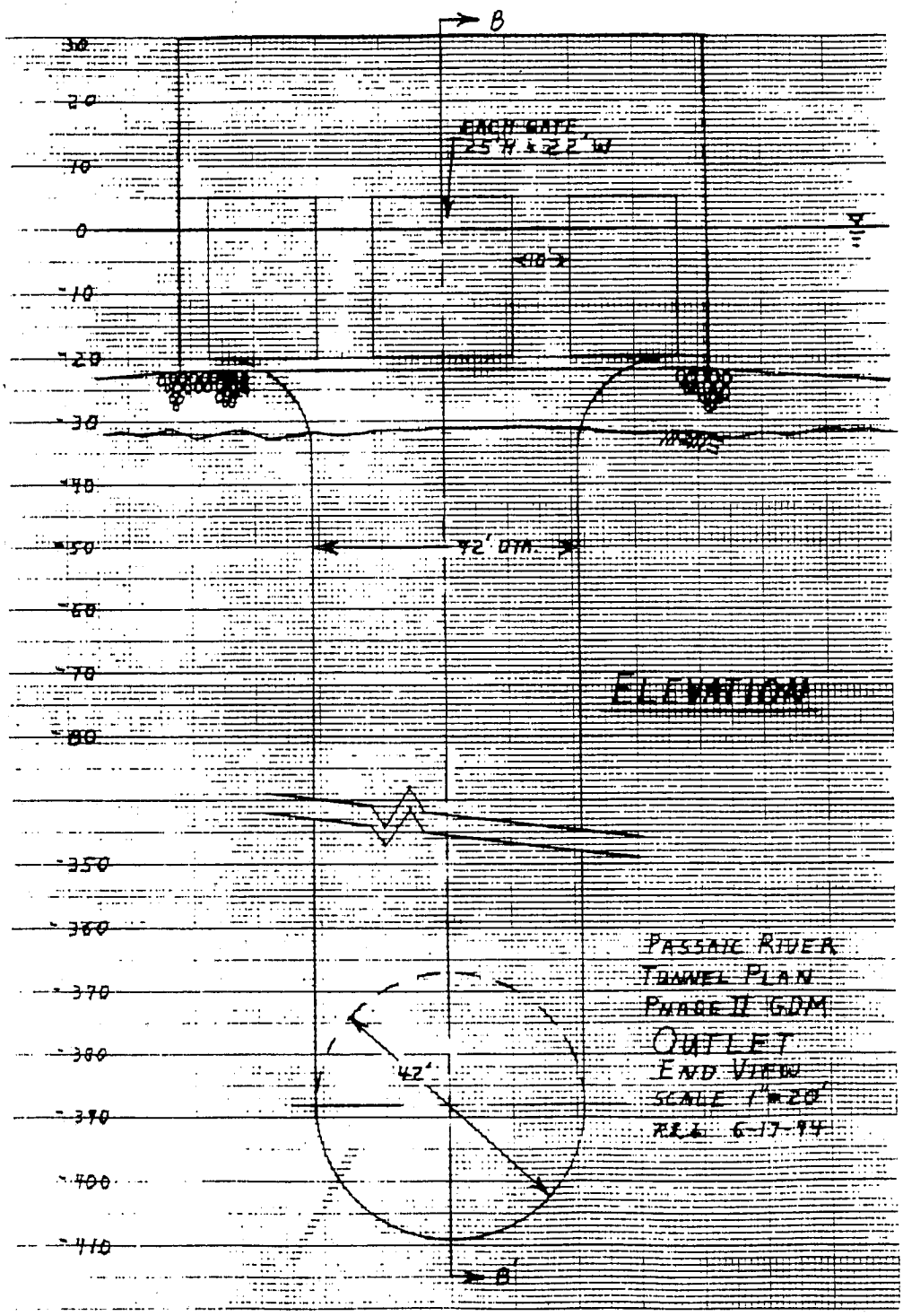

Fig. 2.4 End–view of the downstream outlet

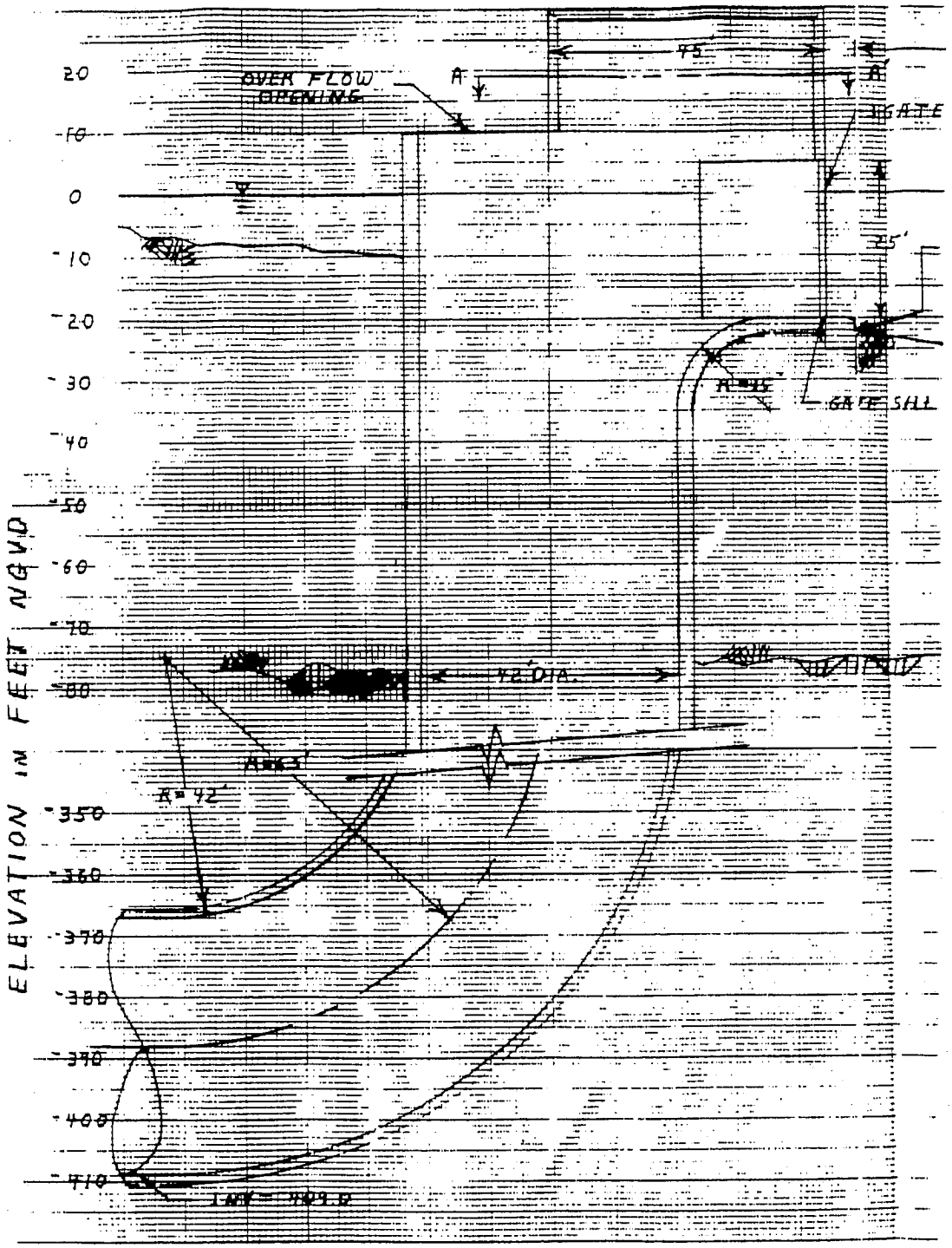

Fig. 2.5 Side–view of the downstream outlet

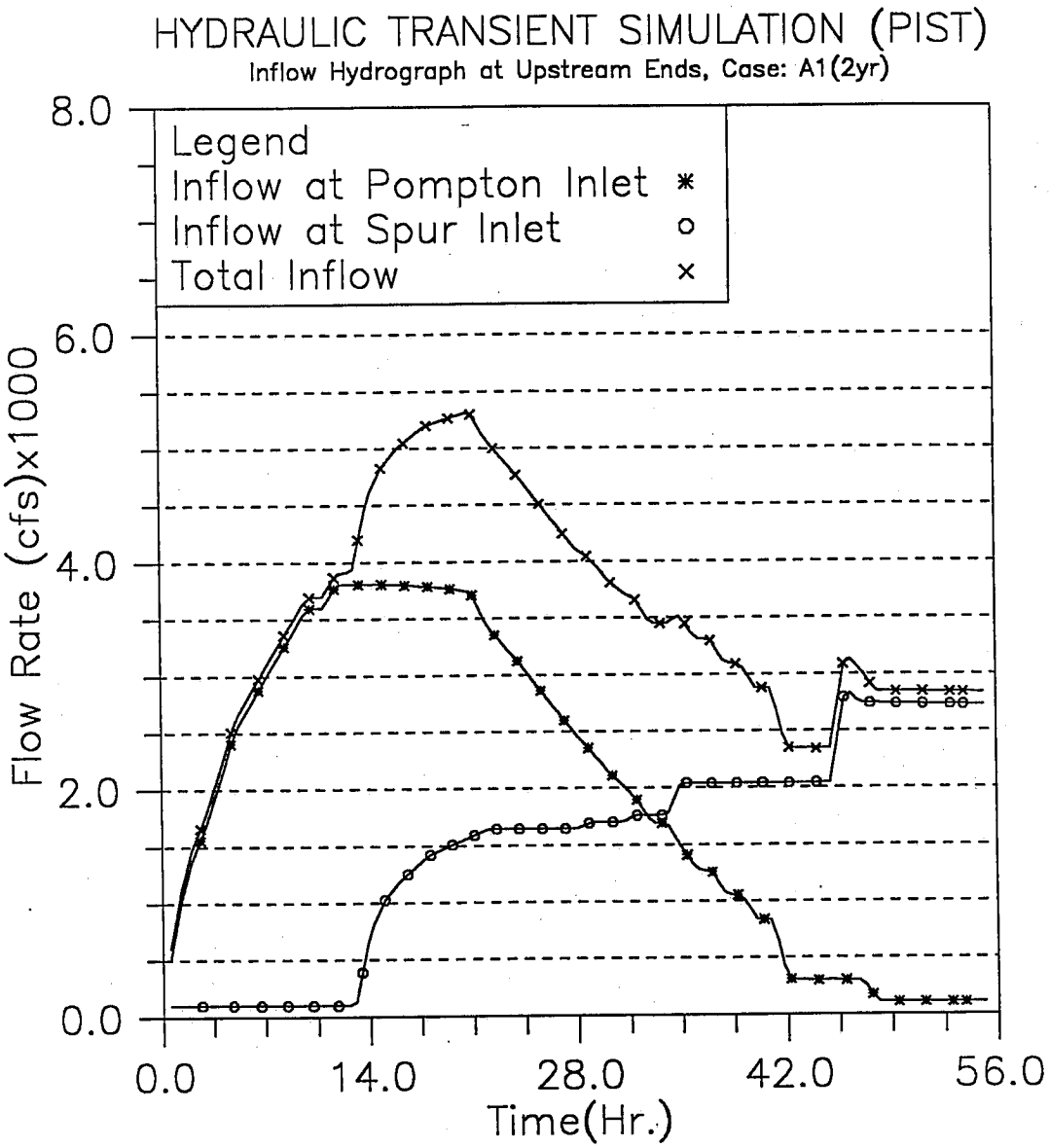

Fig. 2.6 2yr Storm Inflow Hydrograph at Pompton and Spur Inlets

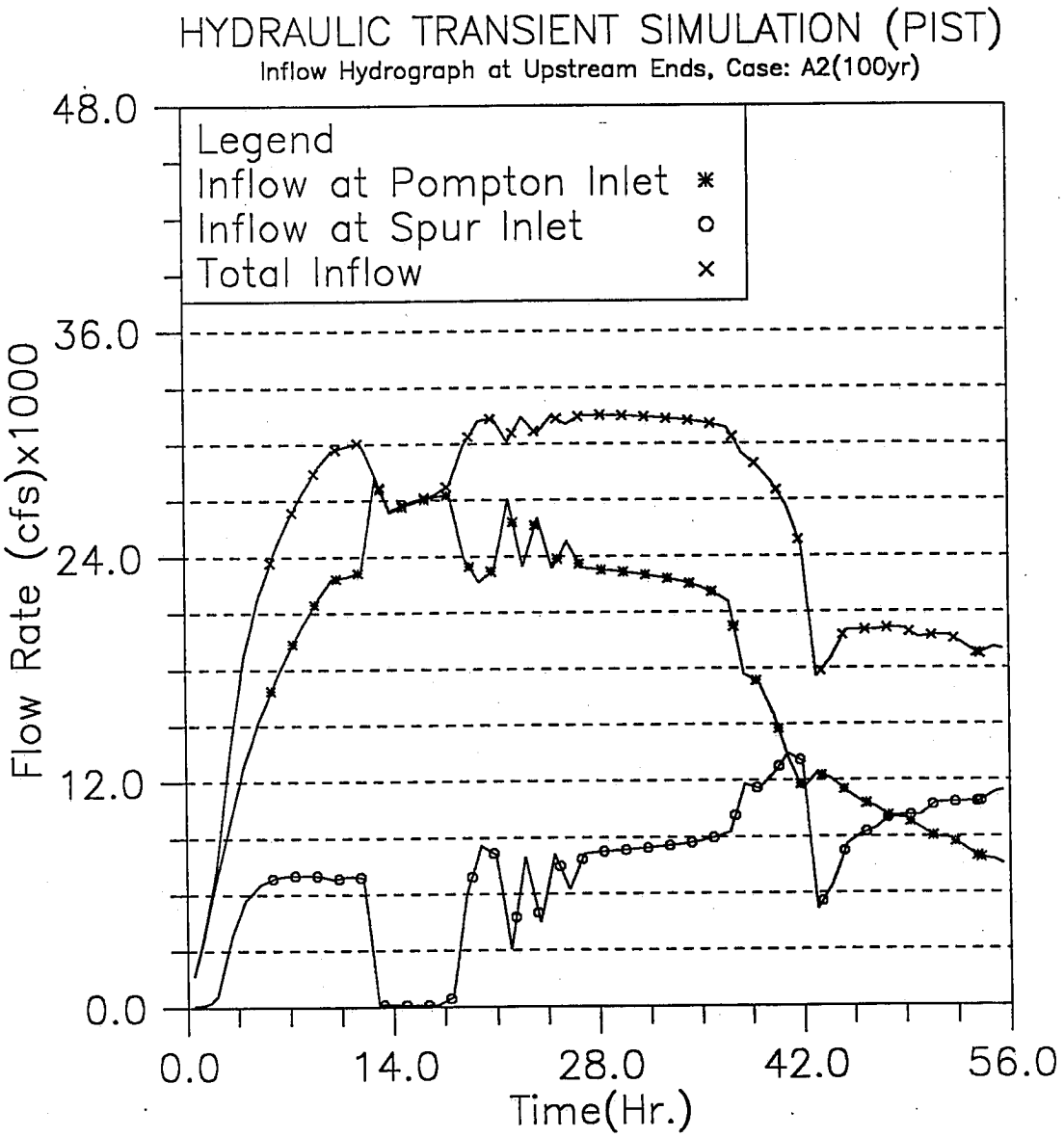

Fig. 2.7 100yr Storm Inflow Hydrograph at Pompton and Spur Inlets

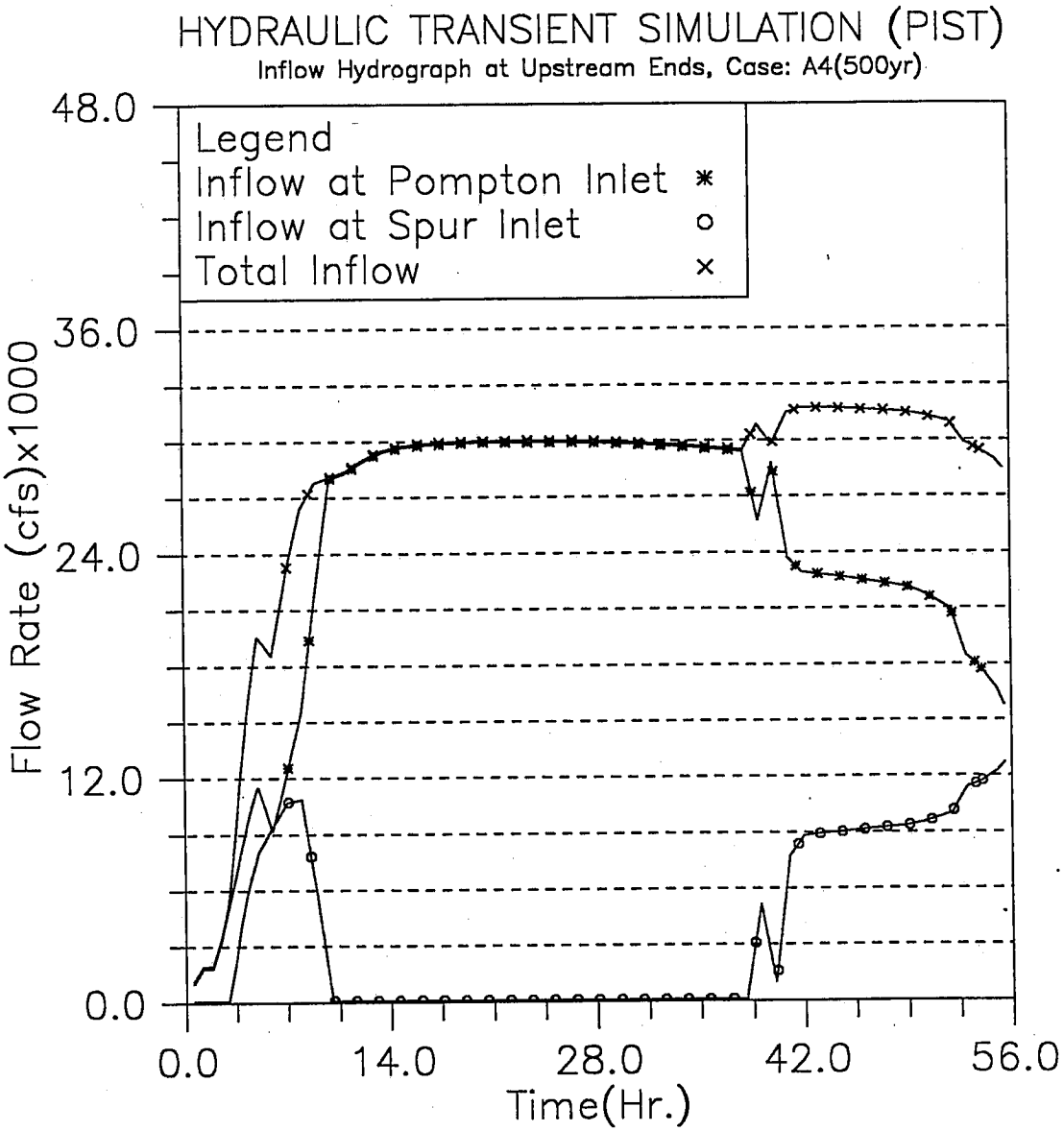

Fig. 2.8 500yr Storm Inflow Hydrograph at Pompton and Spur Inlets

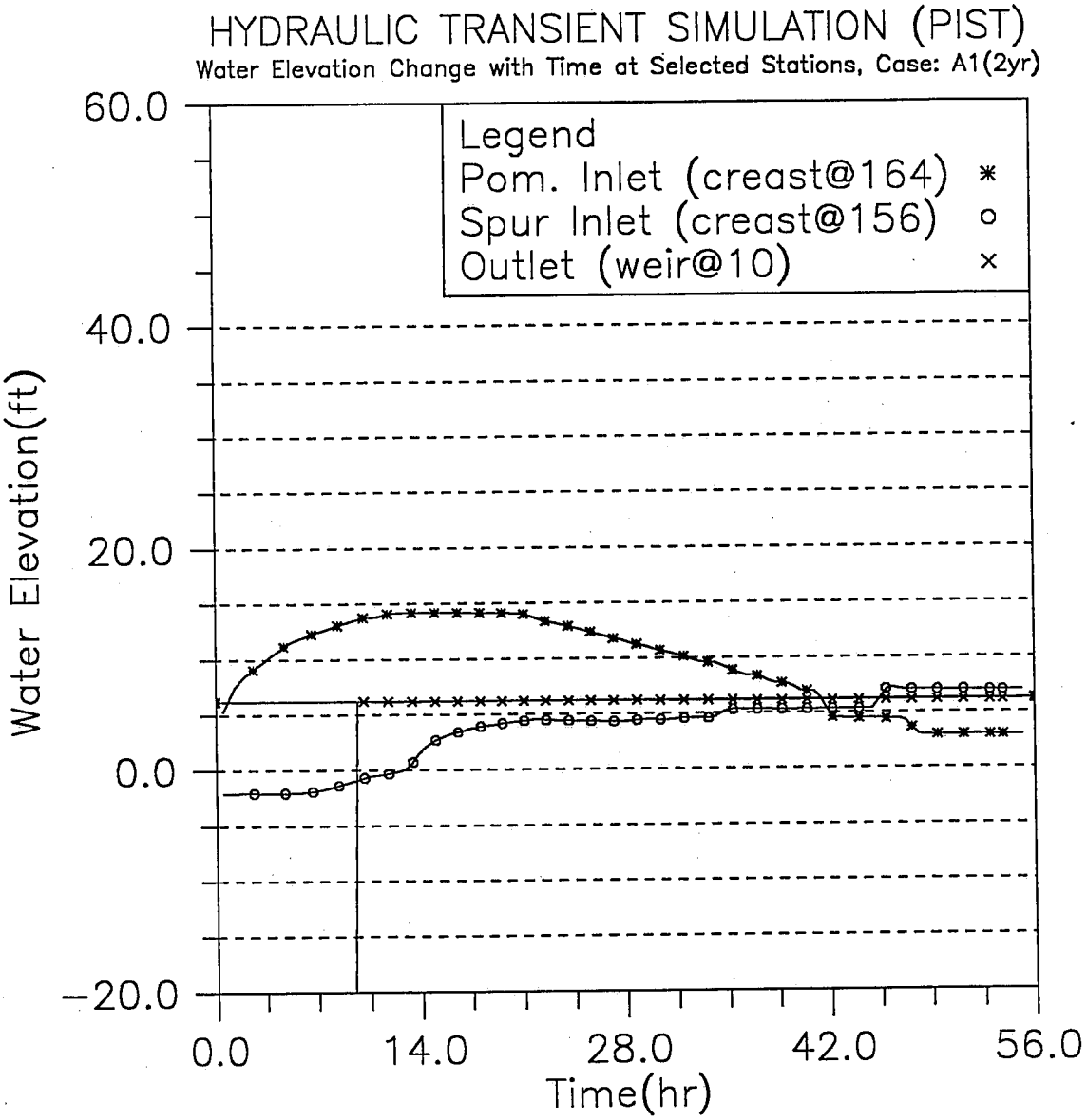

Fig. 3.1 Time variation of water surface elevations at Pompton inlet, Spur inlet and downstream end; modeling case: 2yr storm and dry tunnel (Case A1)

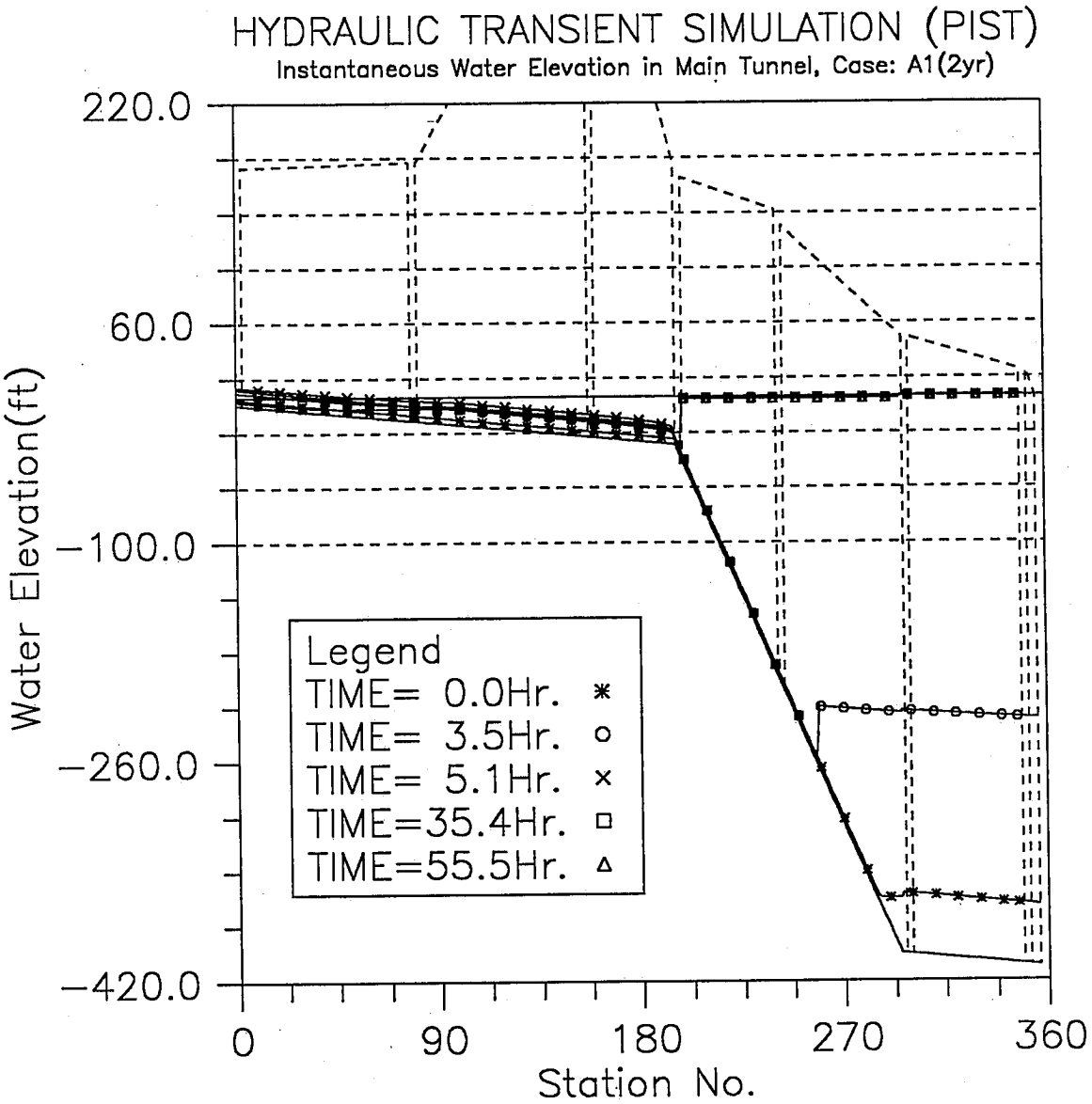

Fig. 3.2 Instantaneous hydraulic gradelines along the main tunnel; modeling case: 2yr storm and dry tunnel (Case A1)

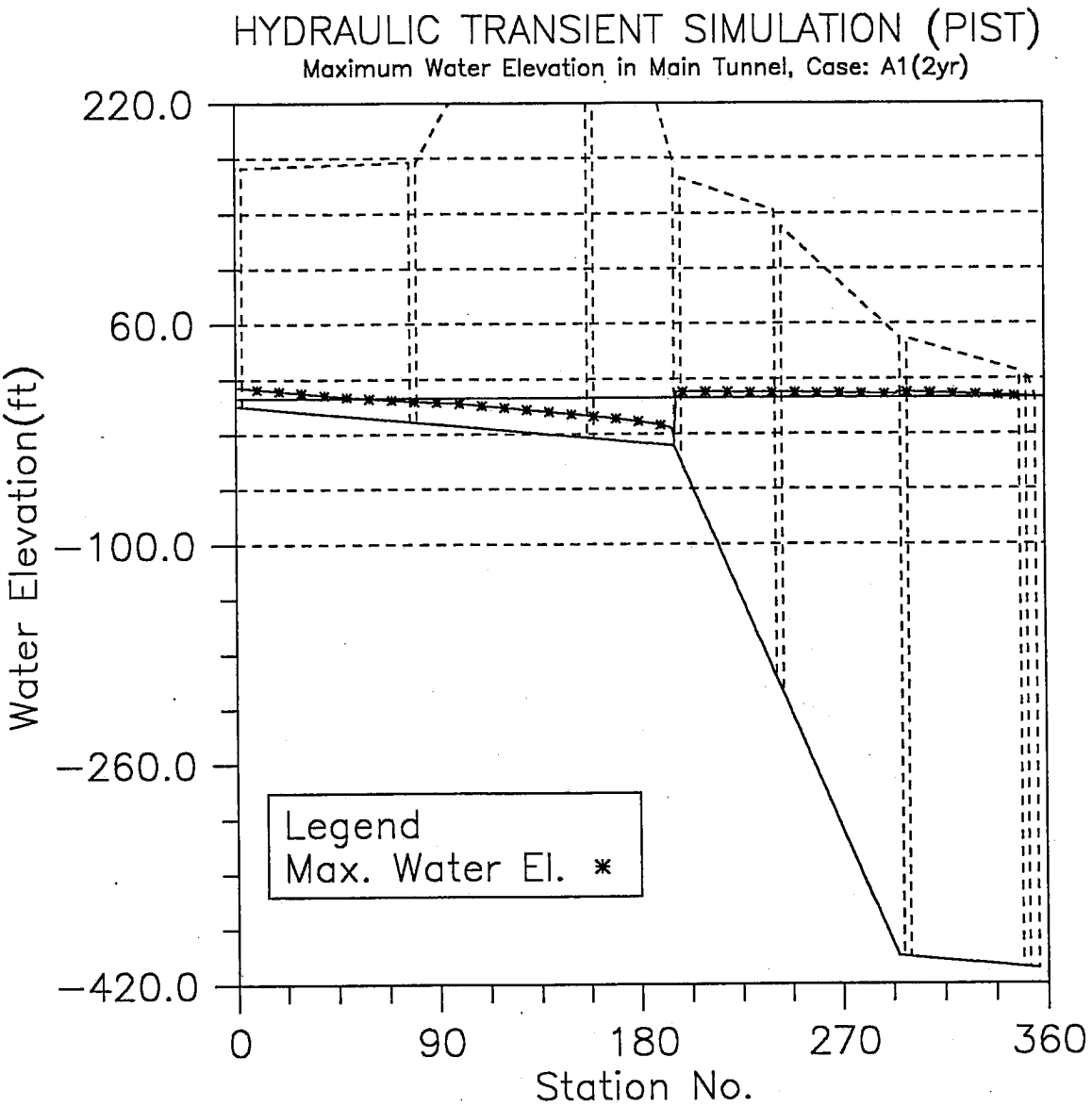

Fig. 3.3 The maximum water surface elevations along the main tunnel; modeling case: 2yr storm and dry tunnel (Case A1)

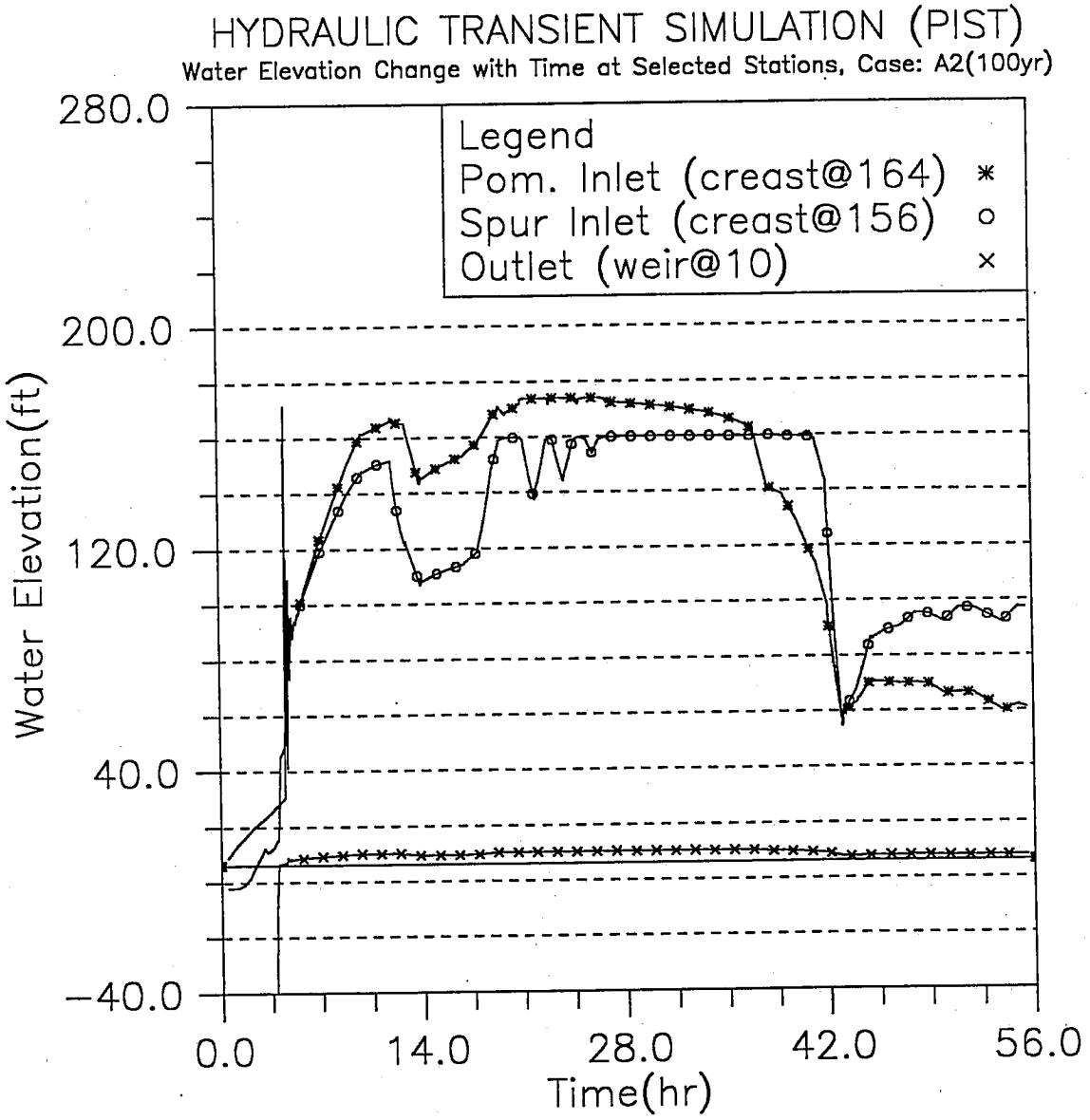

Fig. 3.4 Time variation of water surface elevations at Pompton inlet, Spur inlet and downstream end during the simulated time period; modeling case: 100yr storm and dry tunnel (Case A2)

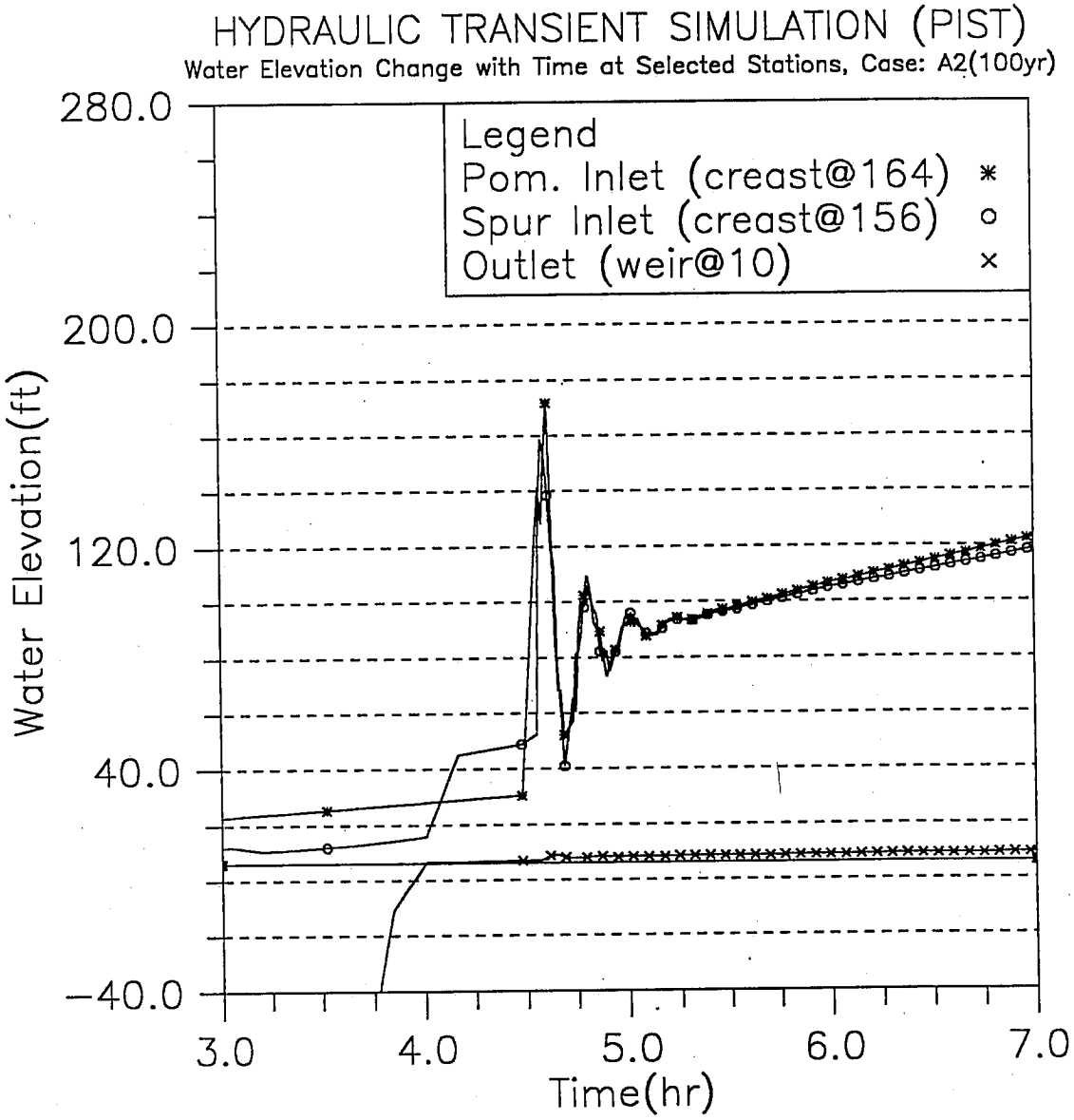

Fig. 3.5 Detailed time variation of water surface elevations at Pompton inlet, Spur inlet and downstream end during the early surging period; modeling case: 100yr storm and dry tunnel (Case A2)

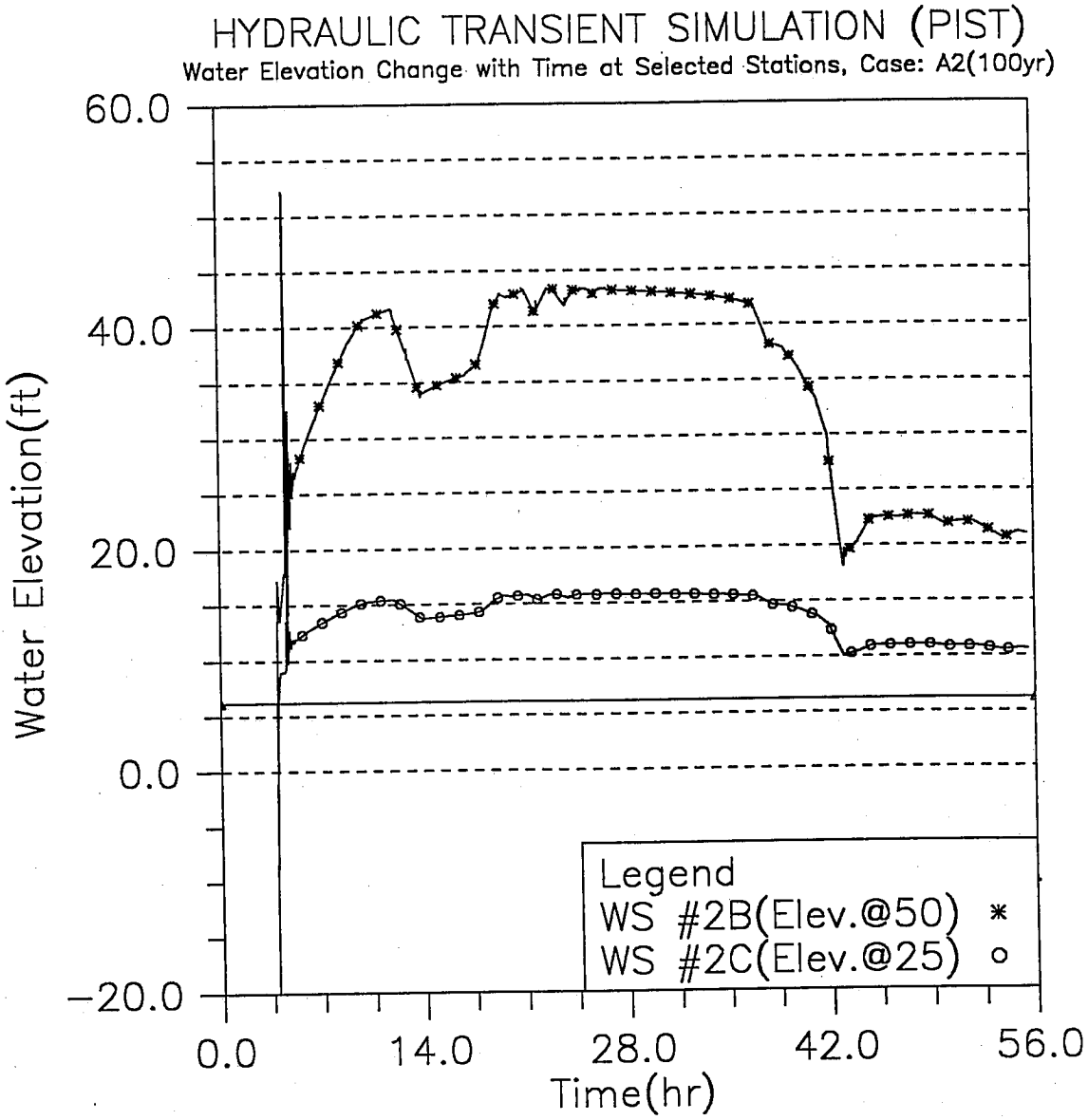

Fig. 3.6 Time variation of water surface elevations at Workshafts #2B and #2C during the simulated time period; modeling case: 100yr storm and dry tunnel (Case A2)

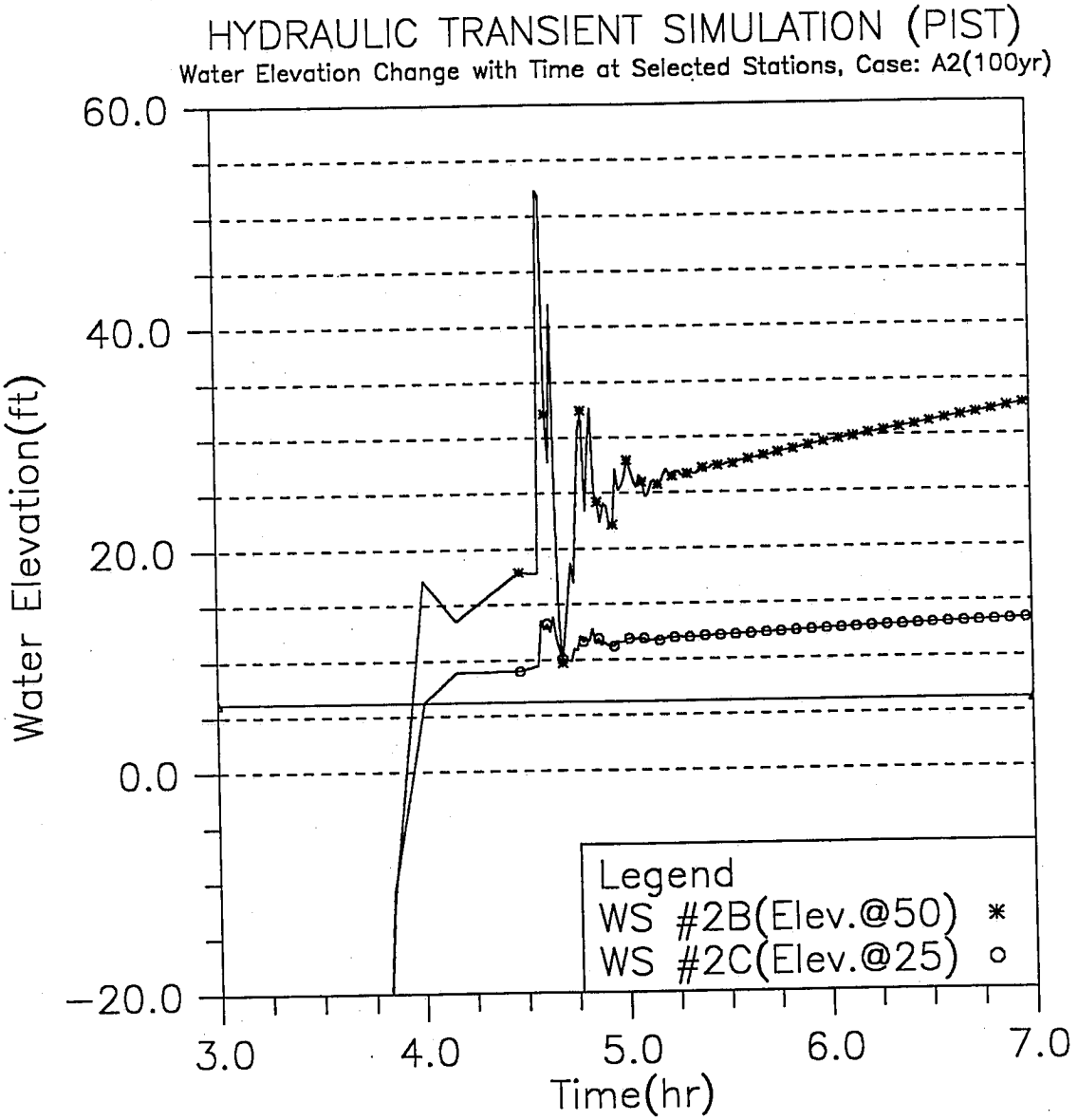

Fig. 3.7 Detailed time variation of water surface elevations at Workshafts #2B and #2C during the early surging period; modeling case: 100yr storm and dry tunnel (Case A2)

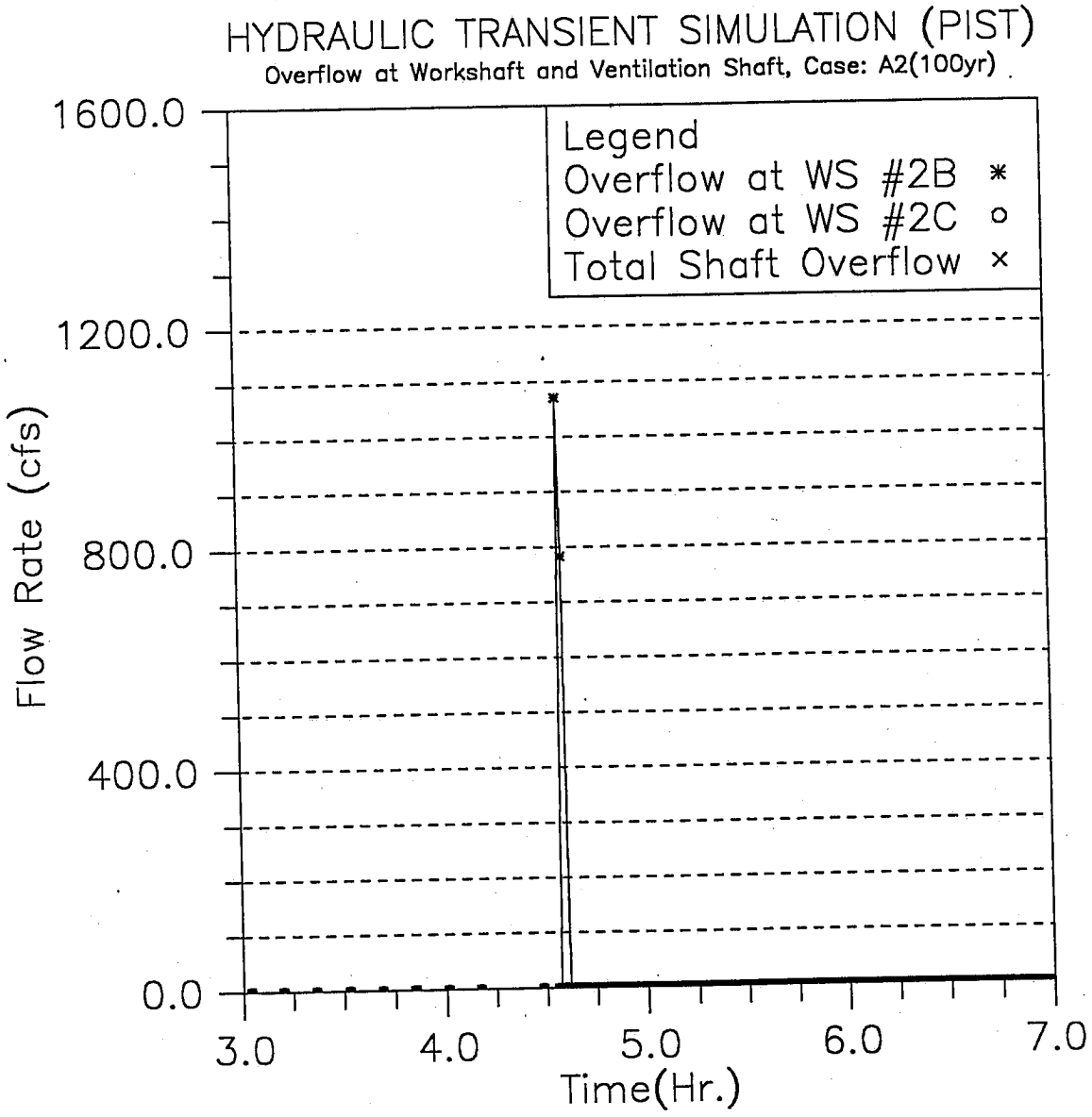

Fig. 3.8 Detailed time variation of the overflow at Workshafts #2B and #2C during the early surging period; modeling case: 100yr storm and dry tunnel (Case A2)

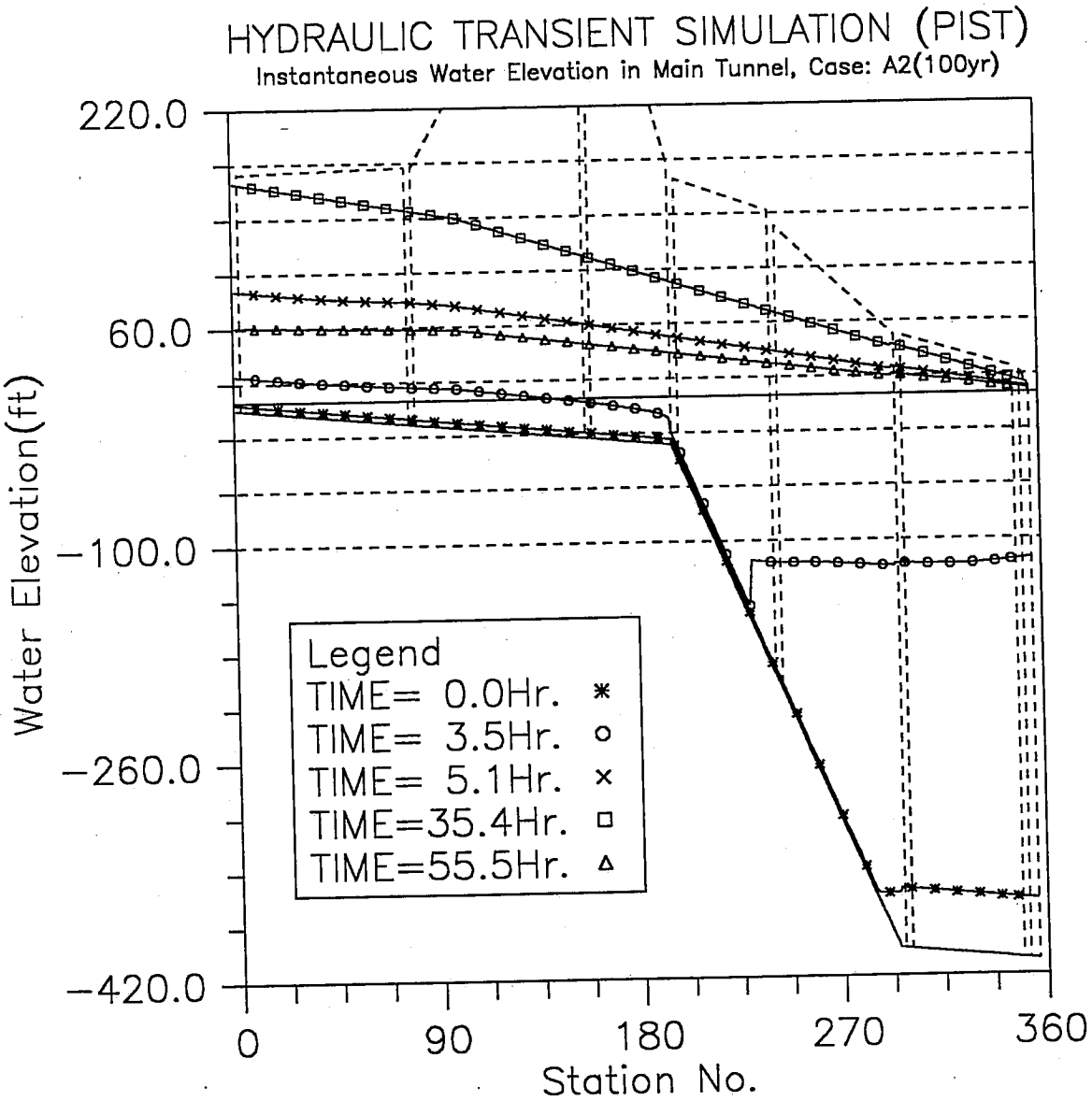

Fig. 3.9 Instantaneous hydraulic gradelines along the main tunnel; modeling case: 100yr storm and dry tunnel (Case A2)

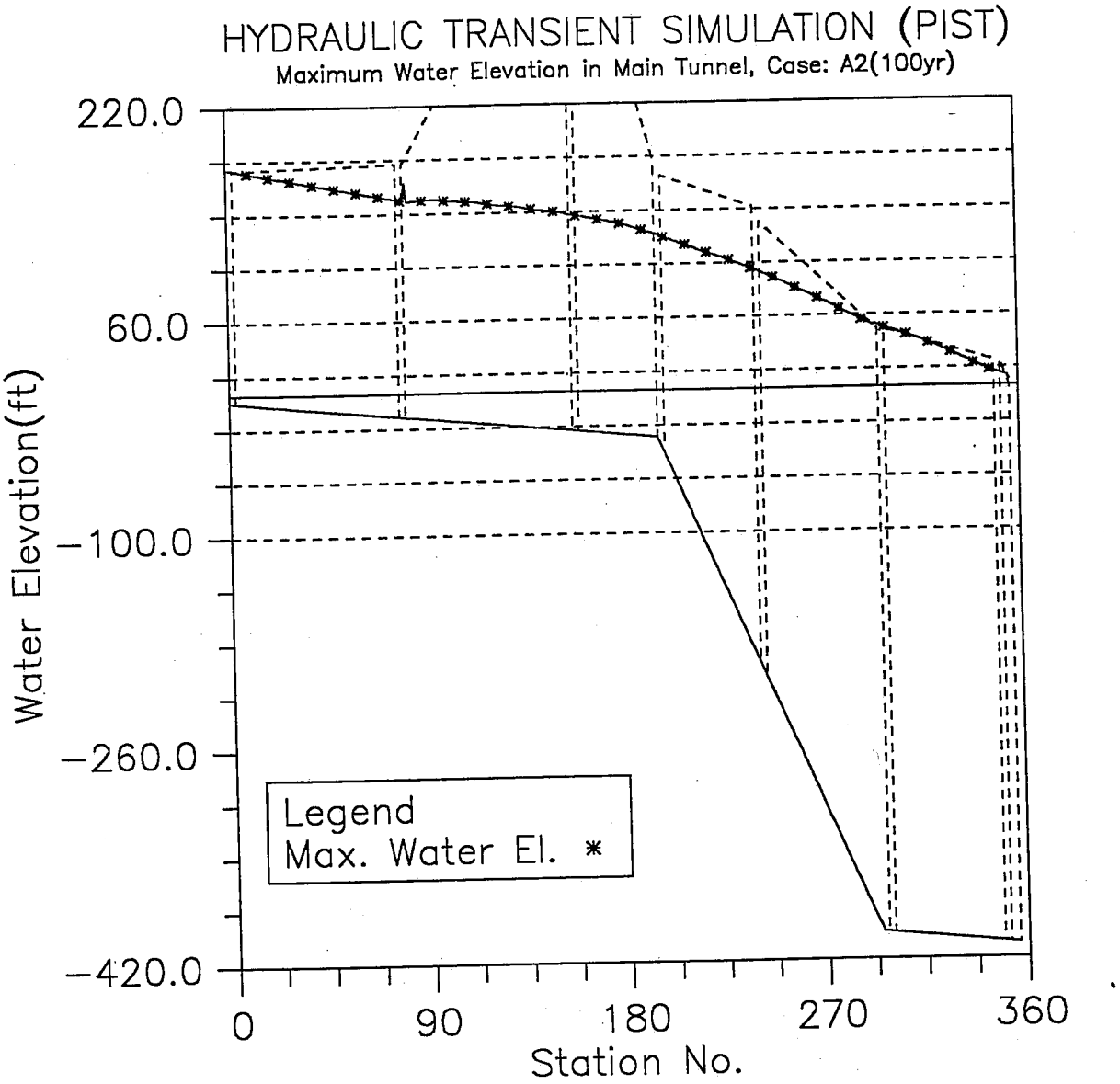

Fig. 3.10 The maximum water surface elevations along the main tunnel; modeling case: 100yr storm and dry tunnel (Case A2)

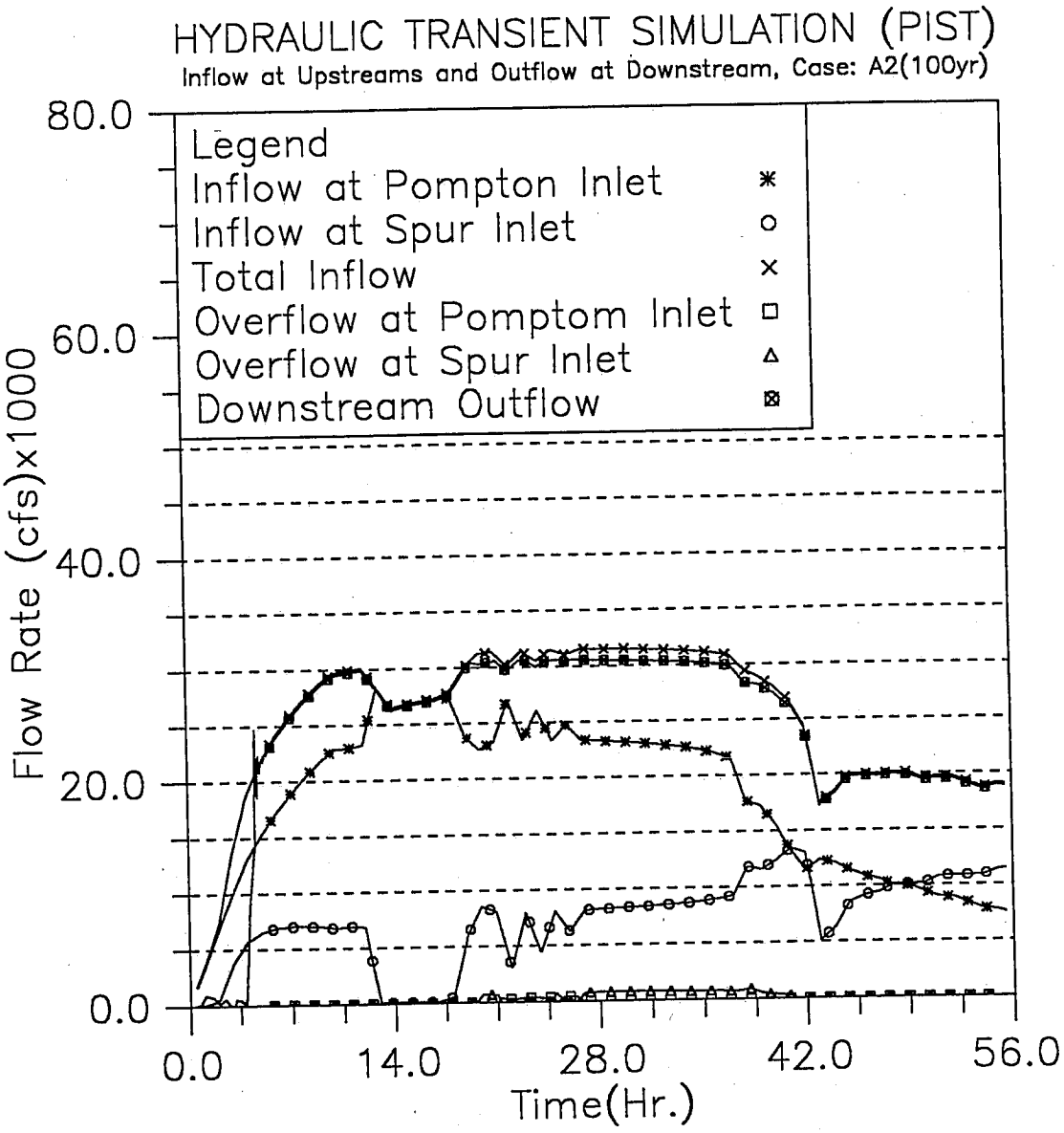

Fig. 3.11 Inflow and overflow hydrographs at Pompton and Spur inlets, and outflow hydrograph at the downstream; modeling case: 100yr storm and dry tunnel (Case A2)

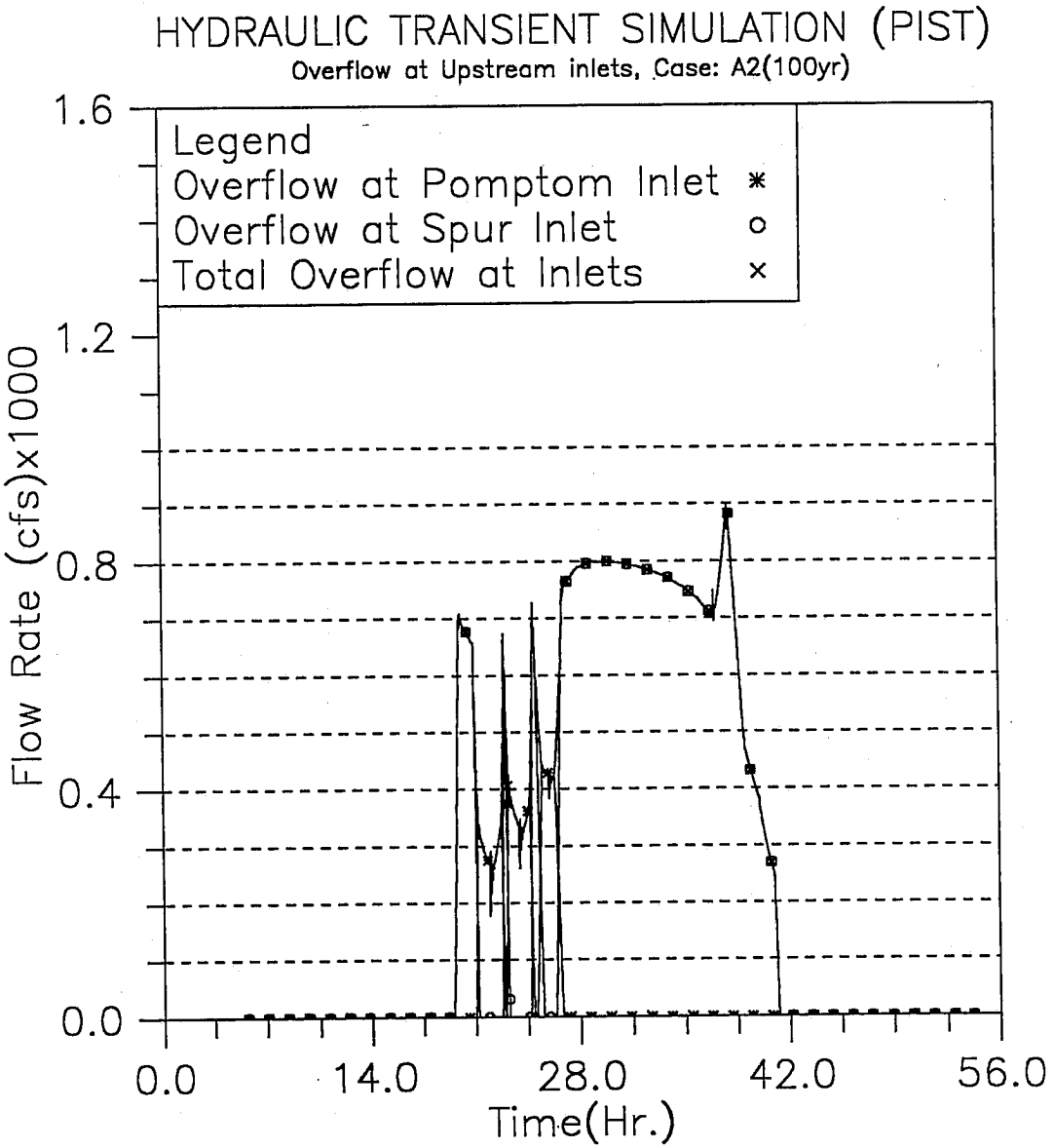

Fig. 3.12 Overflow hydrographs at Pompton and Spur inlets; modeling case: 100yr storm and dry tunnel (Case A2)

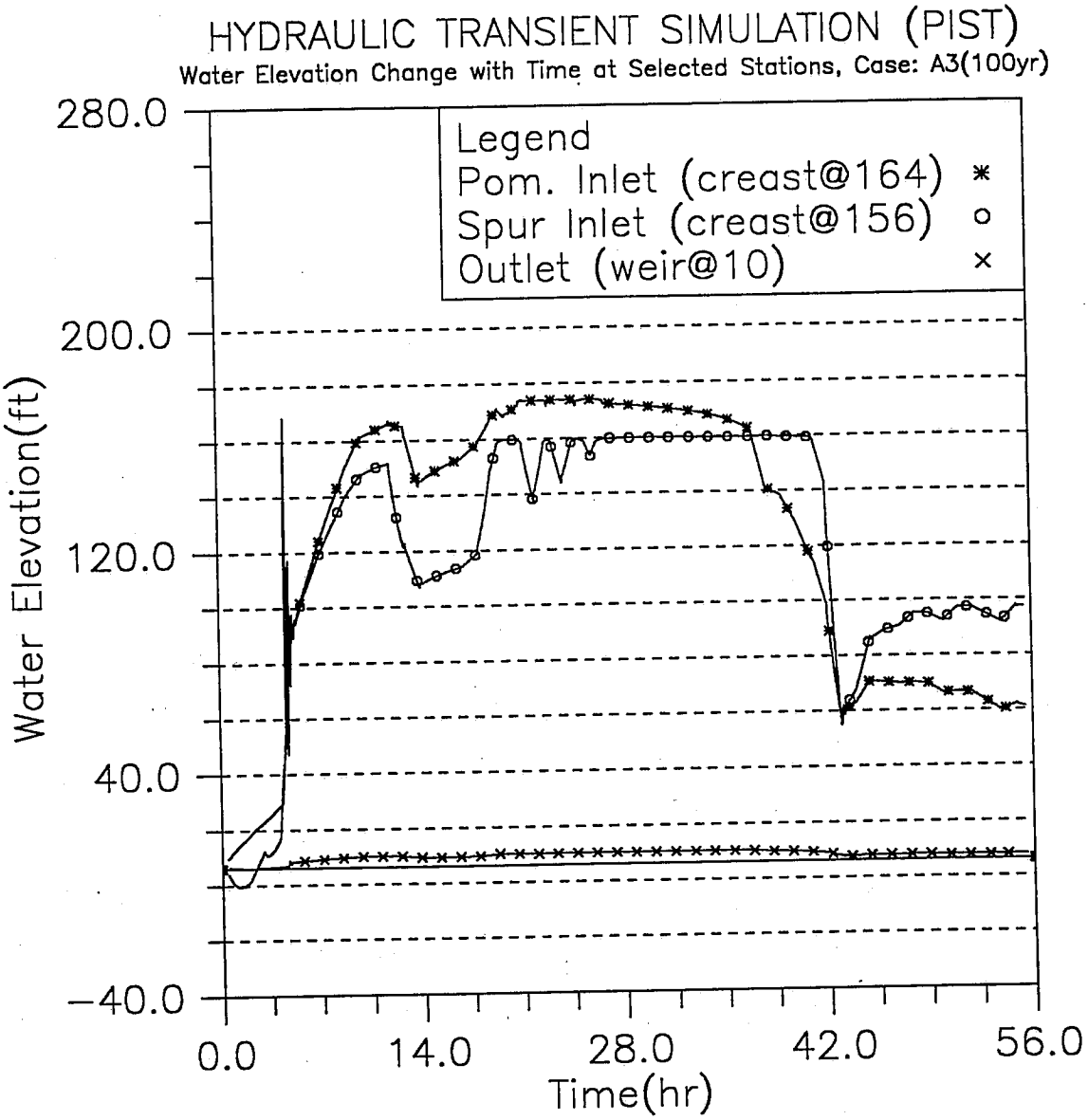

Fig. 3.13 Time variation of water surface elevations at Pompton inlet, Spur inlet and downstream end during the simulated time period; modeling case: 100yr storm and wet tunnel (Case A3)

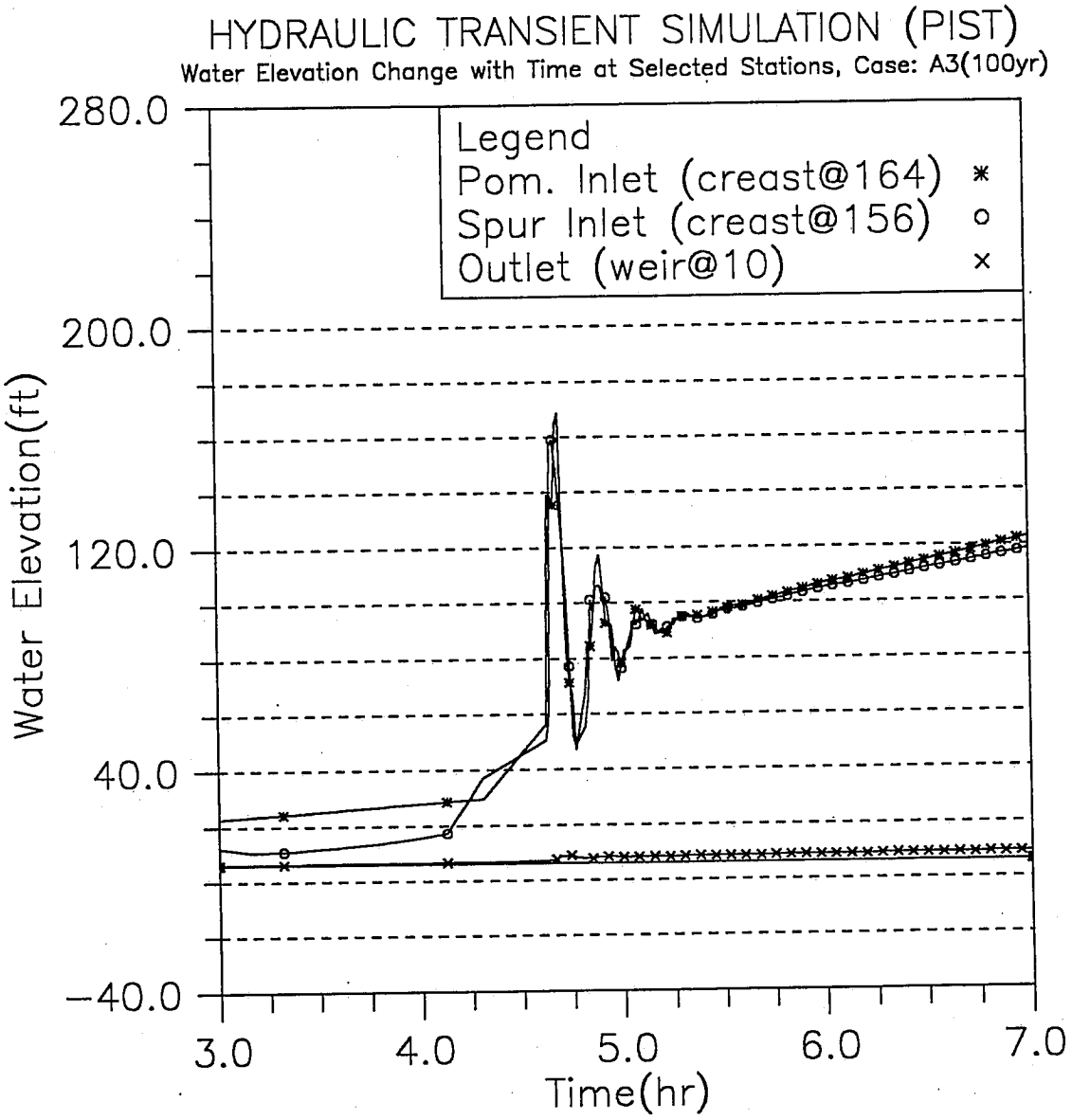

Fig. 3.14 Detailed time variation of water surface elevations at Pompton inlet, Spur inlet and downstream end during the early surging period; modeling case: 100yr storm and wet tunnel (Case A3)

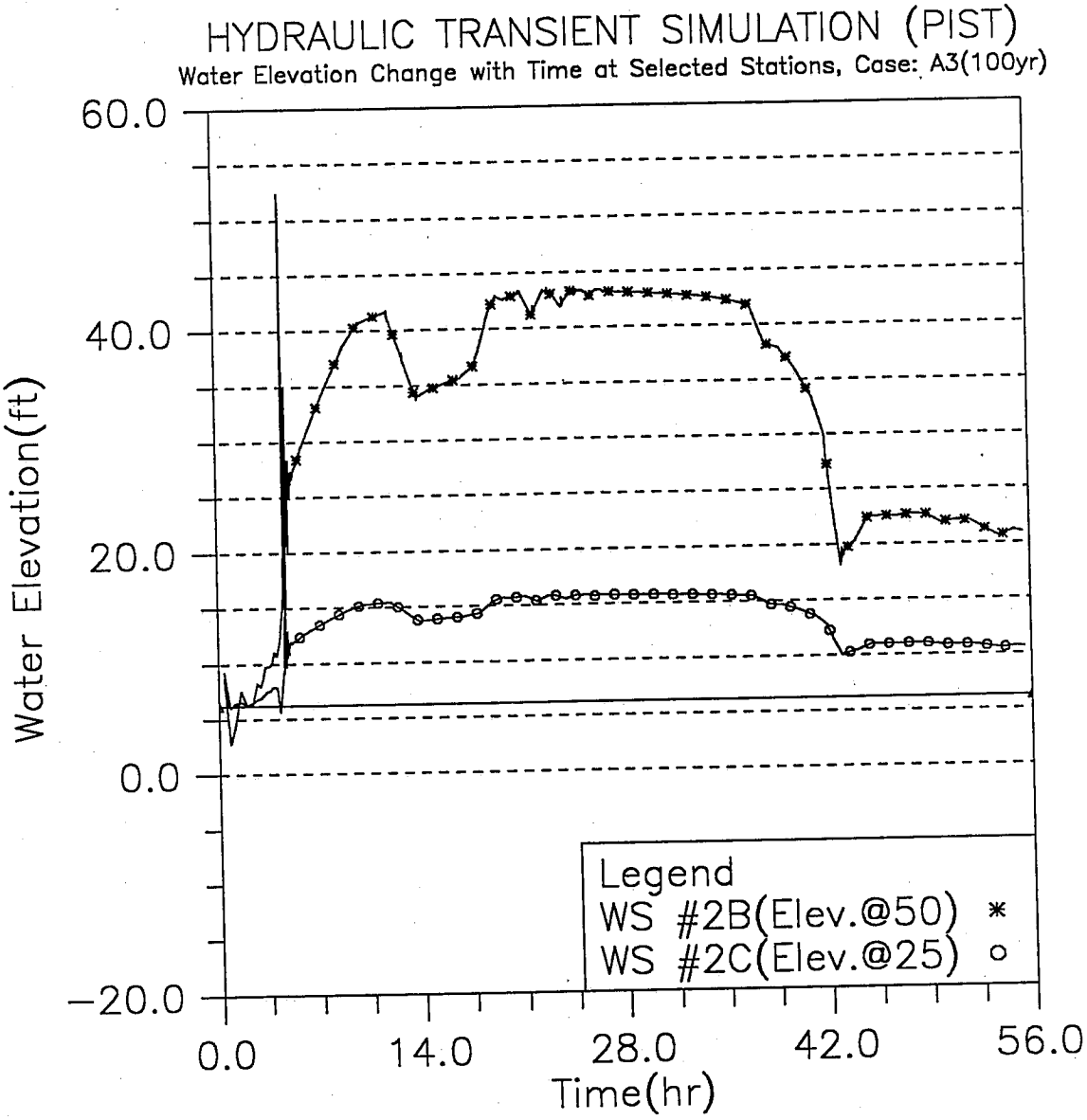

Fig. 3.15 Time variation of water surface elevations at Workshafts #2B and #2C during the simulated time period; modeling case: 100yr storm and wet tunnel (Case A3)

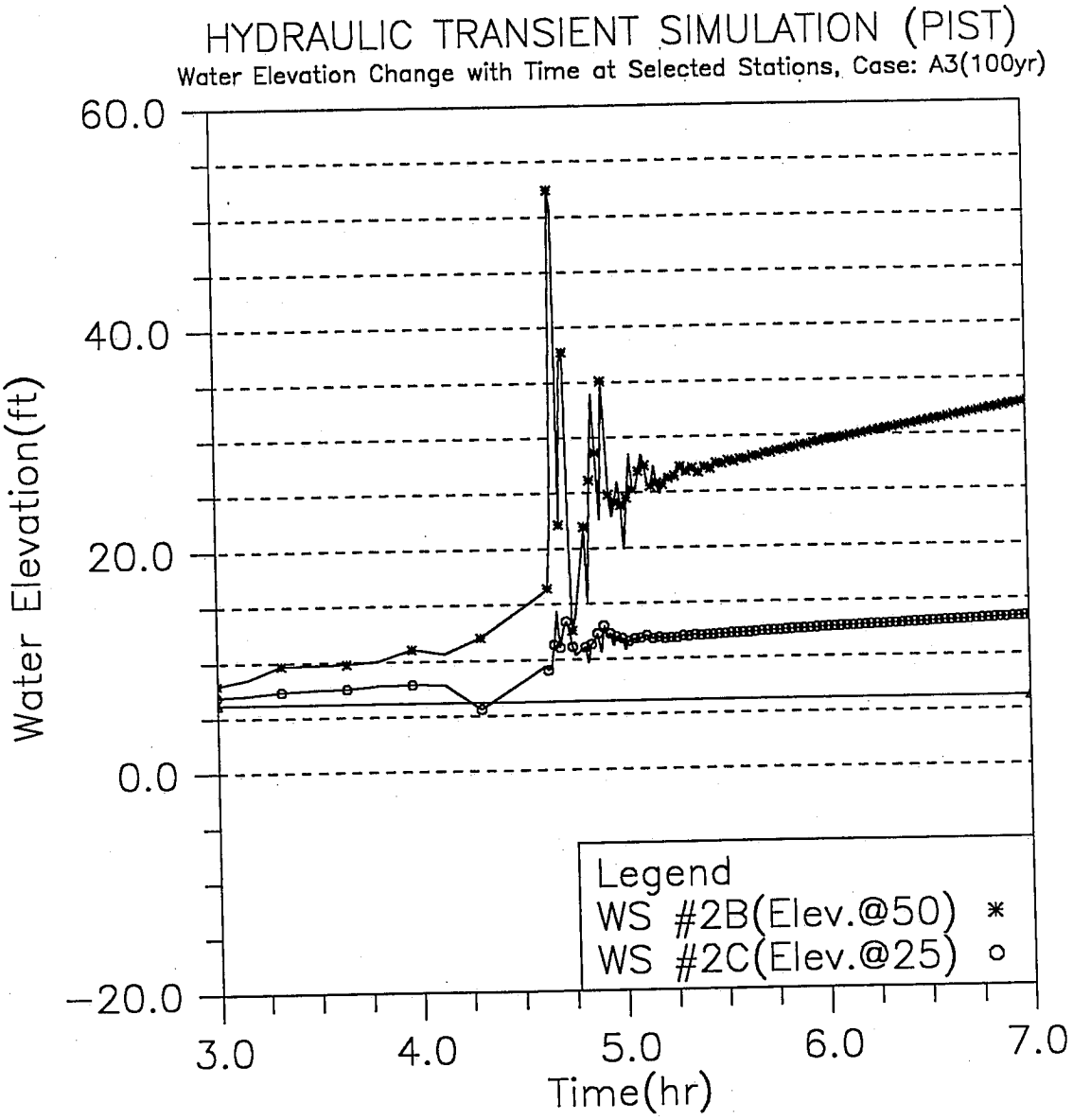

Fig. 3.16 Detailed time variation of water surface elevations at Workshafts #2B and #2C during the early surging period; modeling case: 100yr storm and wet tunnel (Case A3)

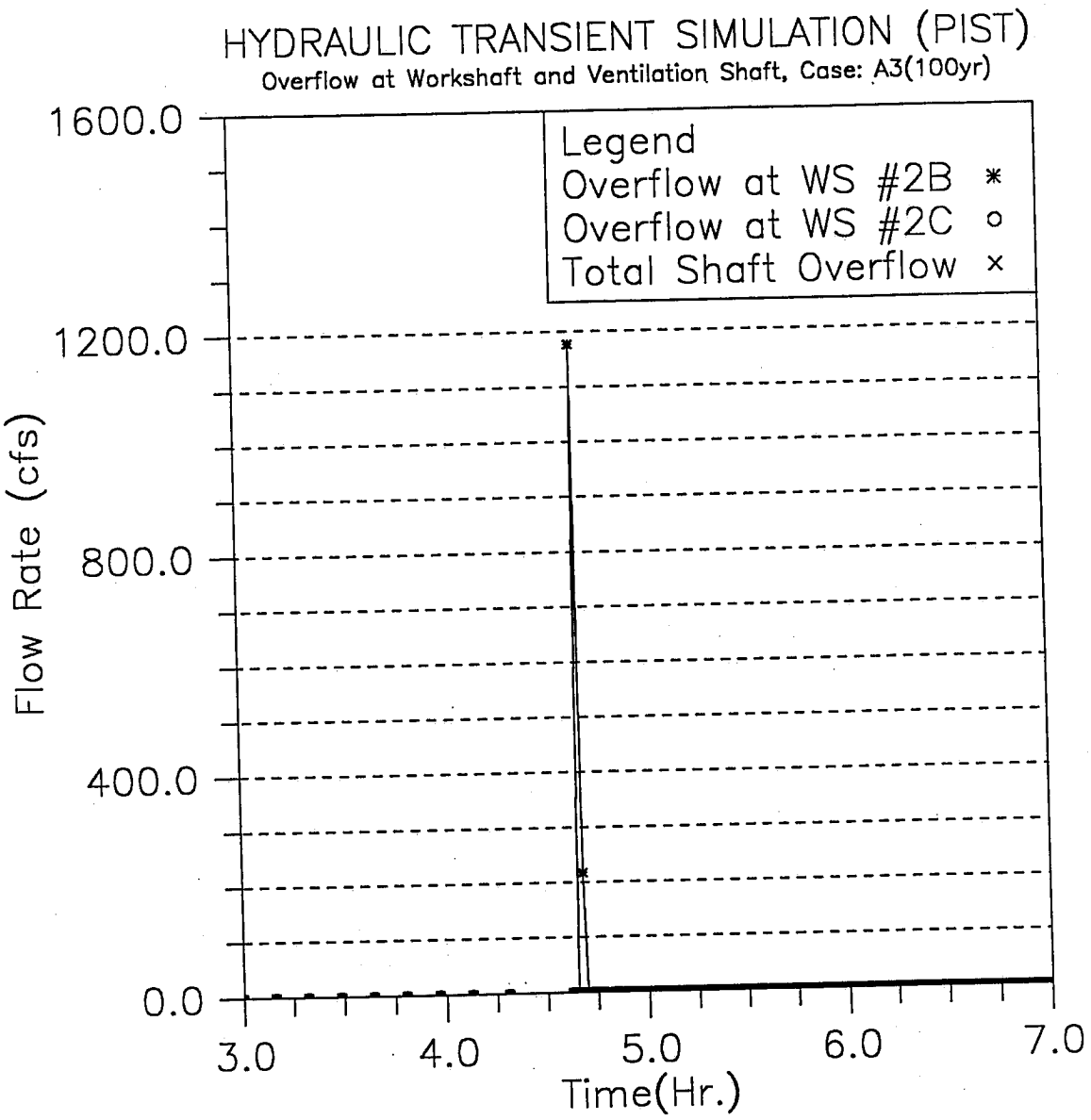

Fig. 3.17 Detailed time variation of the overflow at Workshafts #2B and #2C during the early surging period; modeling case: 100yr storm and wet tunnel (Case A3)

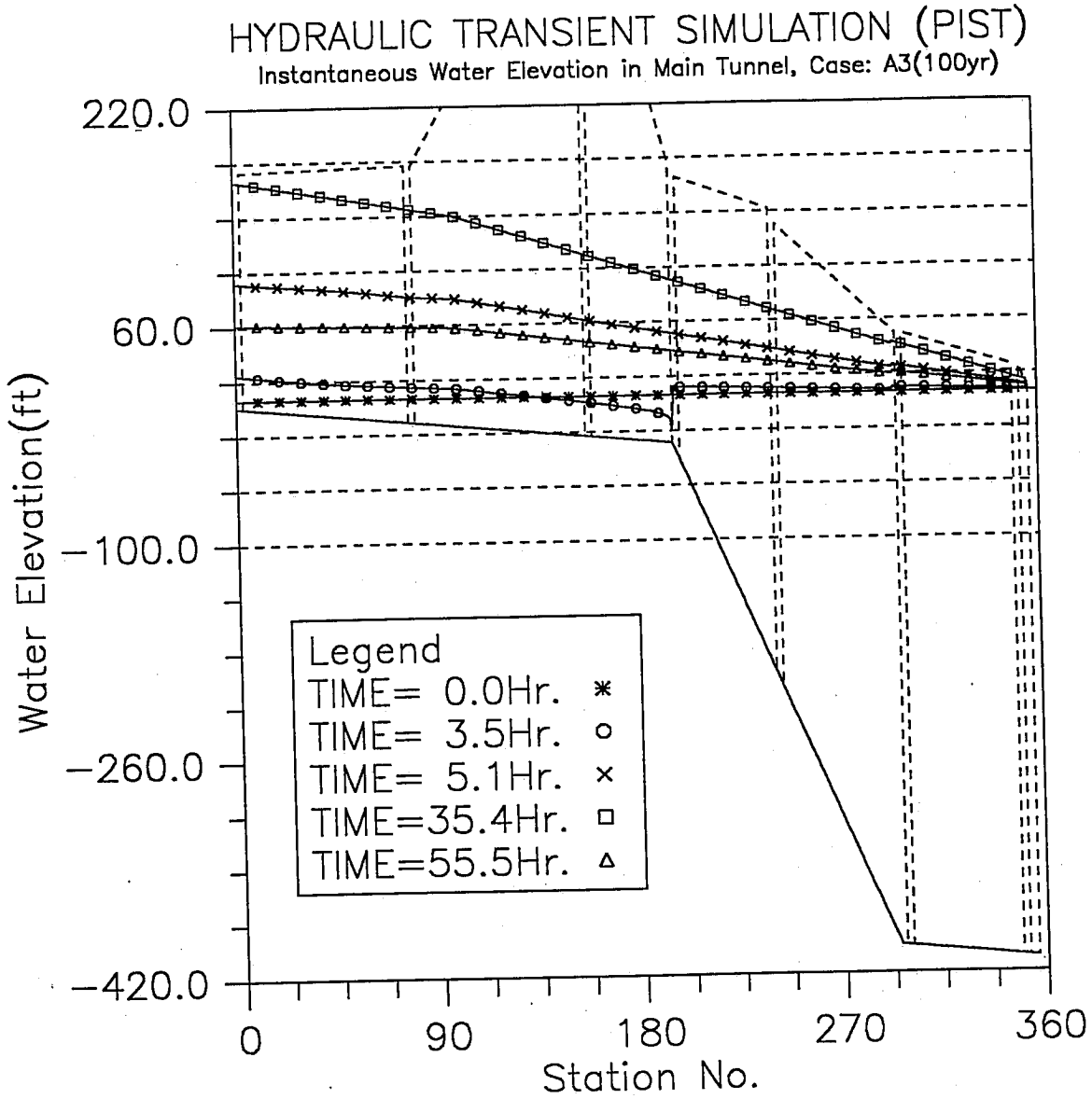

Fig. 3.18 Instantaneous hydraulic gradelines along the main tunnel; modeling case: 100yr storm and wet tunnel (Case A3)

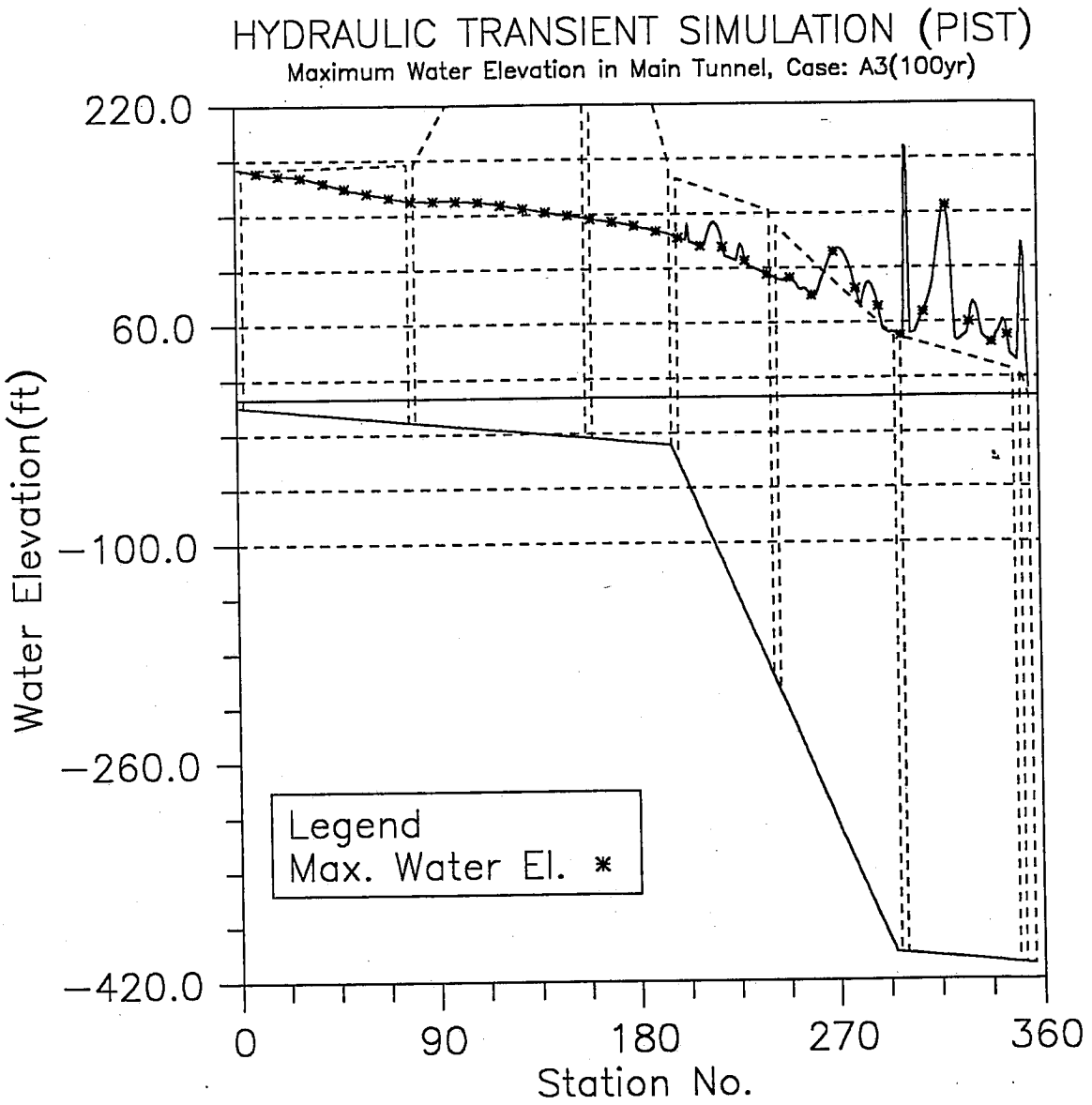

Fig. 3.19 The maximum water surface elevations along the main tunnel; modeling case: 100yr storm and wet tunnel (Case A3)

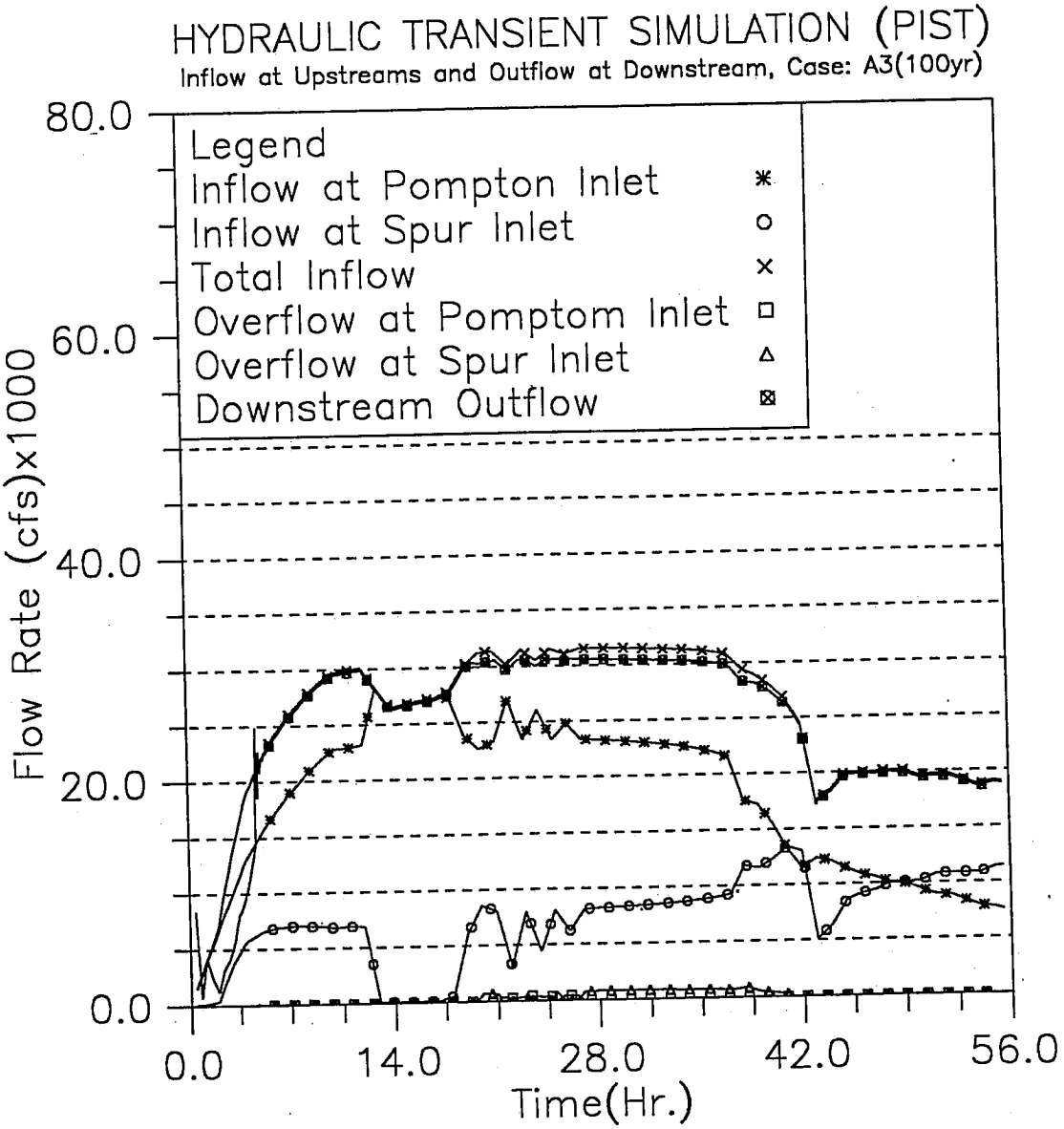

Fig. 3.20 Inflow and overflow hydrographs at Pompton and Spur inlets, and outflow hydrograph at the downstream; modeling case: 100yr storm and wet tunnel (Case A3)

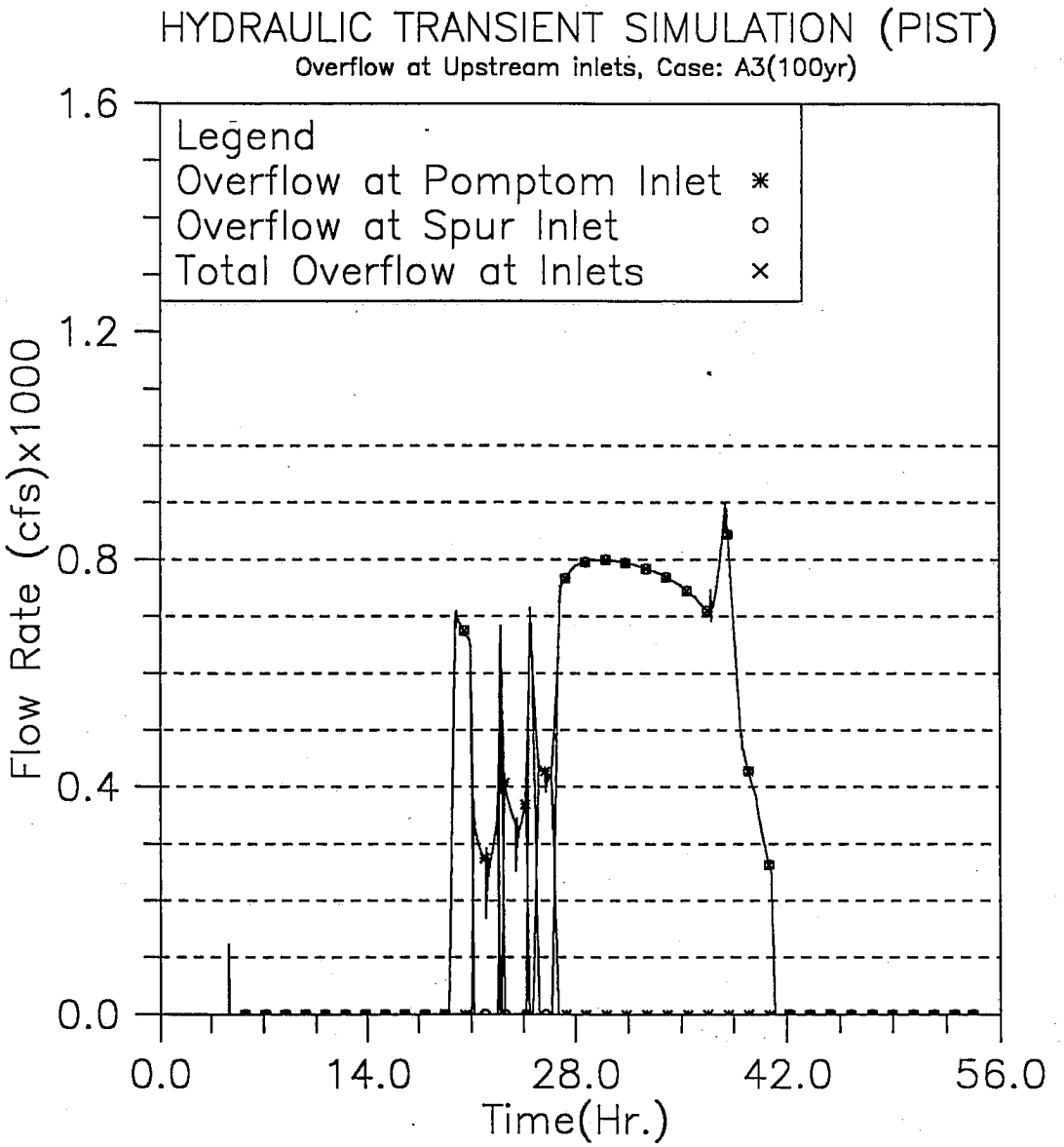

Fig. 3.21 Overflow hydrographs at Pompton and Spur inlets; modeling case: 100yr storm and wet tunnel (Case A3)

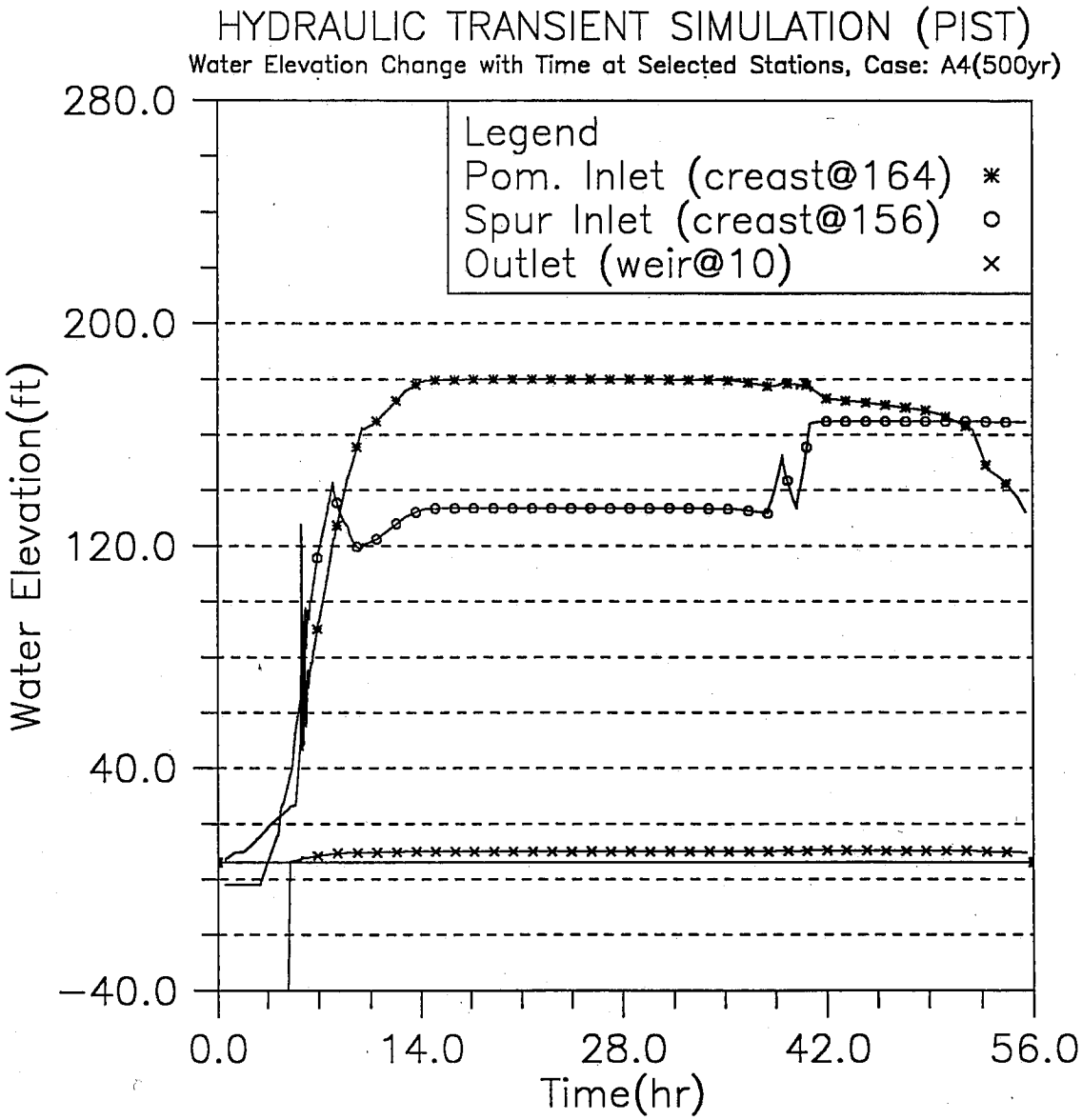

Fig. 3.22 Time variation of water surface elevations at Pompton inlet, Spur inlet and downstream end during the simulated time period; modeling case: 500yr storm and dry tunnel (Case A4)

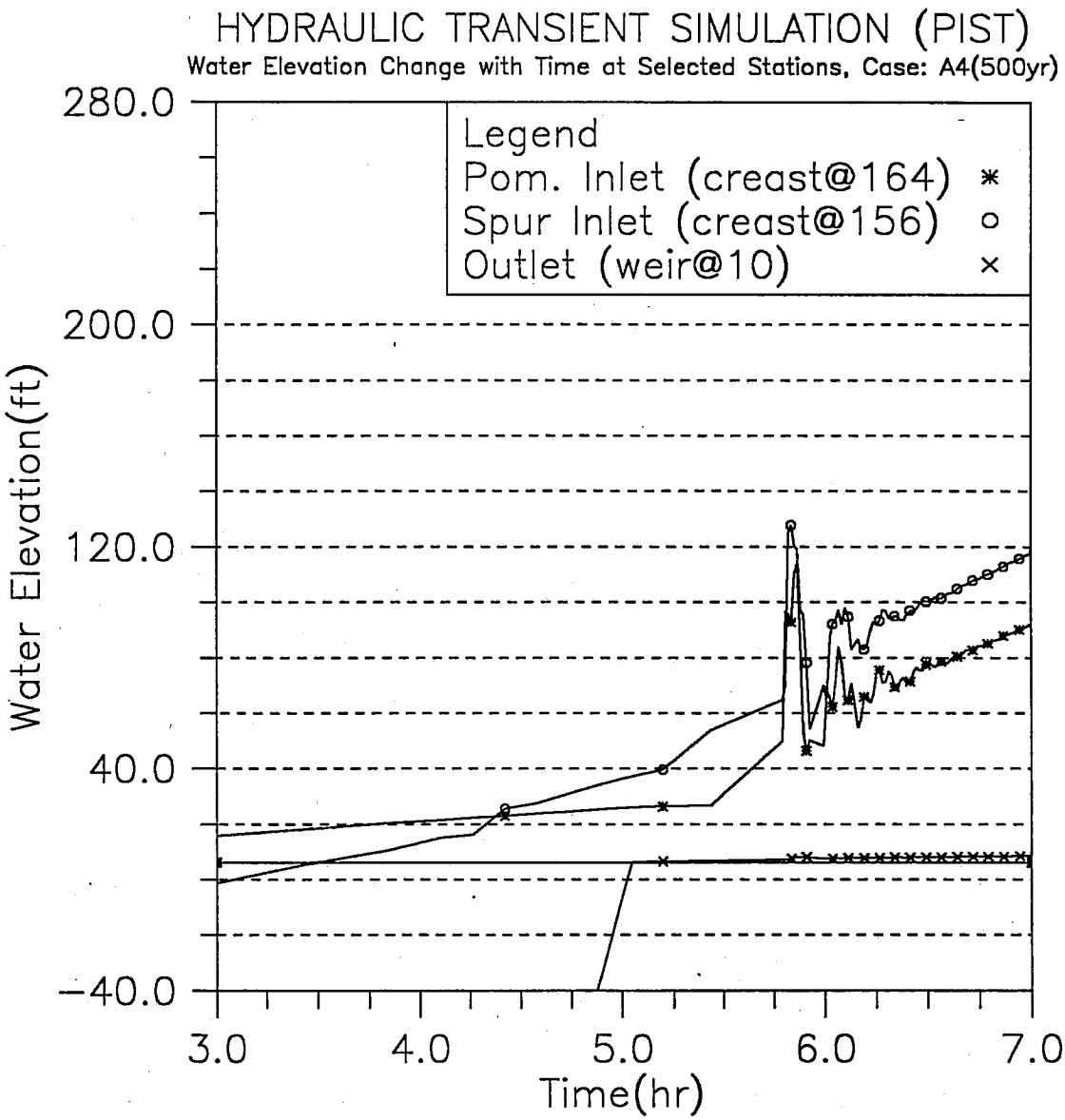

Fig. 3.23 Detailed time variation of water surface elevations at Pompton inlet, Spur inlet and downstream end during the early surging period; modeling case: 500yr storm and dry tunnel (Case A4)

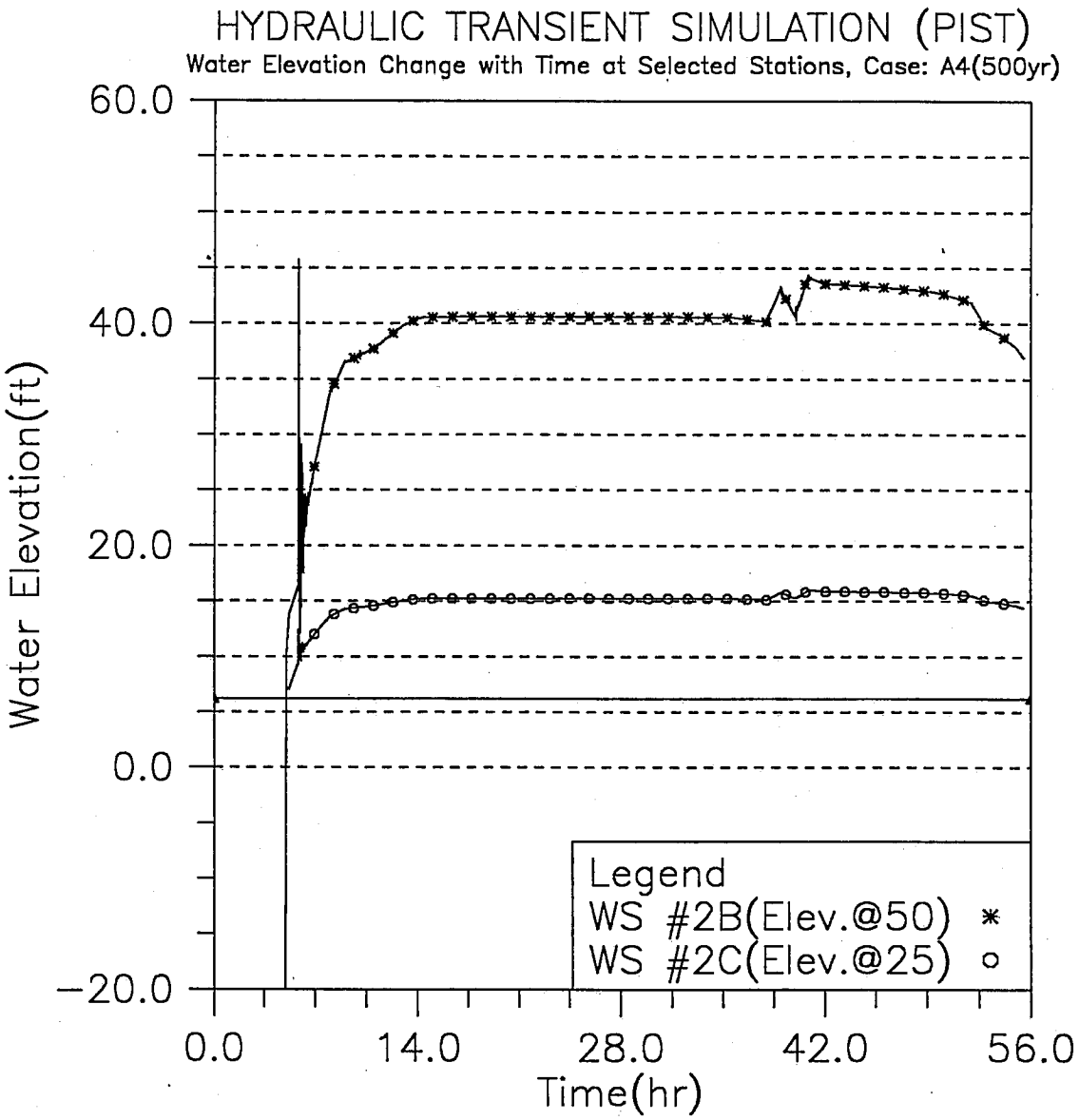

Fig. 3.24 Time variation of water surface elevations at Workshafts #2B and #2C during the simulated time period; modeling case: 500yr storm and dry tunnel (Case A4)

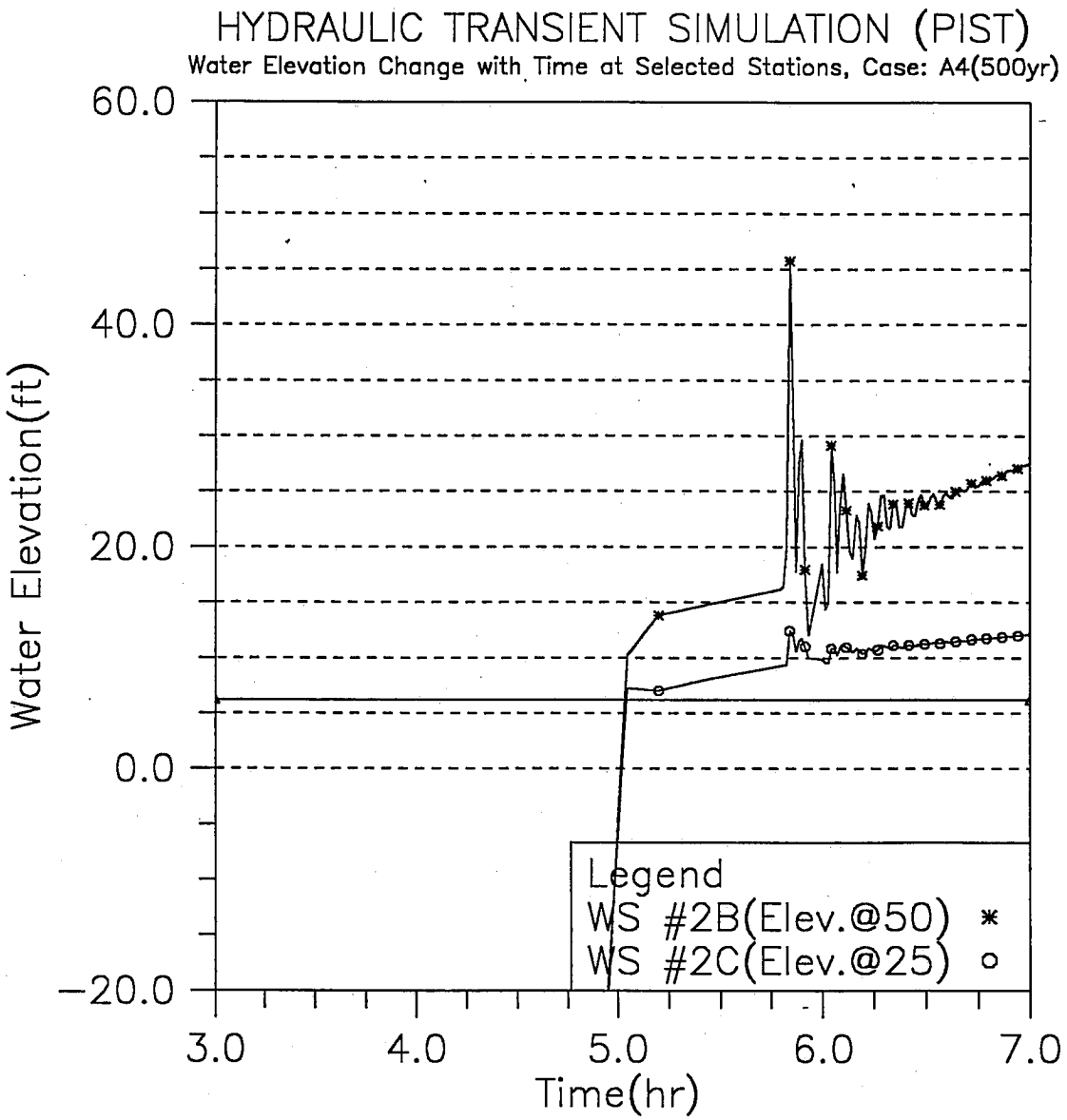

Fig. 3.25 Detailed time variation of water surface elevations at Workshafts #2B and #2C during the early surging period; modeling case: 500yr storm and dry tunnel (Case A4)

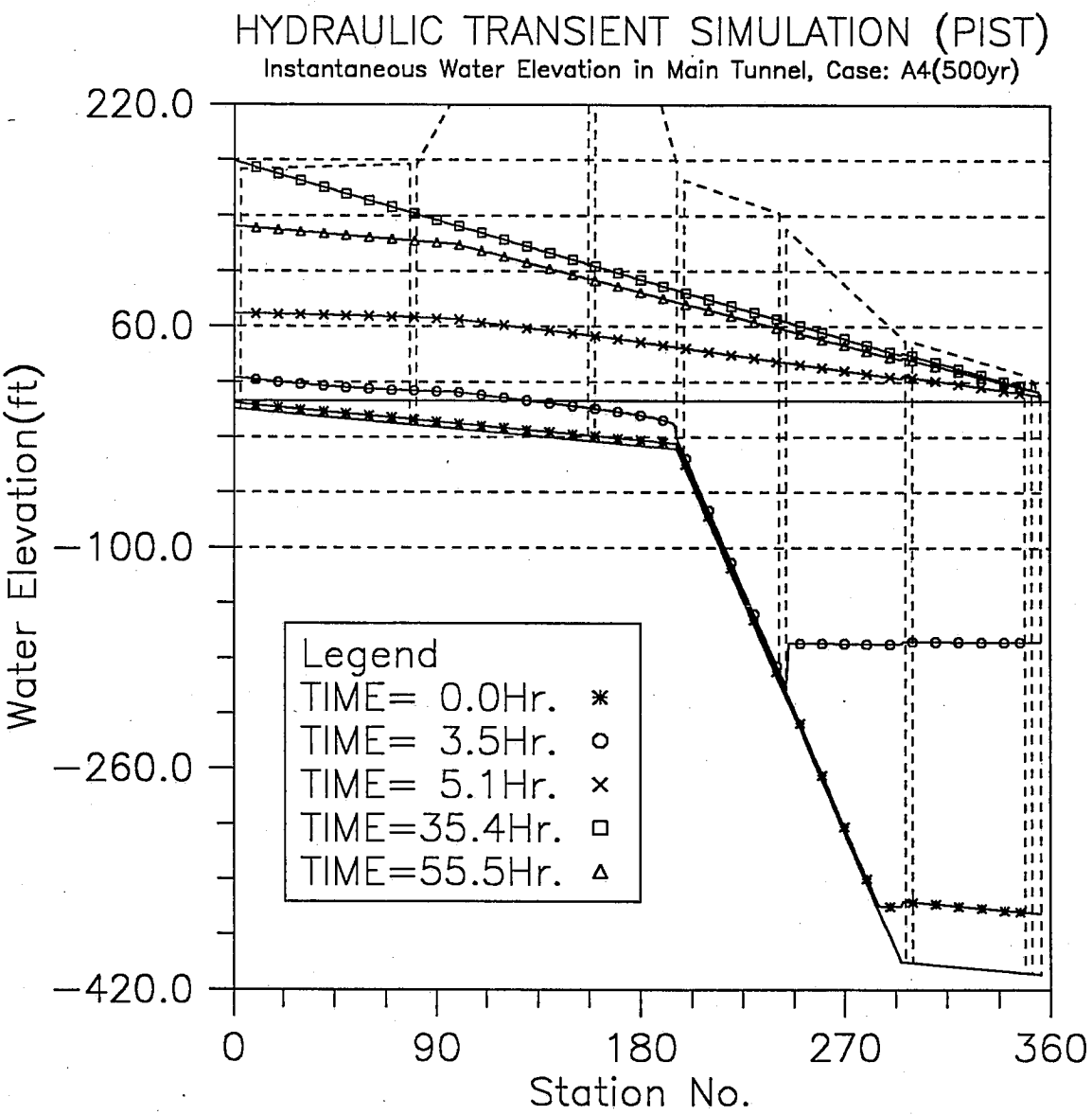

Fig. 3.26 Instantaneous hydraulic gradelines along the main tunnel; modeling case: 500yr storm and dry tunnel (Case A4)

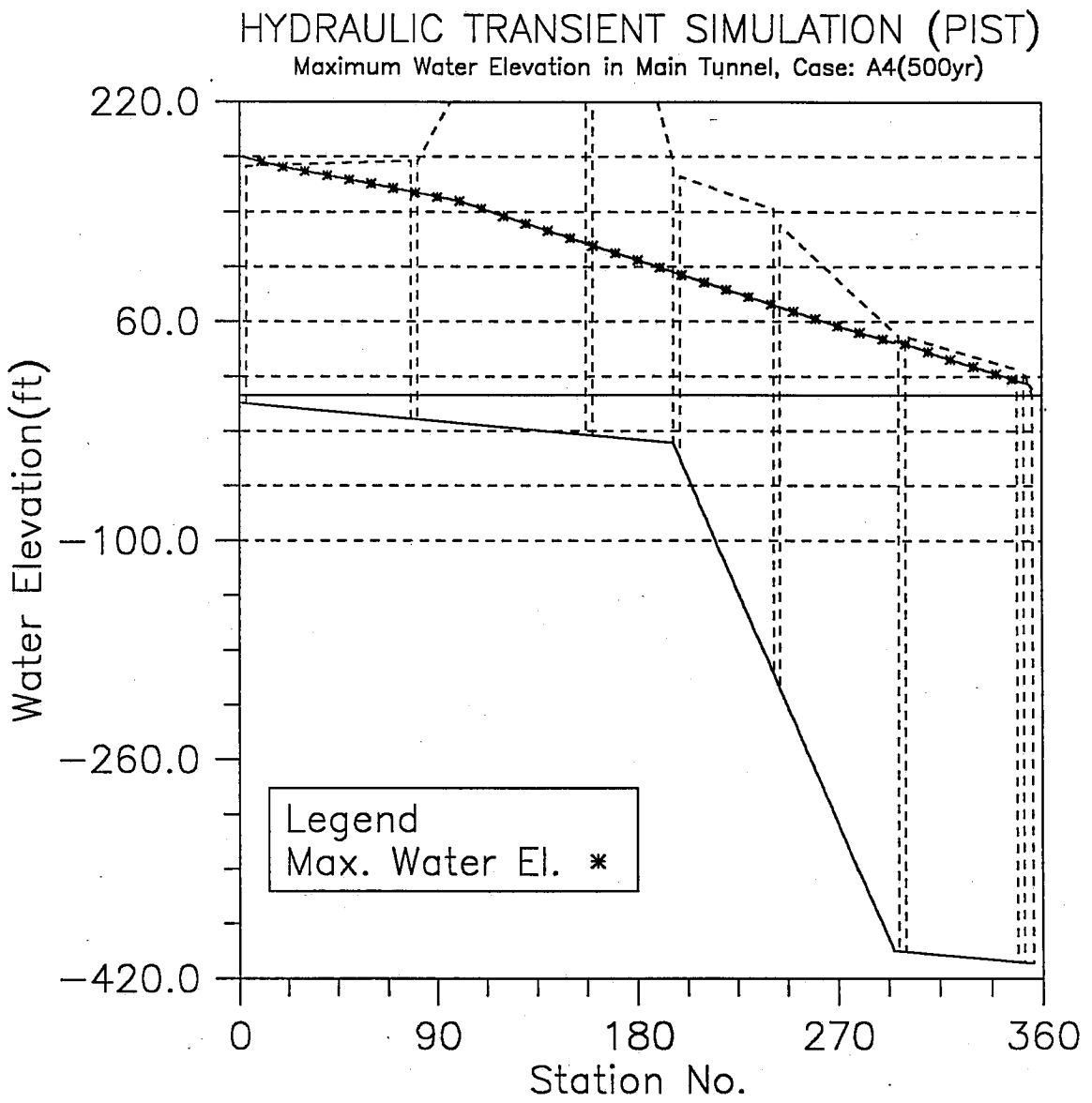

Fig. 3.27 The maximum water surface elevations along the main tunnel; modeling case: 500yr storm and dry tunnel (Case A4)

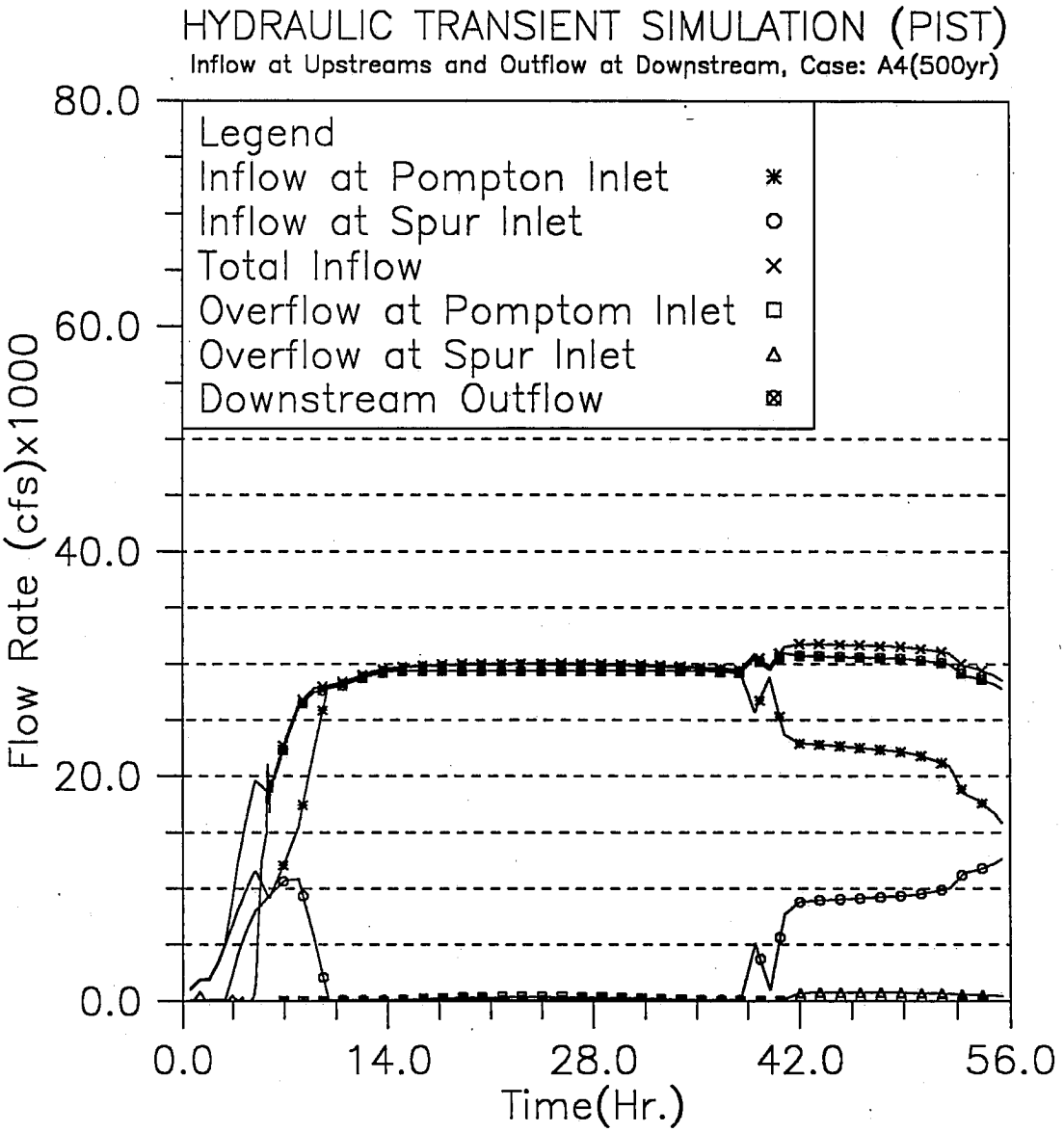

Fig. 3.28 Inflow and overflow hydrographs at Pompton and Spur inlets, and outflow hydrograph at the downstream; modeling case: 500yr storm and dry tunnel (Case A4)

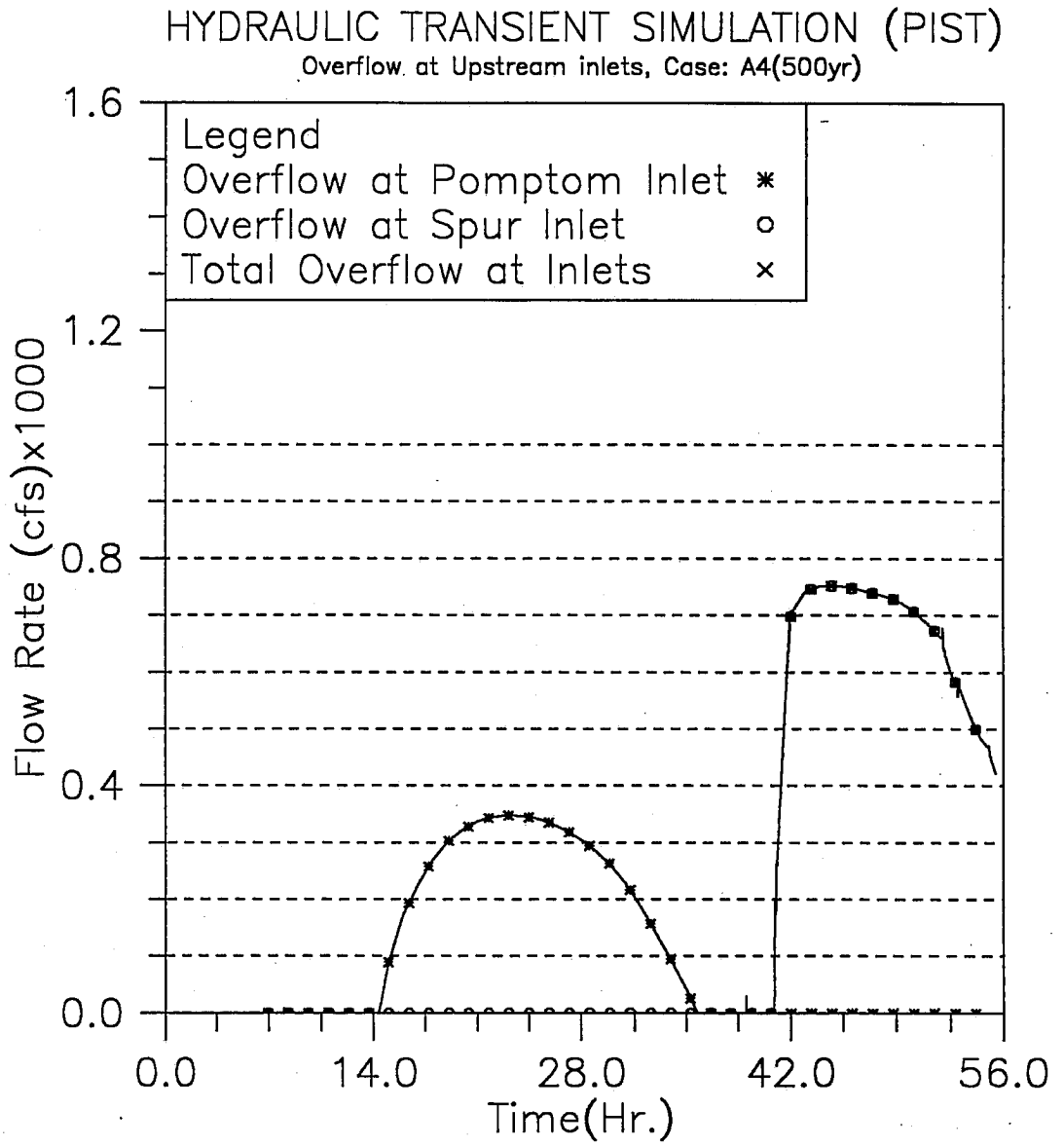

Fig. 3.29 Overflow hydrographs at Pompton and Spur inlets; modeling case: 500yr storm and dry tunnel (Case A4)

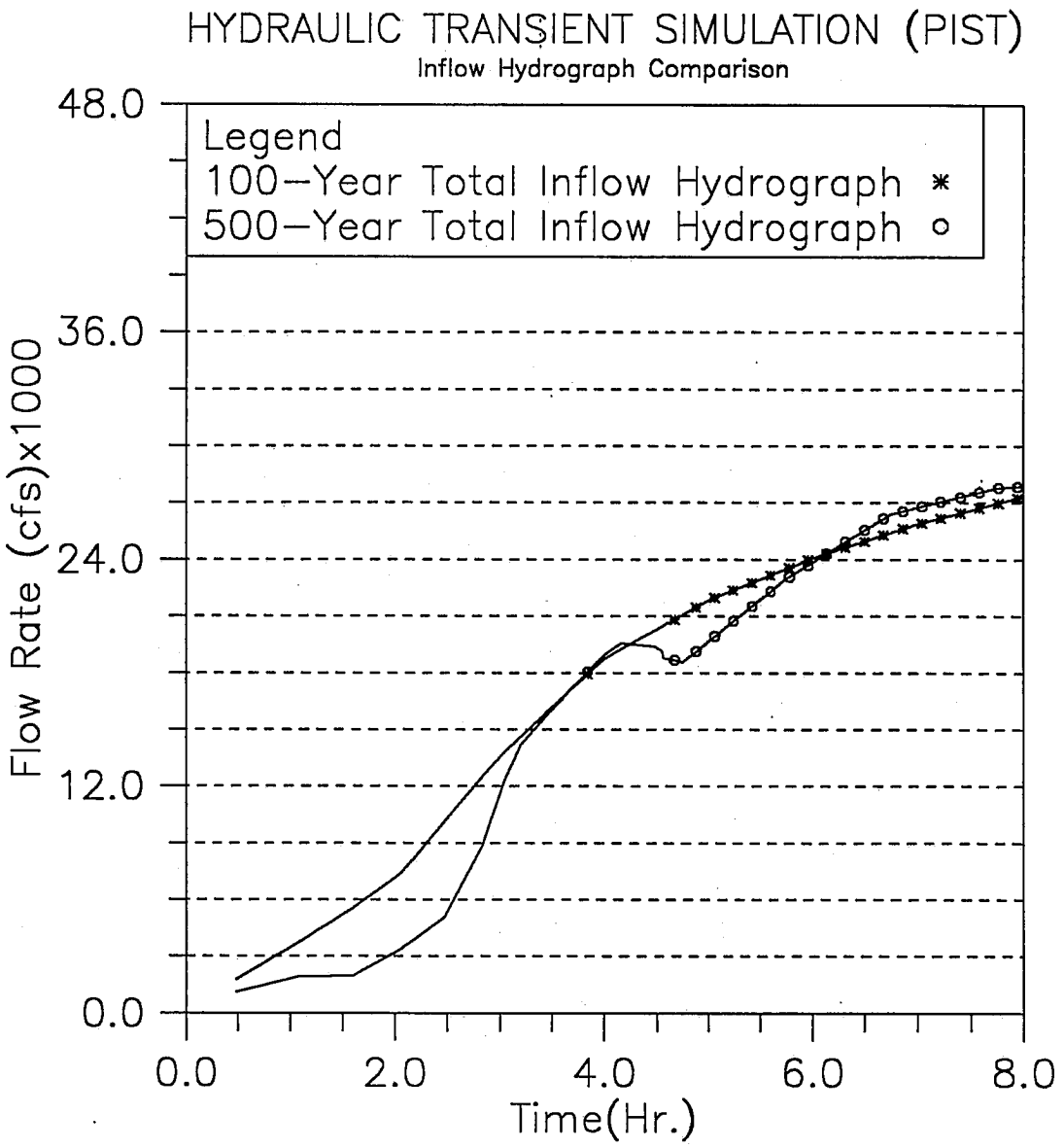

FIg. 3.30 The total inflow hydrographs of the 100–year and 500–year storms during the first 8 hours.

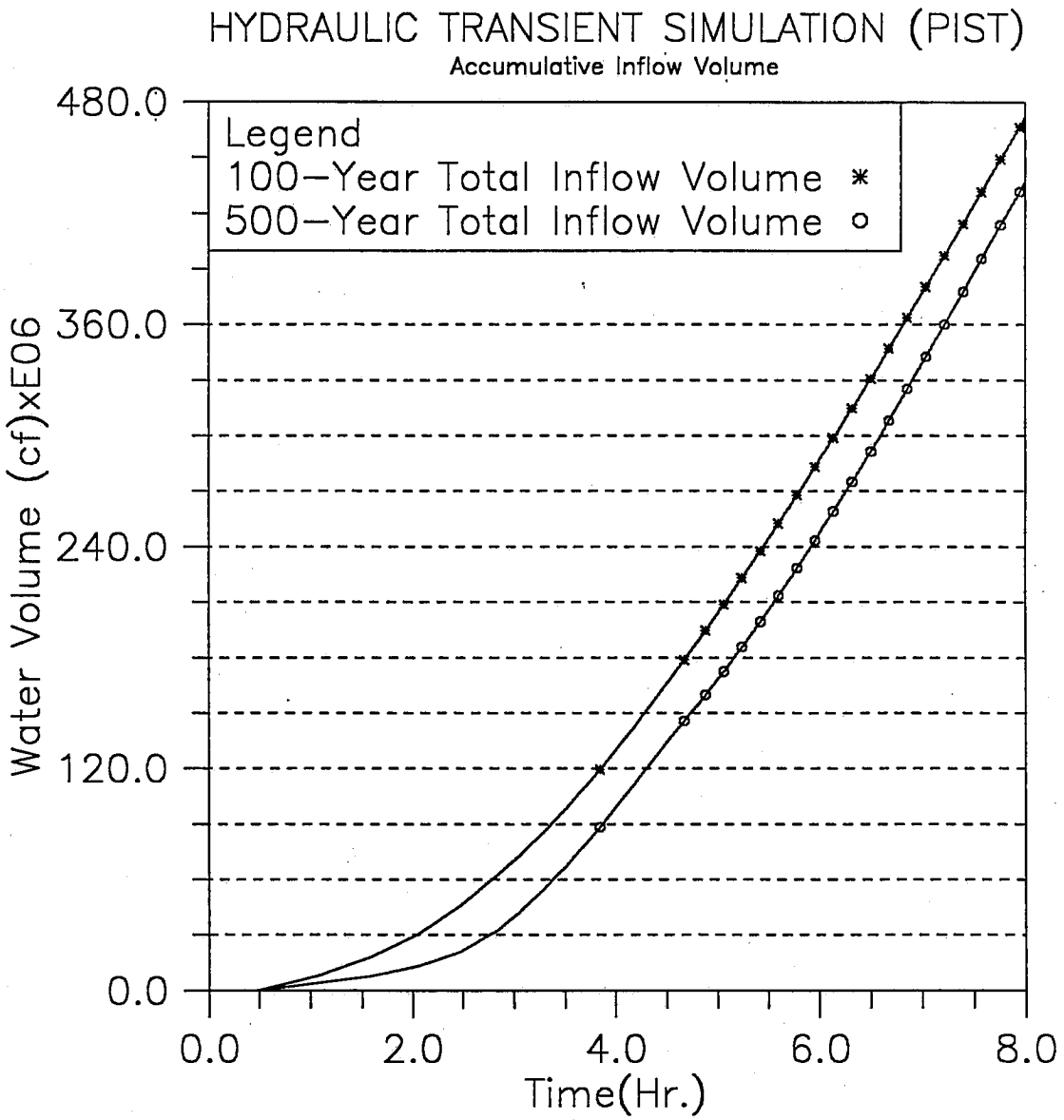

FIg. 3.31 The total inflow accumulative water volume of the 100–year and 500–year storms during the first 8 hours.

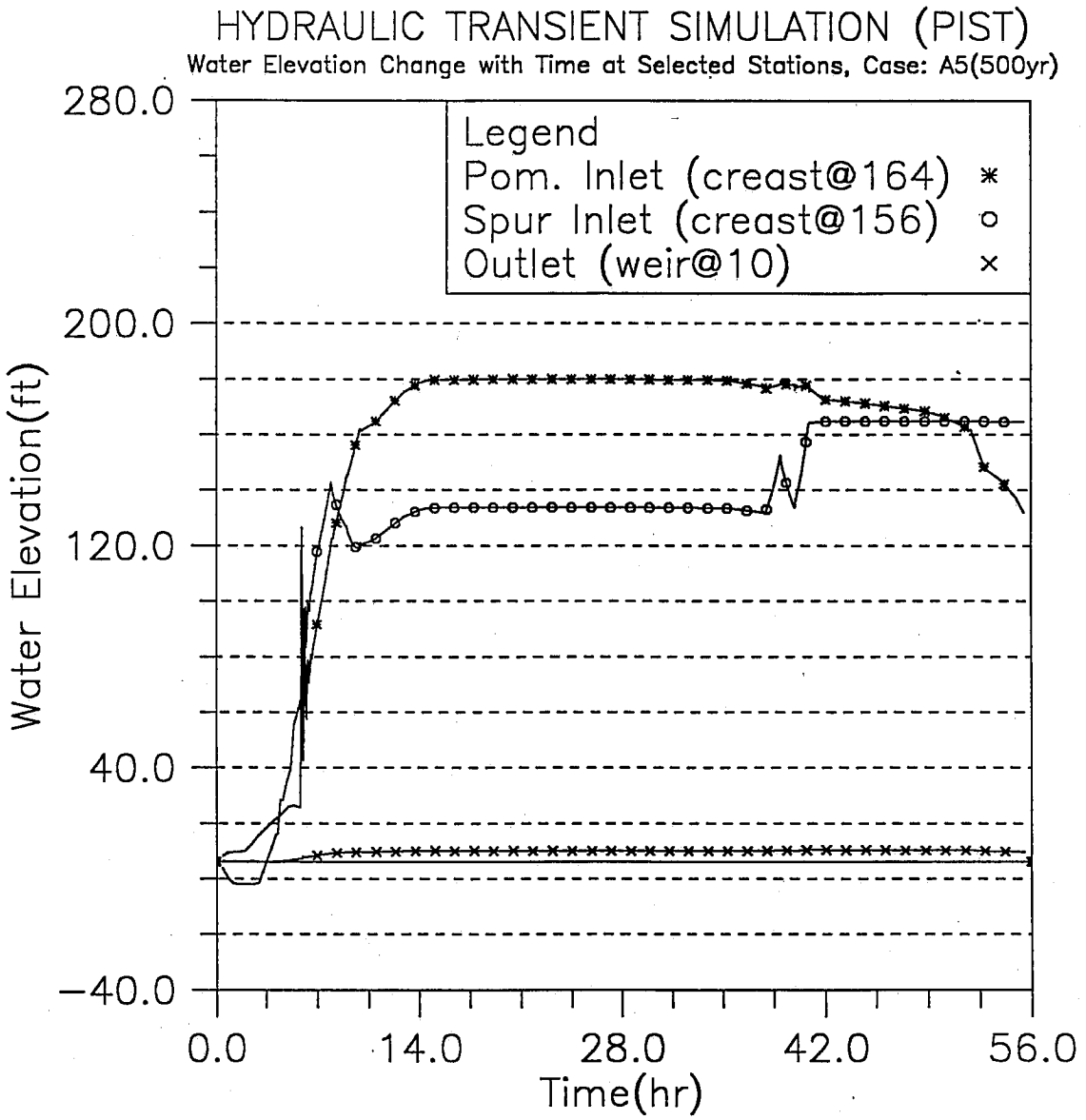

Fig. 3.32 Time variation of water surface elevations at Pompton inlet, Spur inlet and downstream end during the simulated time period; modeling case: 500yr storm and wet tunnel (Case A5)

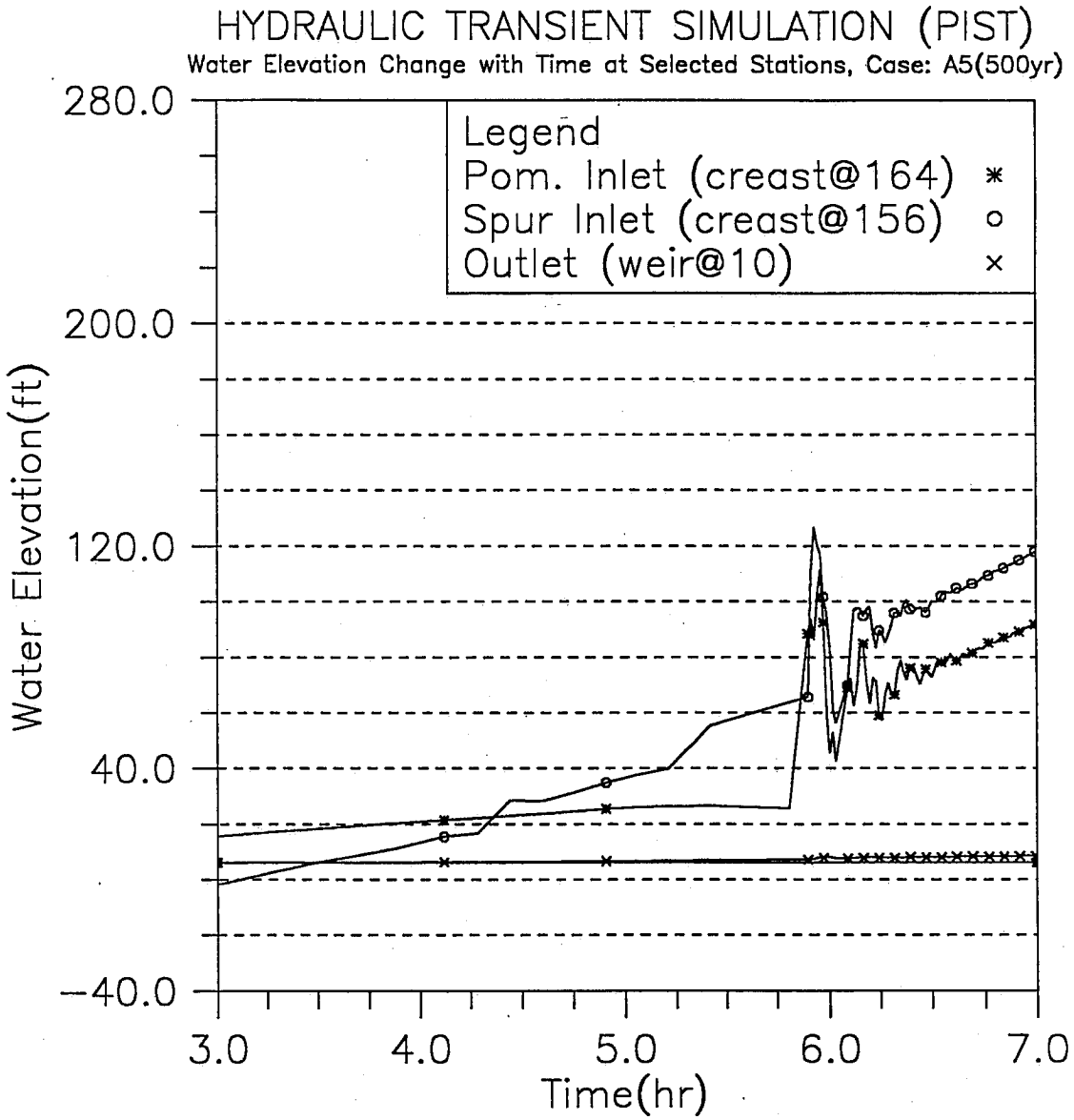

Fig. 3.33 Detailed time variation of water surface elevations at Pompton inlet, Spur inlet and downstream end during the early surging period; modeling case: 500yr storm and wet tunnel (Case A5)

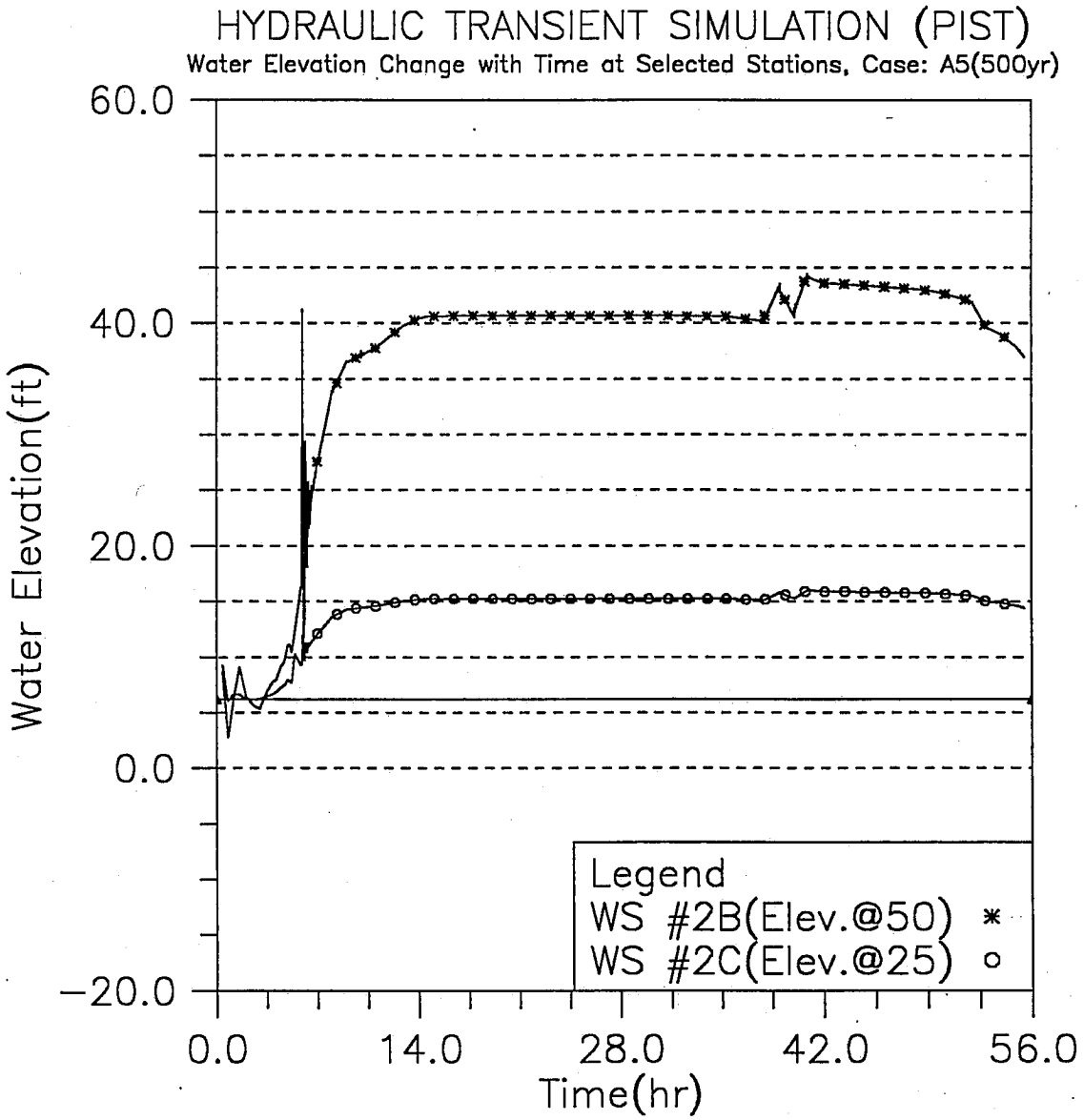

Fig. 3.34 Time variation of water surface elevations at Workshafts #2B and #2C during the simulated time period; modeling case: 500yr storm and wet tunnel (Case A5)

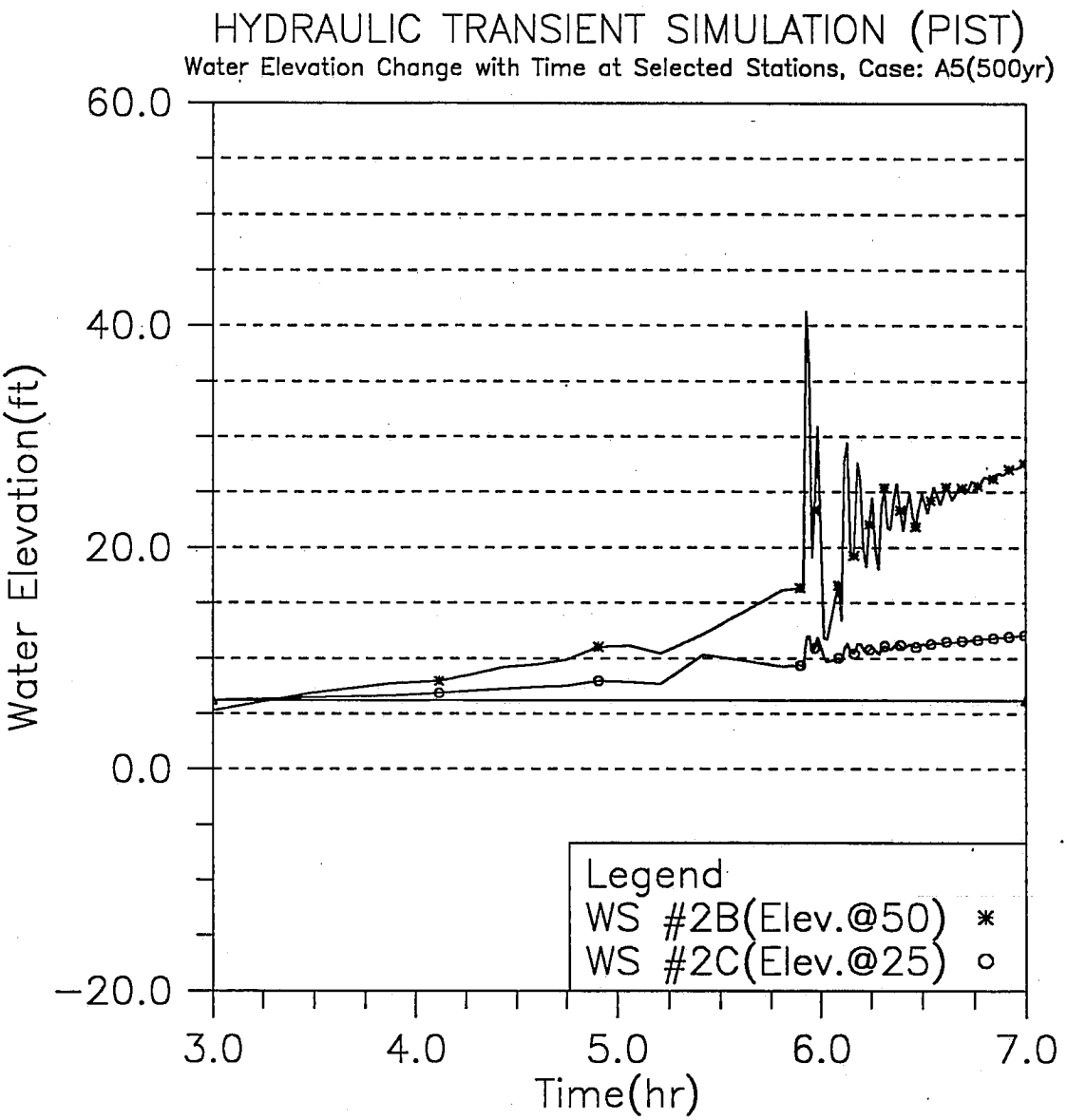

Fig. 3.35 Detailed time variation of water surface elevations at Workshafts #2B and #2C during the early surging period; modeling case: 500yr storm and wet tunnel (Case A5)

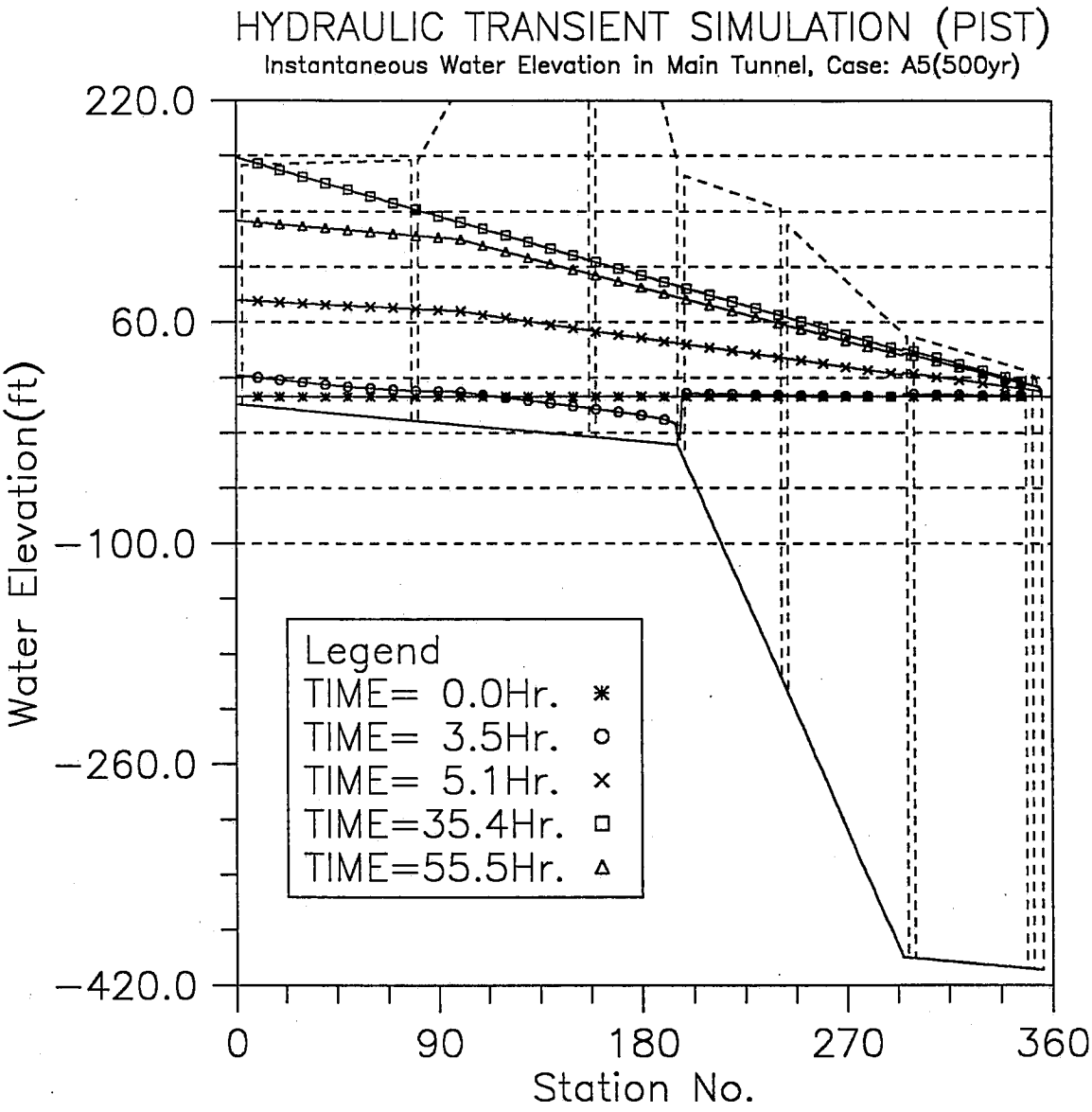

Fig. 3.36 Instantaneous hydraulic gradelines along the main tunnel; modeling case: 500yr storm and wet tunnel (Case A5)

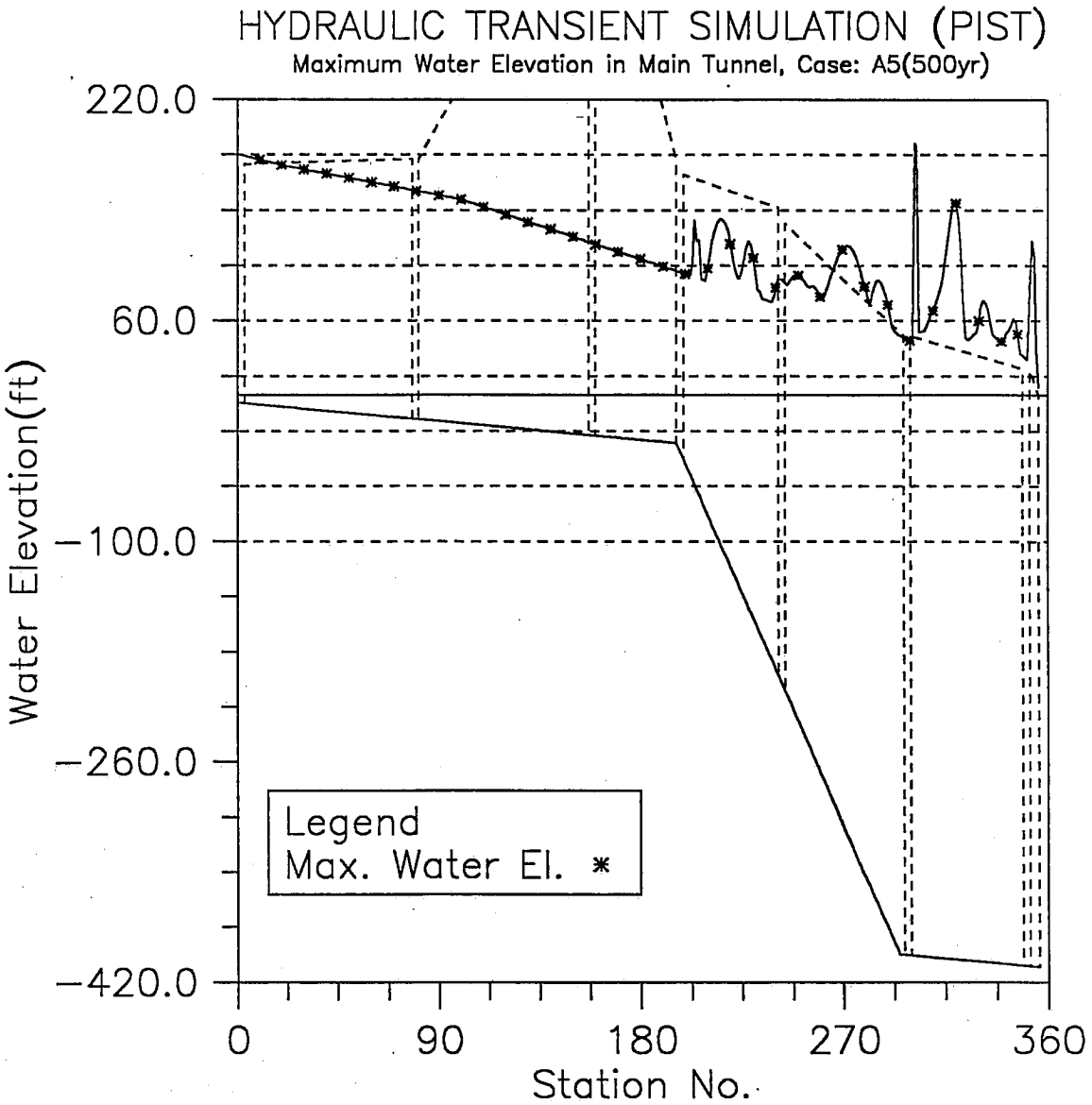

Fig. 3.37 The maximum water surface elevations along the main tunnel; modeling case: 500yr storm and wet tunnel (Case A5)

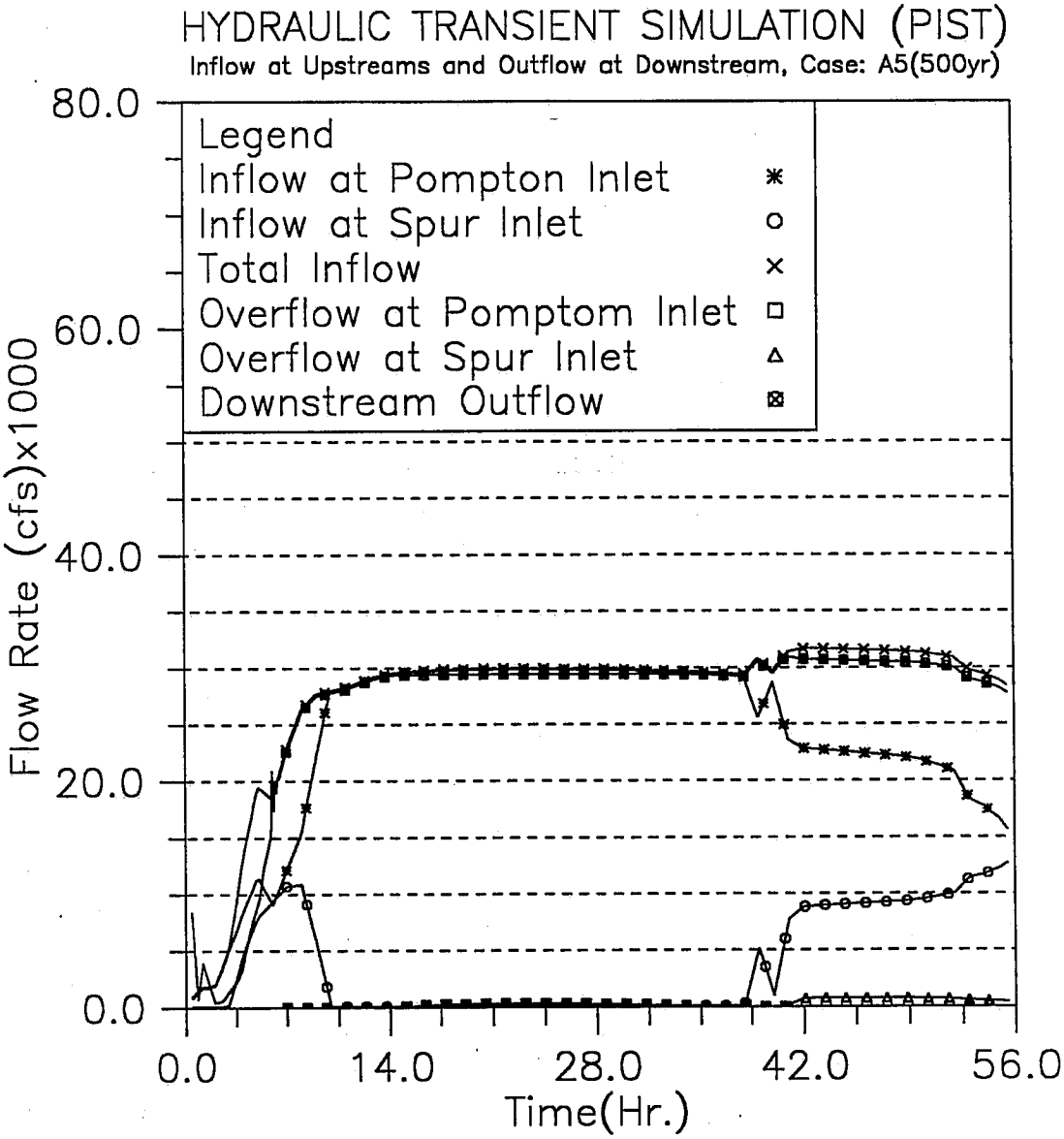

Fig. 3.38 Inflow and overflow hydrographs at Pompton and Spur inlets, and outflow hydrograph at the downstream; modeling case: 500yr storm and wet tunnel (Case A5)

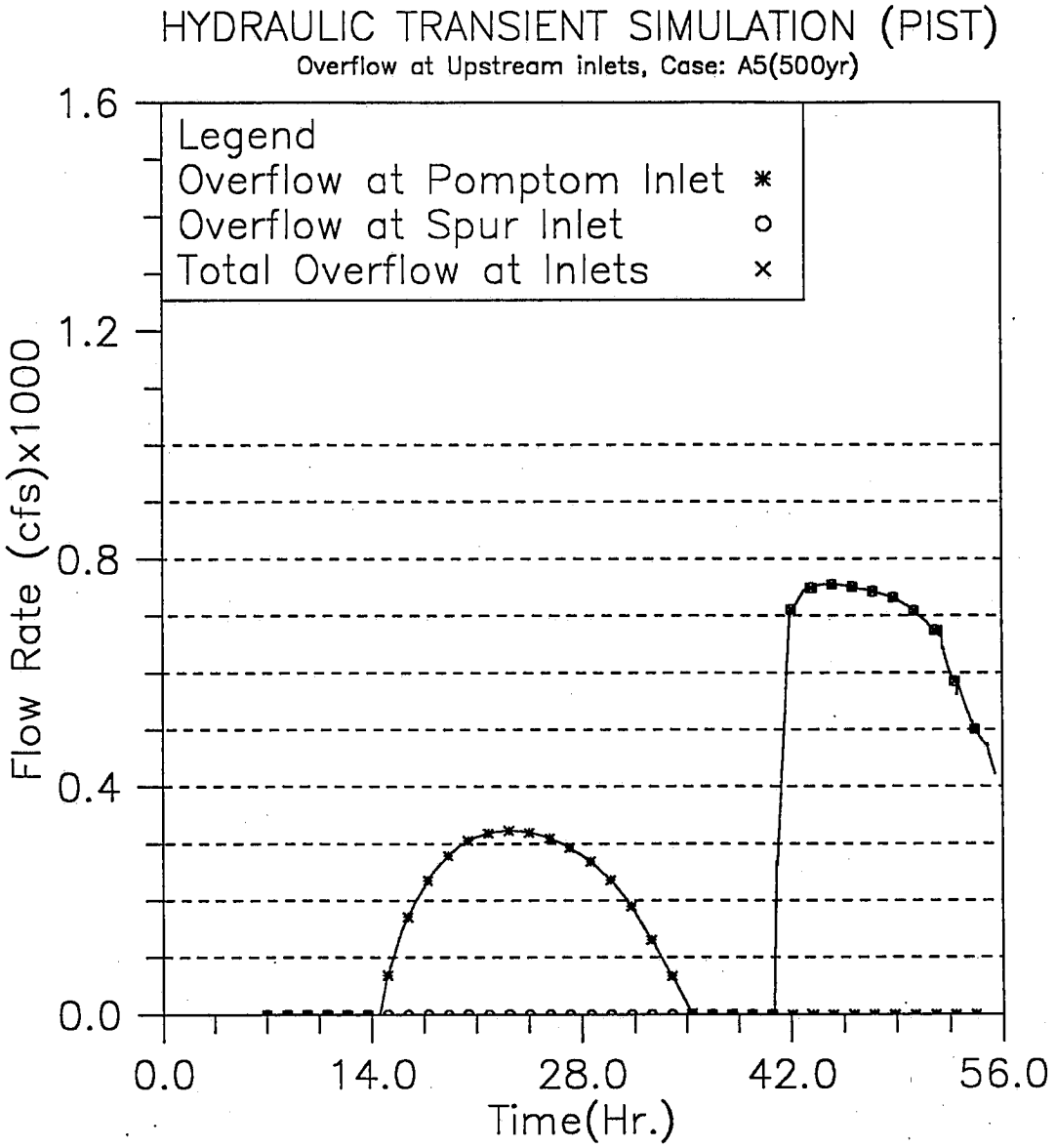

Fig. 3.39 Overflow hydrographs at Pompton and Spur inlets; modeling case: 500yr storm and wet tunnel (Case A5)

Appendix II

The Results of 7 Testing Simulation Runs

As stated in the main part of this report, before the final 5 simulation runs described before were done, 7 testing simulation runs with different input conditions had been conducted. The main parameters of the 7 runs are listed as follows.

II–1. Case Configuration

CASE1: 2yr storm event;
dry tunnel;
Pompton Inlet water level elevation: 164 ft;
Spur Inlet water level elevation: 156 ft;
Gate–control outlet;
Manning Coef. in Pompton Branch and main tunnel: 0.014
Manning Coef. in Spur Branch: 0.016
Sea level elevation: 6.2 ft.

CASE2: 100yr storm event;
dry tunnel;
Pompton Inlet water level elevation: 164 ft;
Spur Inlet water level elevation: 156 ft;
Gate–control outlet;
Manning Coef. in Pompton Branch and main tunnel: 0.014
Manning Coef. in Spur Branch: 0.016
Sea level elevation: 0.0 ft.

CASE3: 500yr storm event;
dry tunnel;
Pompton Inlet water level elevation: 164 ft;
Spur Inlet water level elevation: 156 ft;
Gate–control outlet;
Manning Coef. in Pompton Branch and main tunnel: 0.014
Manning Coef. in Spur Branch: 0.016
Sea level elevation: 0.0 ft.

CASE4: 500yr storm event;
dry tunnel;
Pompton Inlet water level elevation: 164 ft;
Spur Inlet water level elevation: 156 ft;
Gate–control outlet;
Manning Coef. in Pompton Branch and main tunnel: 0.014
Manning Coef. in Spur Branch: 0.016

Sea level elevation: 6.2 ft.

CASE5: 100yr storm event;
dry tunnel;
Pompton Inlet water level elevation: 186 ft;
Spur Inlet water level elevation: 175 ft;
Gate–control outlet;
Manning Coef. in Pompton Branch and main tunnel: 0.014
Manning Coef. in Spur Branch: 0.016
Sea level elevation: 0.0 ft.

CASE6: 500yr storm event;
dry tunnel;
Pompton Inlet water level elevation: 186 ft;
Spur Inlet water level elevation: 175 ft;
Gate–control outlet;
Manning Coef. in Pompton Branch and main tunnel: 0.014
Manning Coef. in Spur Branch: 0.016
Sea level elevation: 0.0 ft.

CASE7: 500yr storm event;
dry tunnel;
Pompton Inlet water level elevation: 186 ft;
Spur Inlet water level elevation: 175 ft;
Gate–control outlet;
Manning Coef. in Pompton Branch and main tunnel: 0.014
Manning Coef. in Spur Branch: 0.016
Sea level elevation: 6.2 ft.

II–2. Highlight of The Modeling Results

Case1 Figs. II–1 to II–3 show the modeling results of this case. The results are almost the same as those in Case A1 of the final simulation runs since the transient process with the 2yr storm event is little affected by their difference.

Case2 Figs. II–4 to II–7 show the modeling results of this case. Since the tunnel friction coefficient in this case is larger than that of the final simulation runs, the overflow in this case at both inlets is increased. However there is no overflow at workshaft due to the lower sea level.

Case3 Figs. II–8 to II–11 show the modeling results of this case. The results are similar to Case2.

Case4 Figs. II–12 to II–16 show the modeling results of this case. A large amount of overflow at both inlets and Workshafts #2B and #2C can be found in this case due to the increase of the downstream sea level. Compared this case with Case A4 of the final simulation runs, it is found that the larger tunnel friction coefficient may cause a serious hydraulic transient problem.

Case5 Figs. II–17 to II–20 show the modeling results of this case. The results indicate that higher upstream water elevation results in a significant decrease of the overflow at both upstream inlets.

Case6 Figs. II–21 to II–24 show the modeling results of this case. Similar results can be found in this case.

Case7 Figs. II–25 to II–29 show the modeling results of this case. Like the above two cases, the overflow at both inlets is reduced. In this case, however, the overflow at the two workshaft is increased because the hydraulic gradeline rises due to the increase of upstream water elevation.

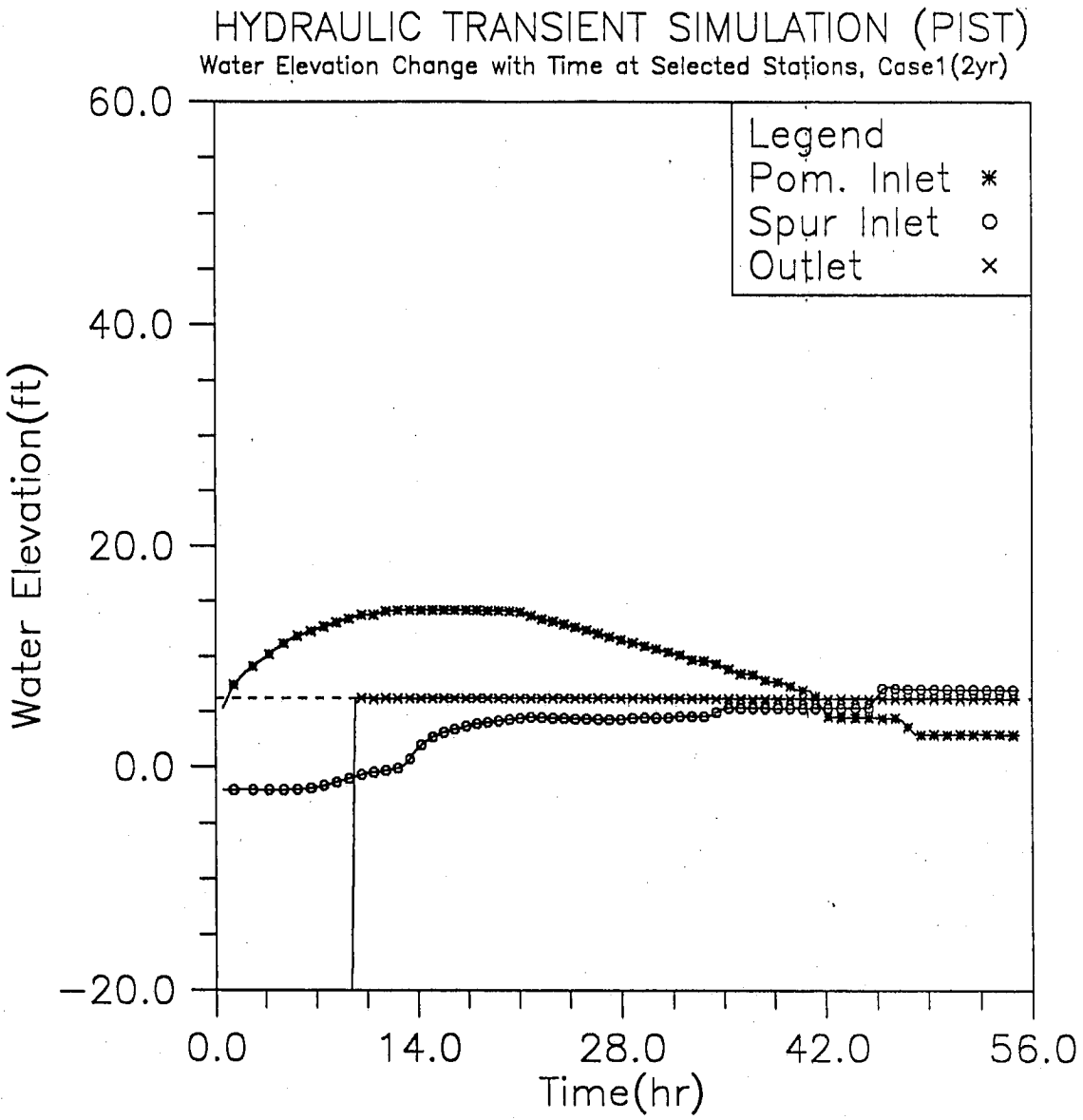

Fig. II–1 Time variation of water elevation at Pompton inlet, Spur inlet and downstream end; modeling case: 2yr storm and 0.0 sea level (testing run: Case1)

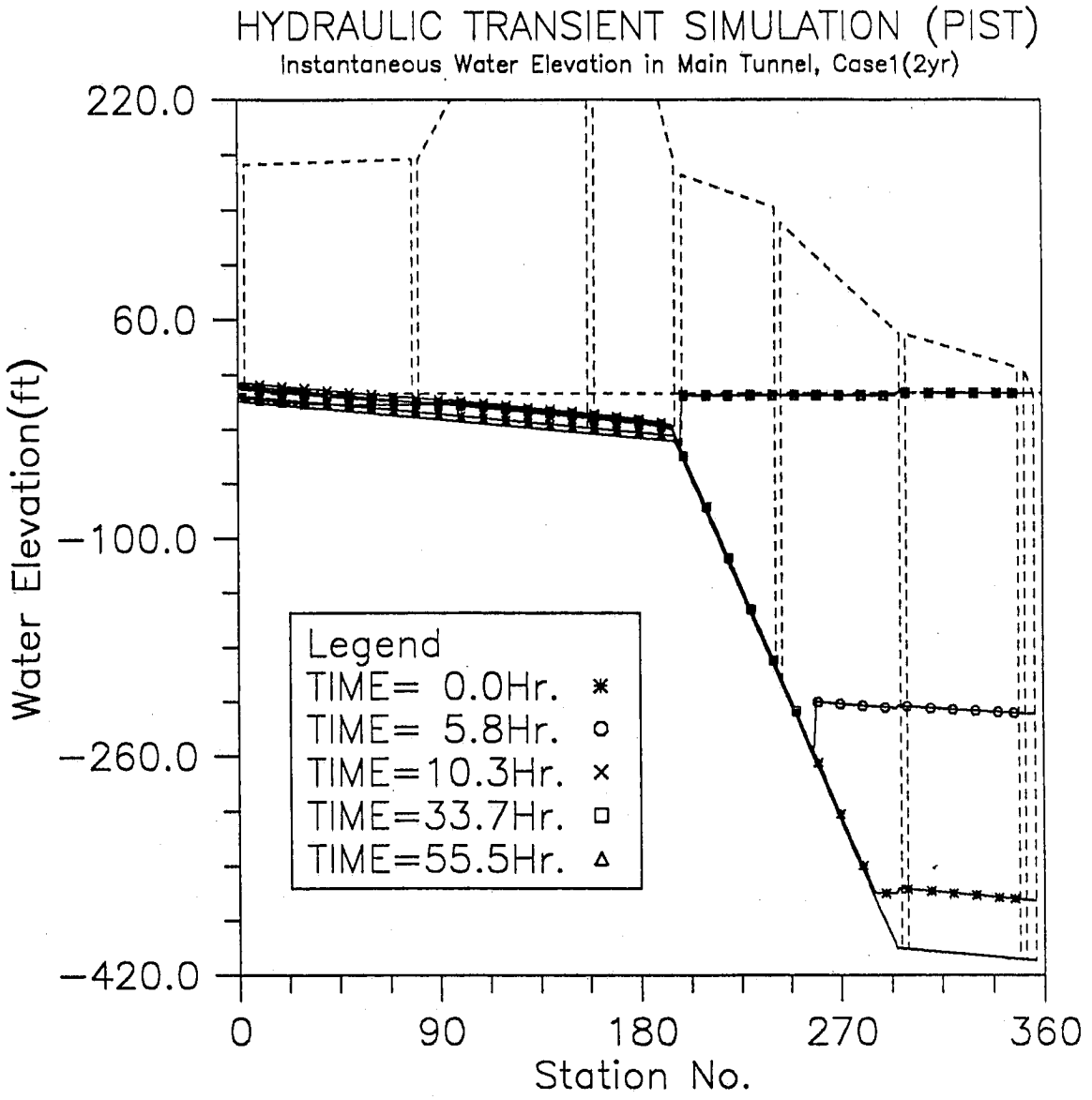

Fig. II–2 Instantaneous hydraulic gradelines along the main tunnel; modeling case: 2yr storm and 0.0 sea level (testing run: Case1)

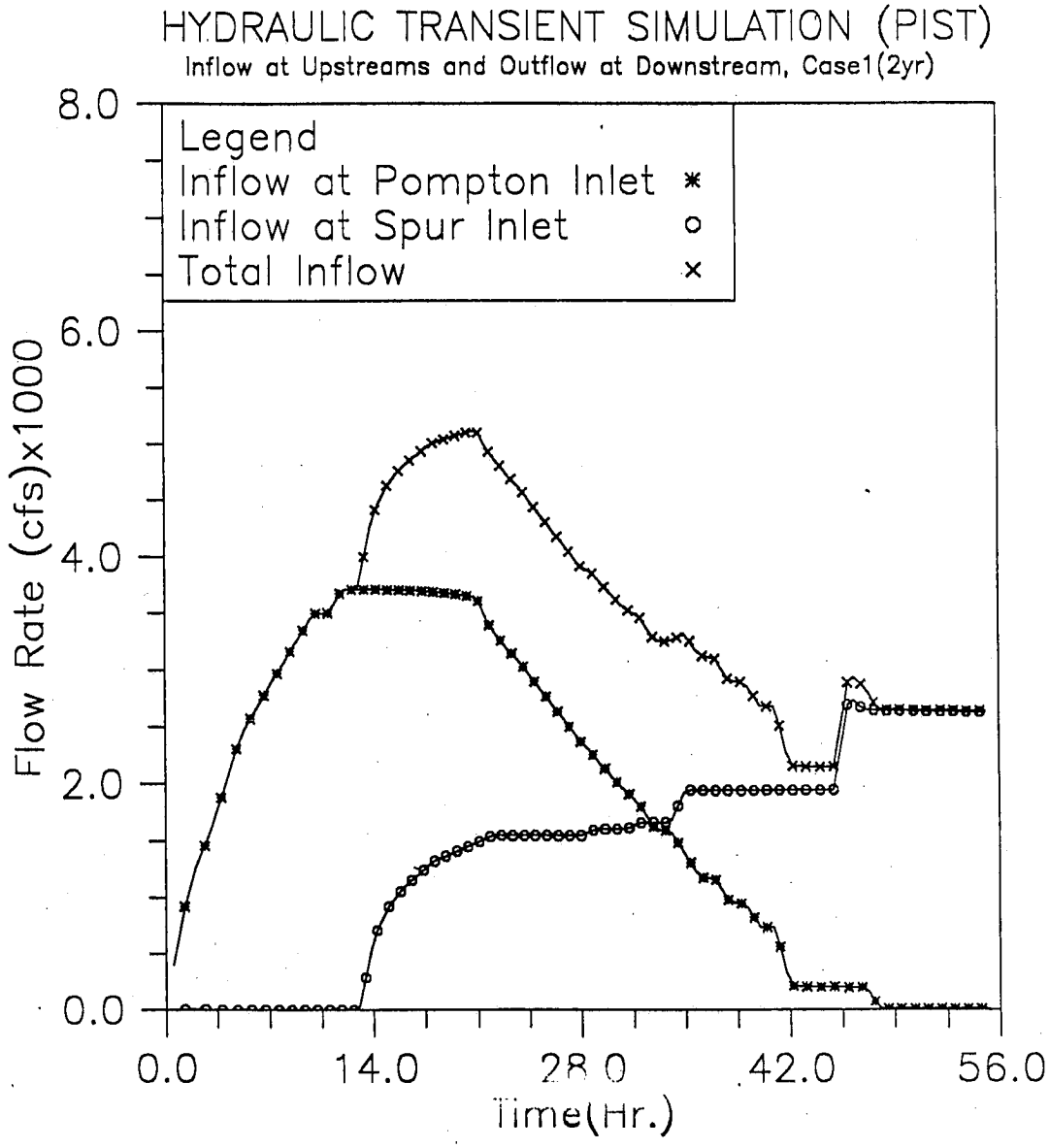

Fig. II–3 Inflow hydrograph of 2 year storm event (testing run: Case1)

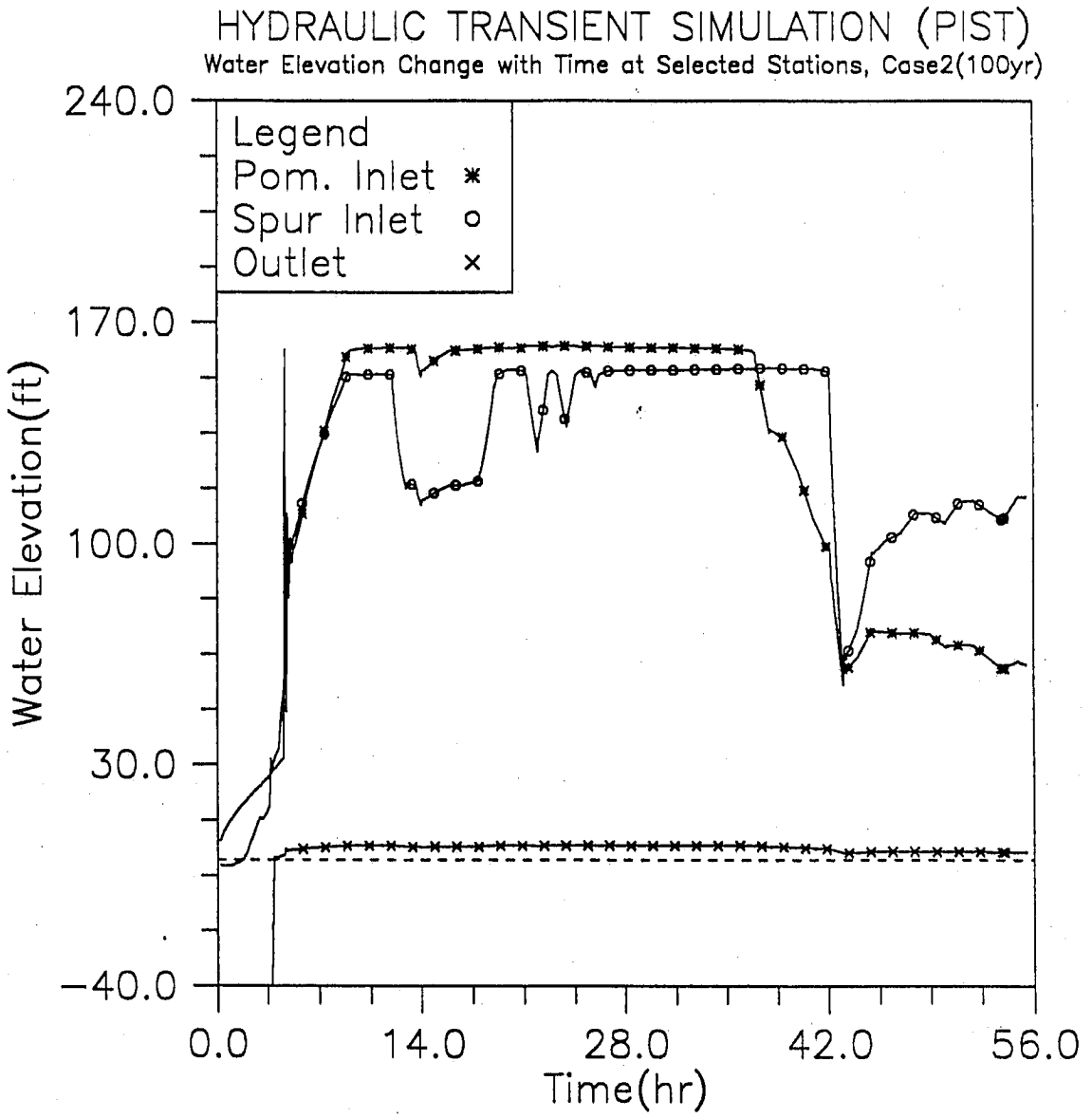

Fig. II–4 Time variation of water elevation at Pompton inlet, Spur inlet and downstream end during the simulated time period; modeling case: 100yr storm and 0.0 sea level (testing run: Case2)

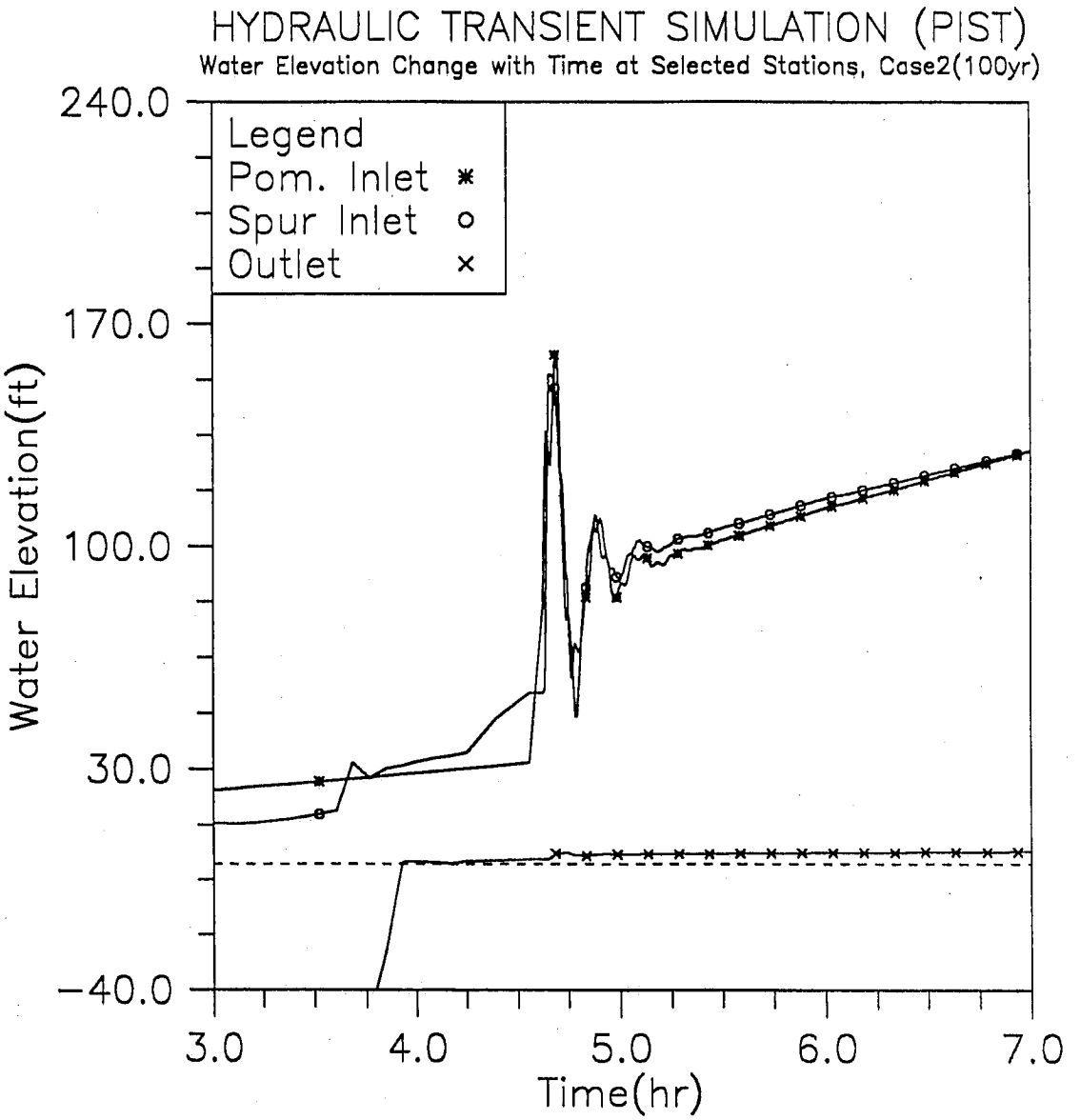

Fig. II–5 More detailed time variation of water elevation at Pompton inlet, Spur inlet and downstream end during the early surging period; modeling case: 100yr storm and 0.0 sea level (testing run: Case2)

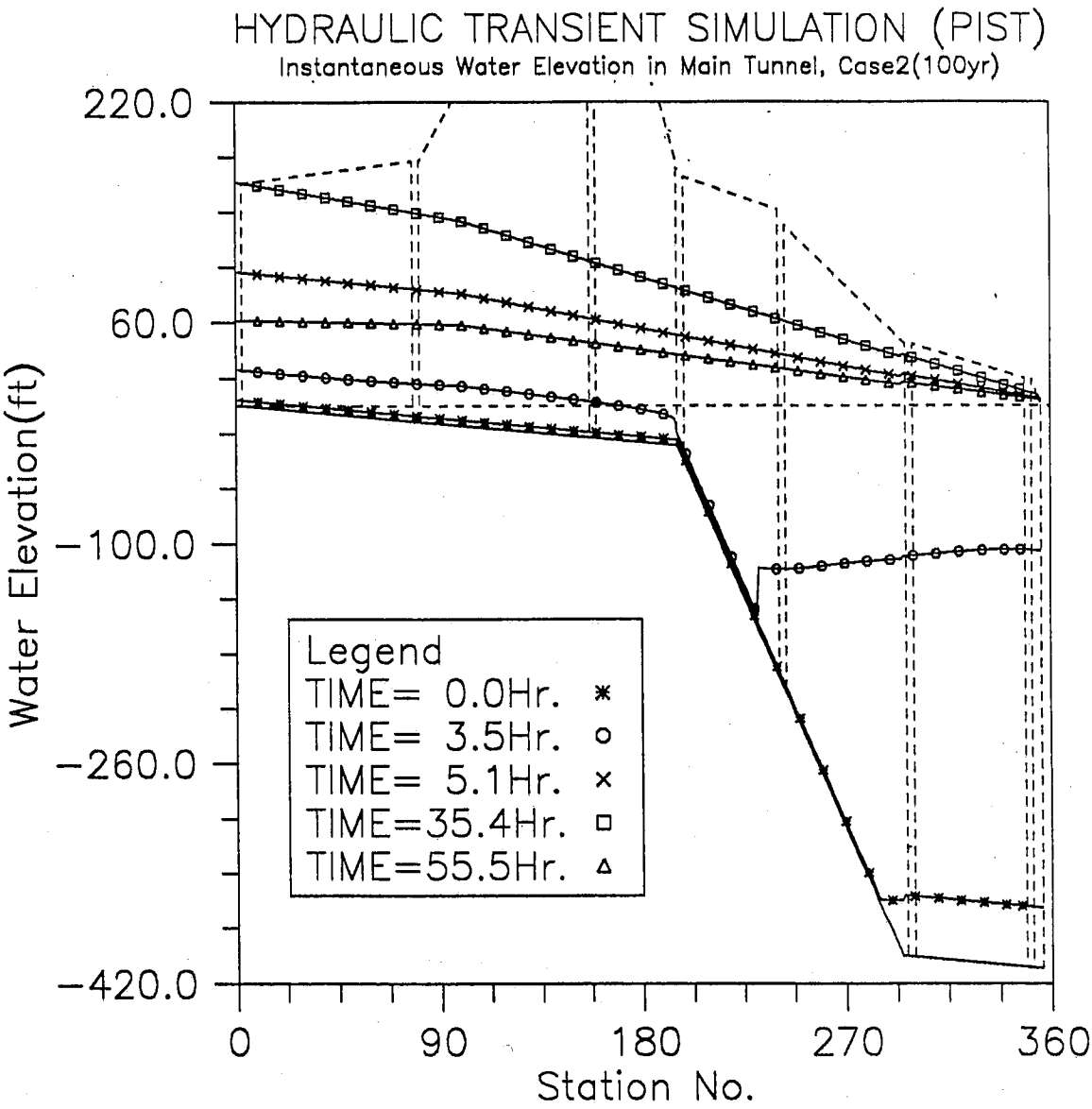

Fig. II–6 Instantaneous hydraulic gradelines along the main tunnel; modeling case: 100yr storm and 0.0 sea level (testing run: Case2)

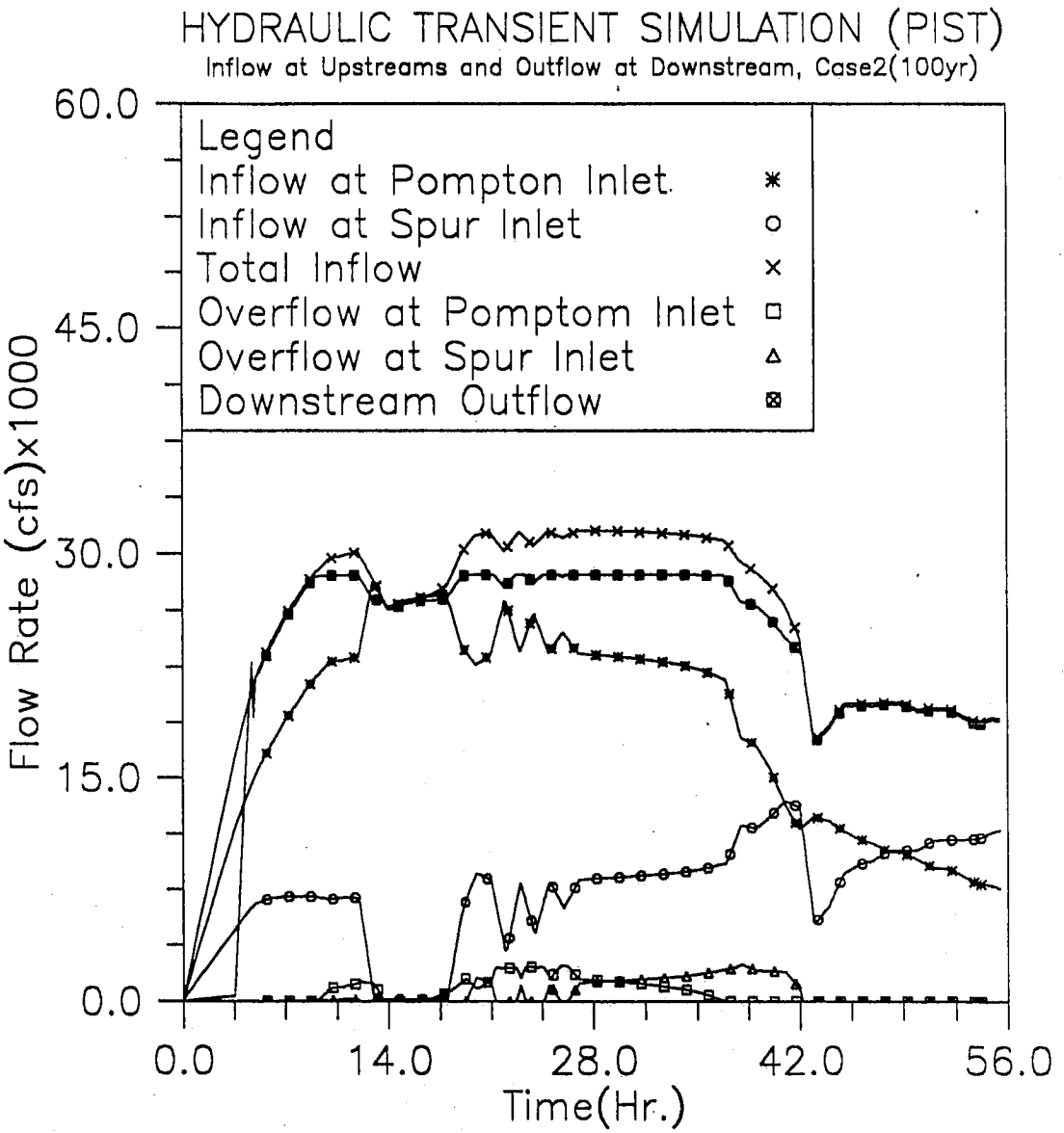

Fig. II–7 Inflow and overflow hydrographs at Pompton and Spur inlets, and outflow hydrograph at the downstream; modeling case: 100yr storm and 0.0 sea level (testing run: Case2)

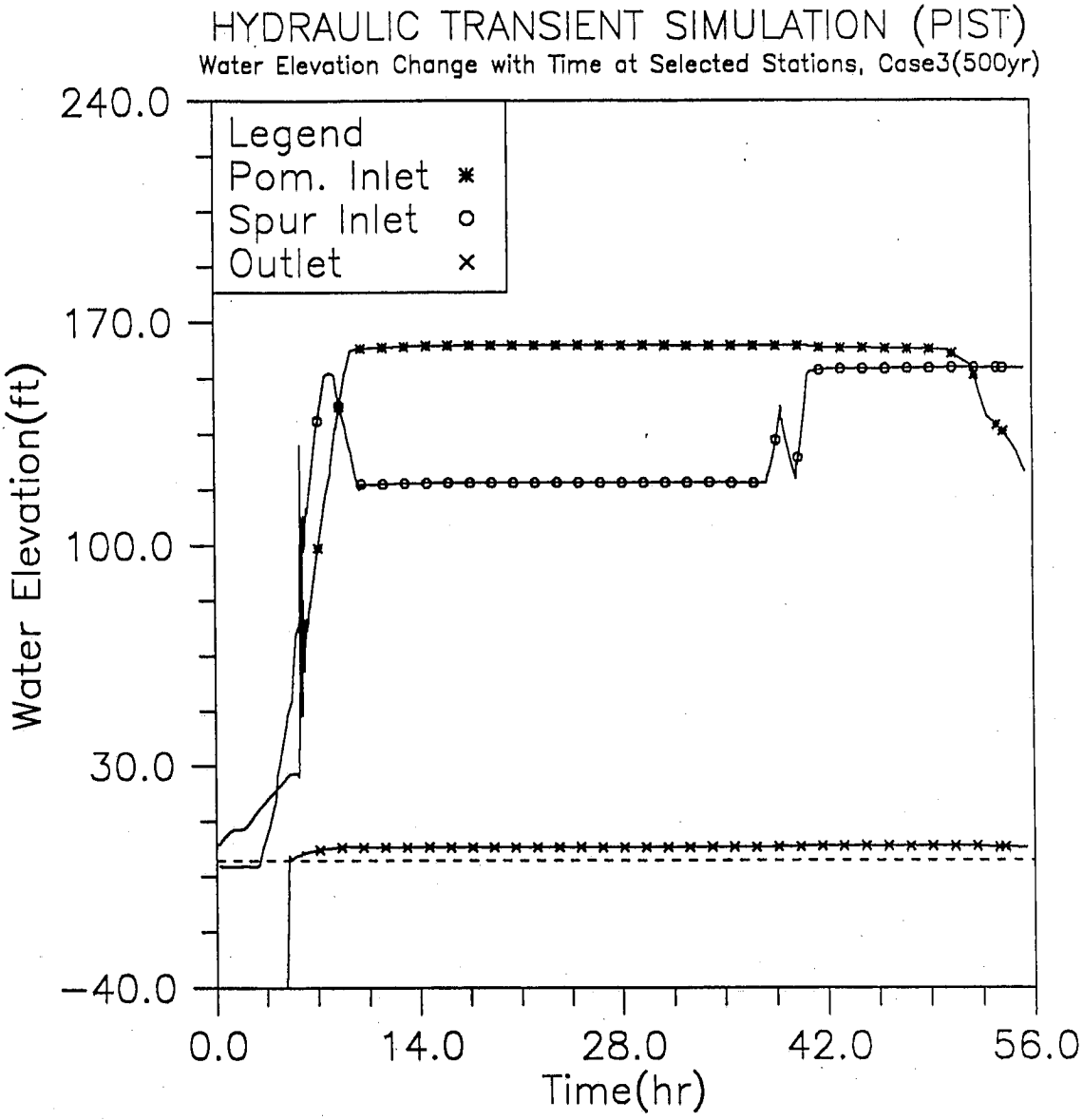

Fig. II–8 Time variation of water elevation at Pompton inlet, Spur inlet and downstream end during the simulated time period; modeling case: 500yr storm and 0.0 sea level (testing run: Case3)

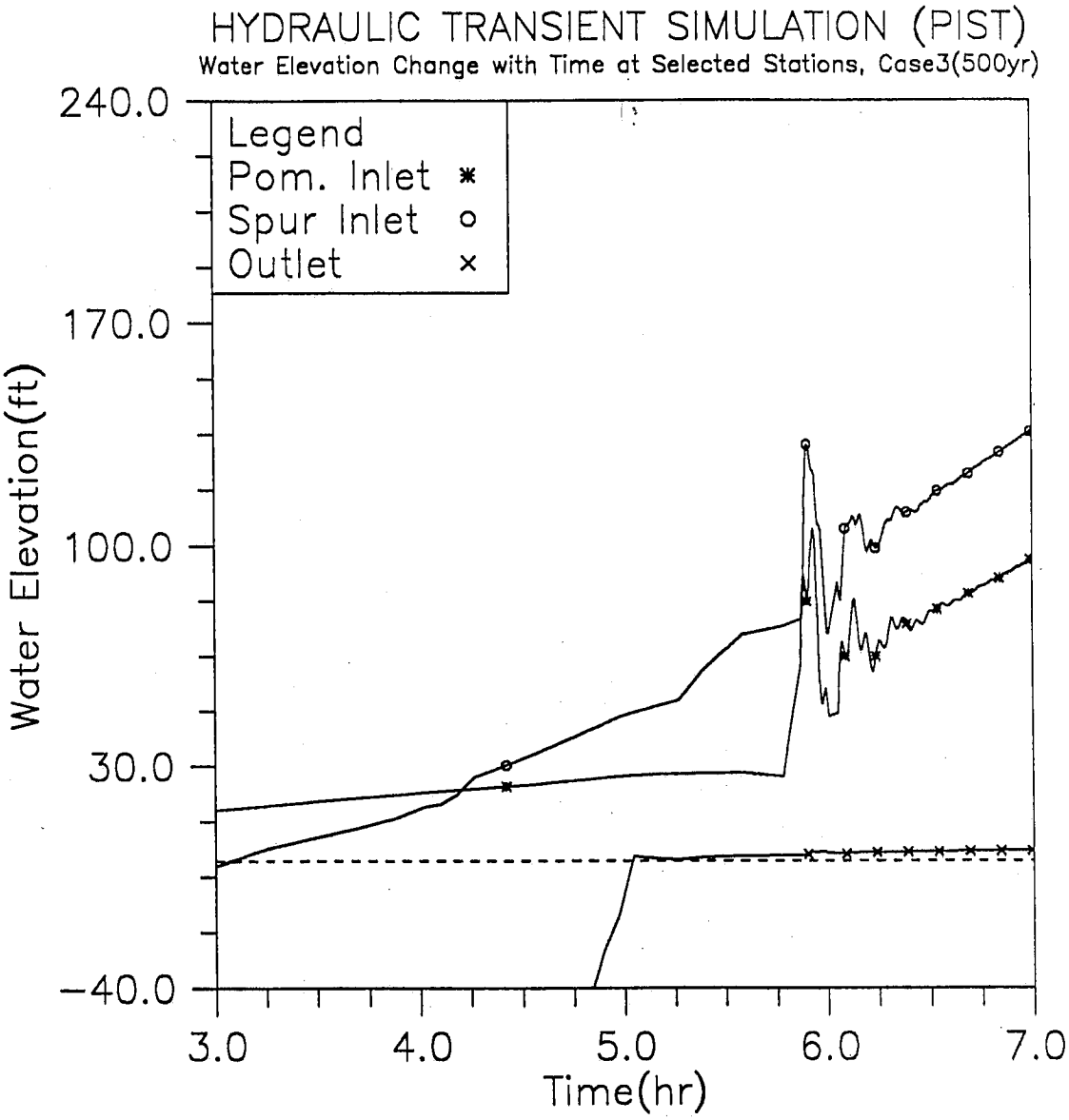

Fig. II-9 More detailed time variation of water elevation at Pompton inlet, Spur inlet and downstream end during the early surging period; modeling case: 500yr storm and 0.0 sea level (testing run: Case3)

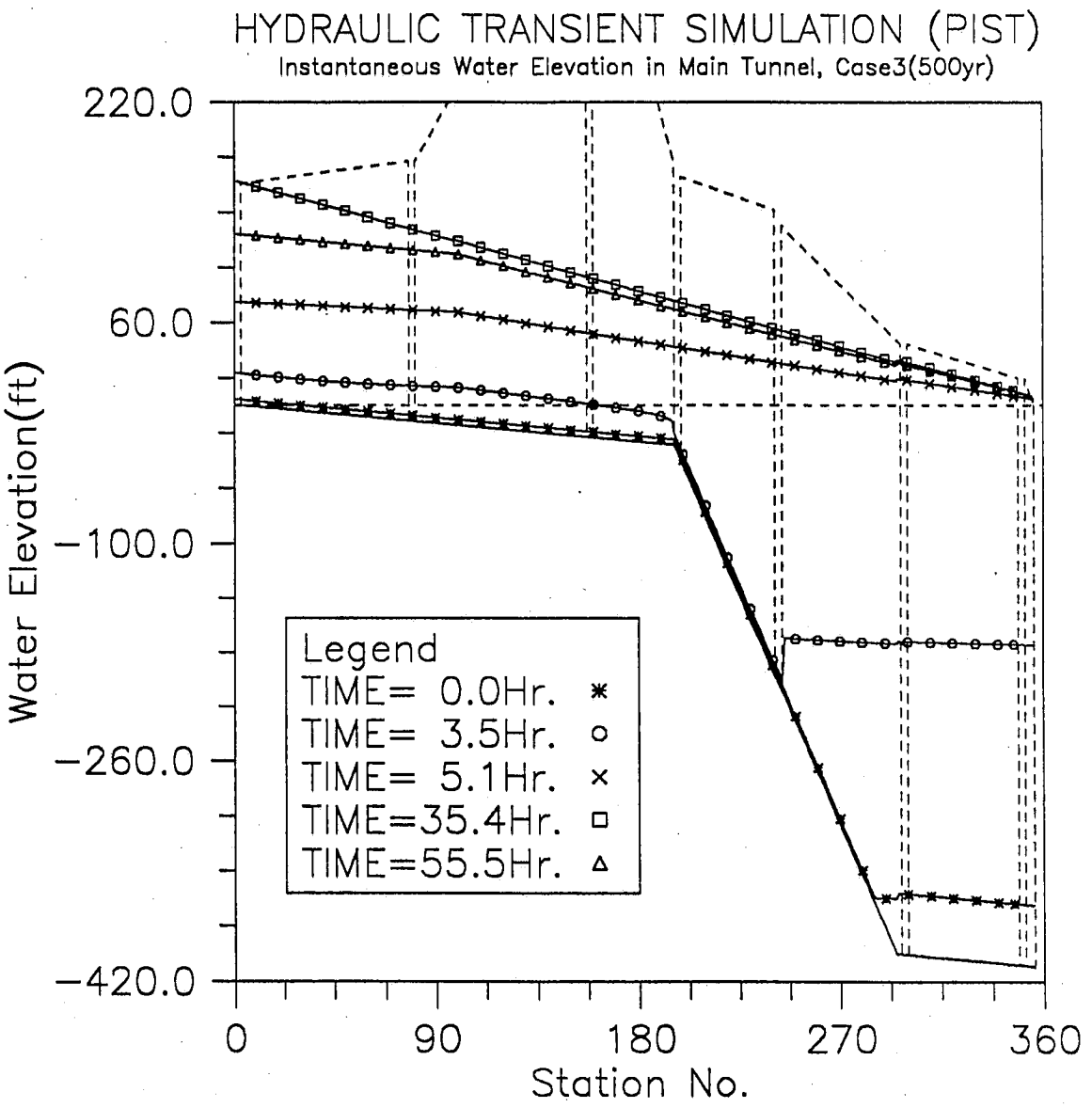

Fig. II–10 Instantaneous hydraulic gradelines along the main tunnel; modeling case: 500yr storm and 0.0 sea level (testing run: Case3)

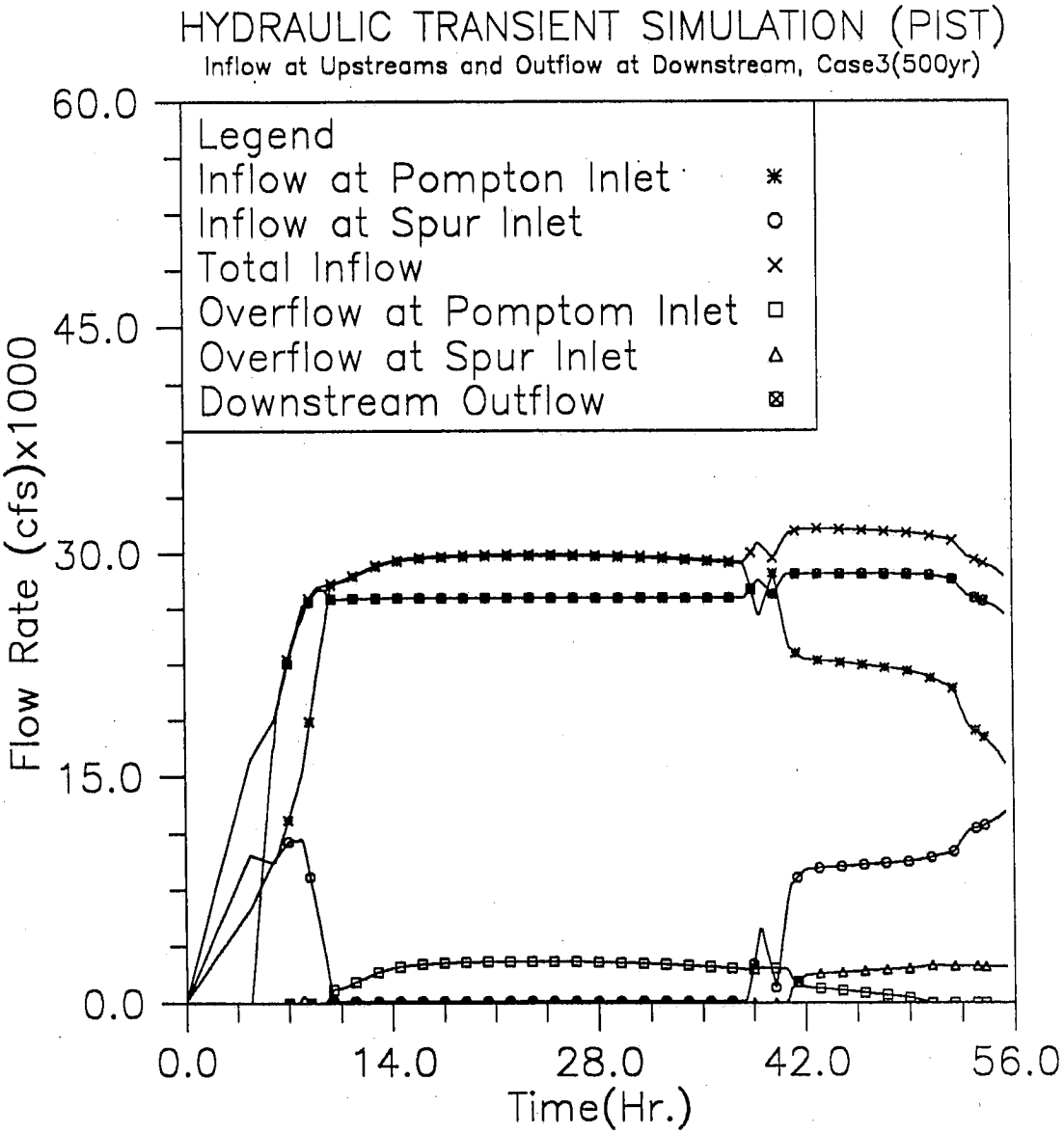

Fig. II–11 Inflow and overflow hydrographs at Pompton and Spur inlets, and outflow hydrograph at the downstream; modeling case: 500yr storm and 0.0 sea level (testing run: Case3)

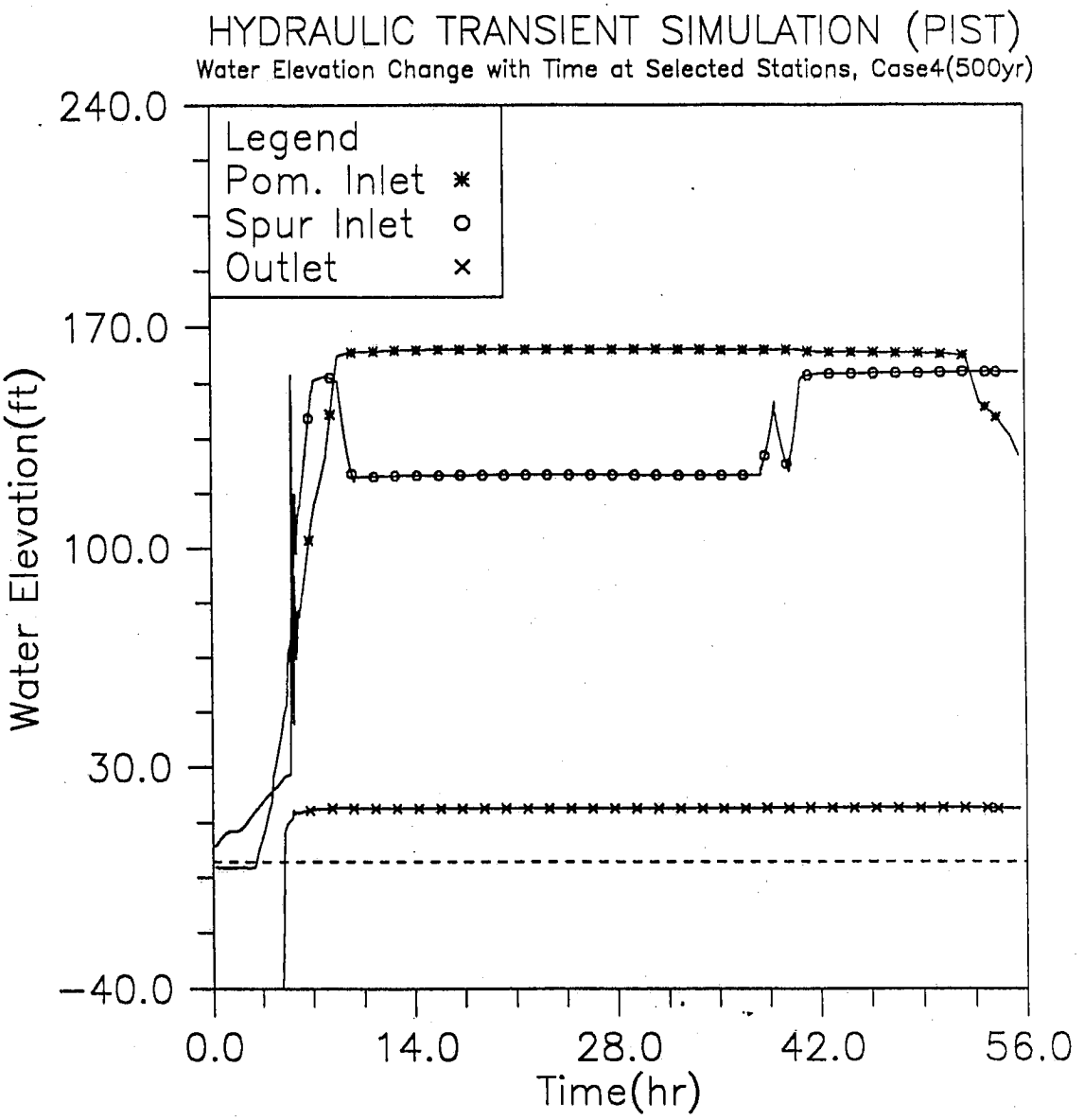

Fig. II–12 Time variation of water elevation at Pompton inlet, Spur inlet and downstream end during the simulated time period; modeling case: 500yr storm and 6.2 sea level (testing run: Case4)

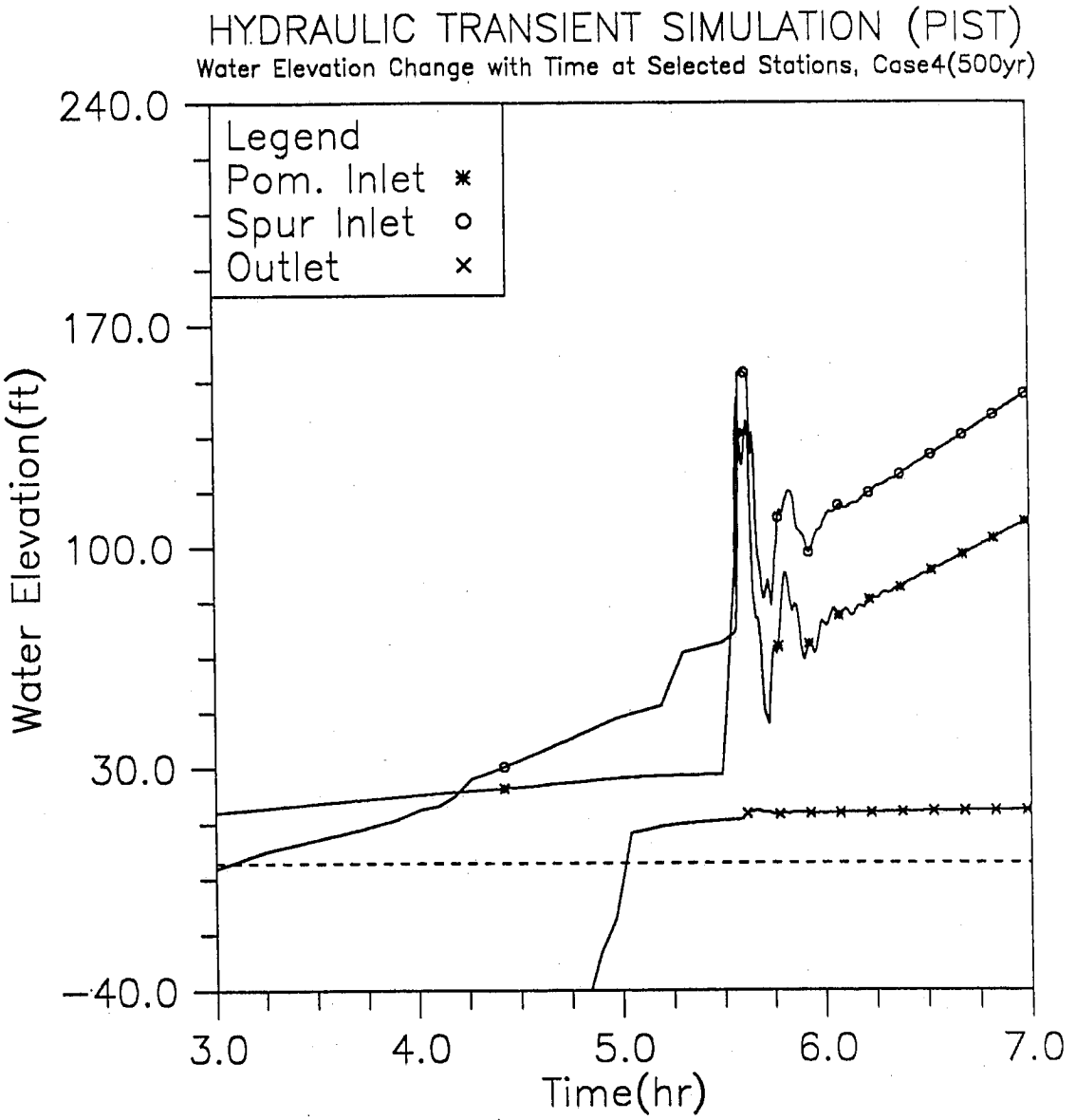

Fig. II–13 More detailed time variation of water elevation at Pompton inlet, Spur inlet and downstream end during the early surging period; modeling case: 500yr storm and 6.2 sea level (testing run: Case4)

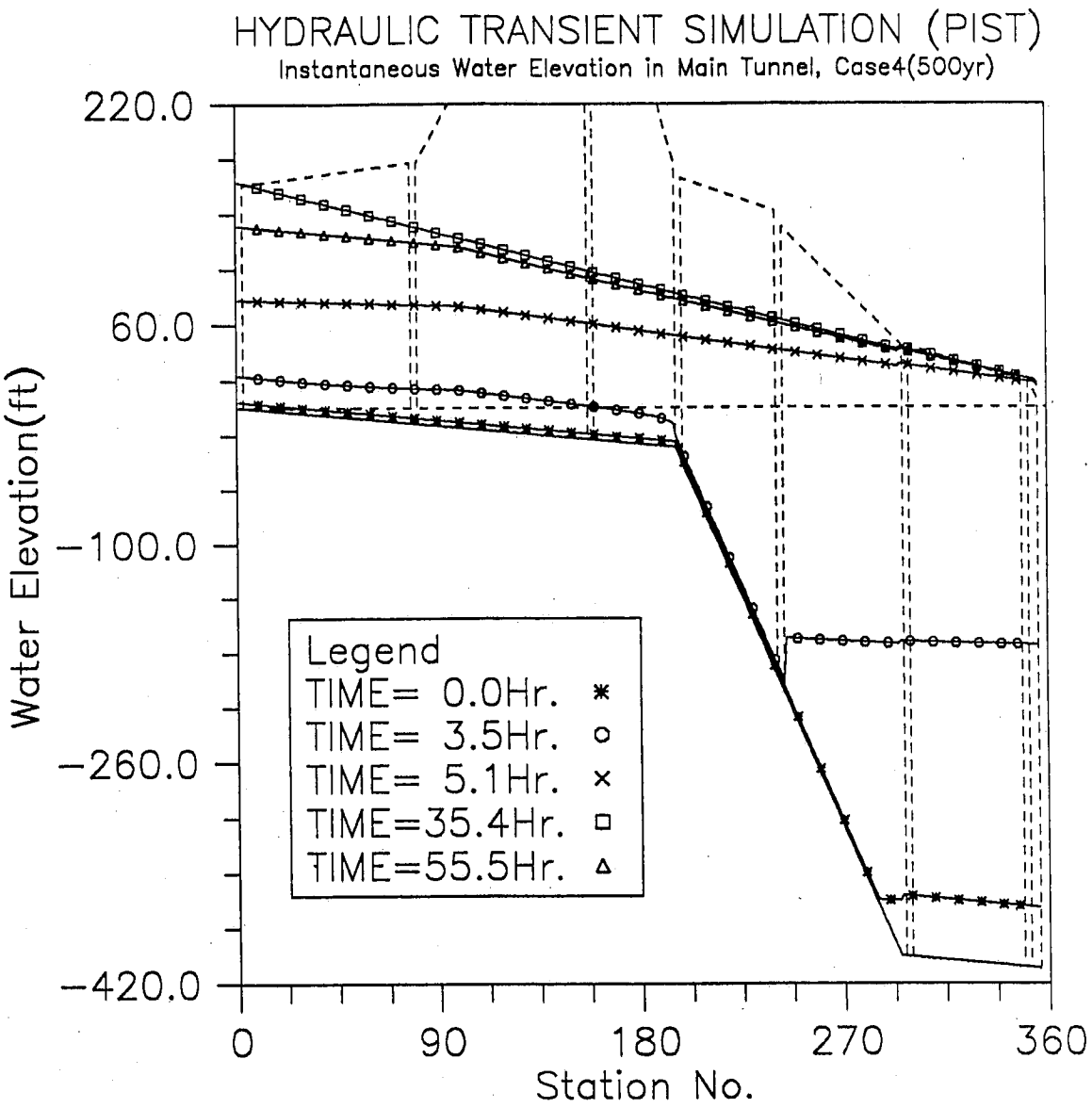

Fig. II–14 Instantaneous hydraulic gradelines along the main tunnel; modeling case: 500yr storm and 6.2 sea level (testing run: Case4)

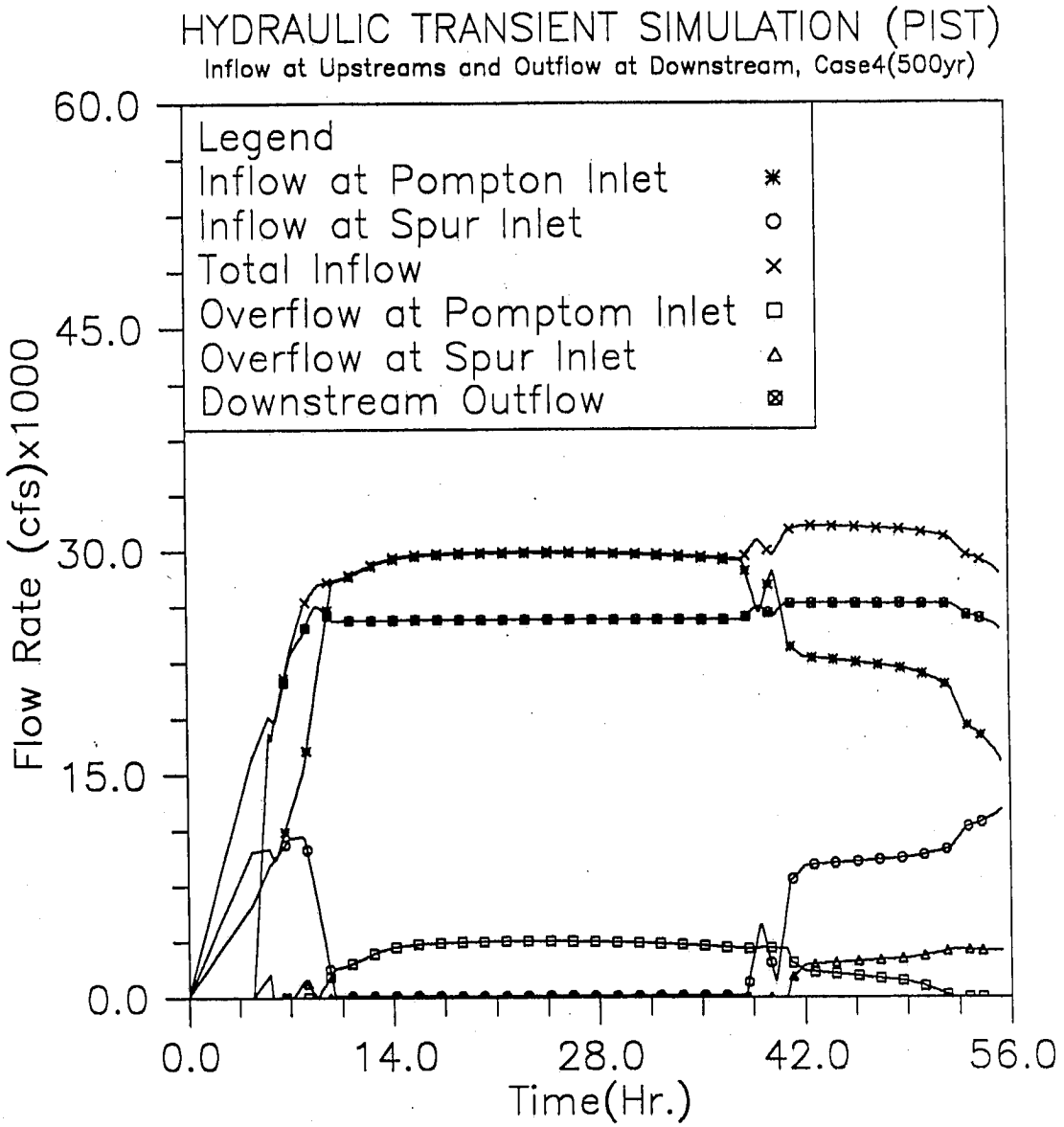

Fig. II–15 Inflow and overflow hydrographs at Pompton and Spur inlets, and outflow hydrograph at the downstream; modeling case: 500yr storm and 6.2 sea level (testing run: Case4)

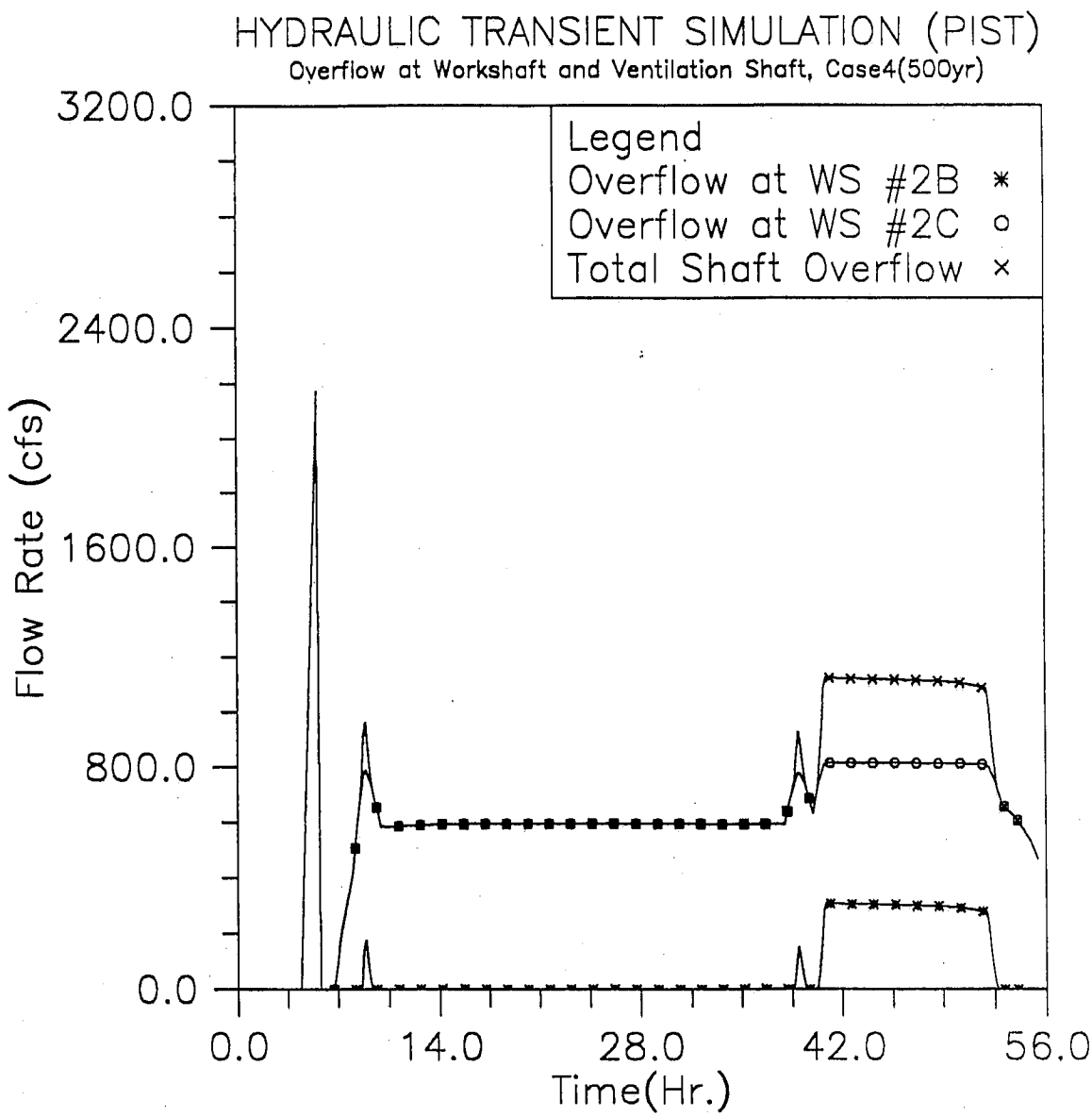

Fig. II–16 Overflow hydrographs at Workshafts #2B and #2C; modeling case: 500yr storm and 6.2 sea level (testing run: Case4)

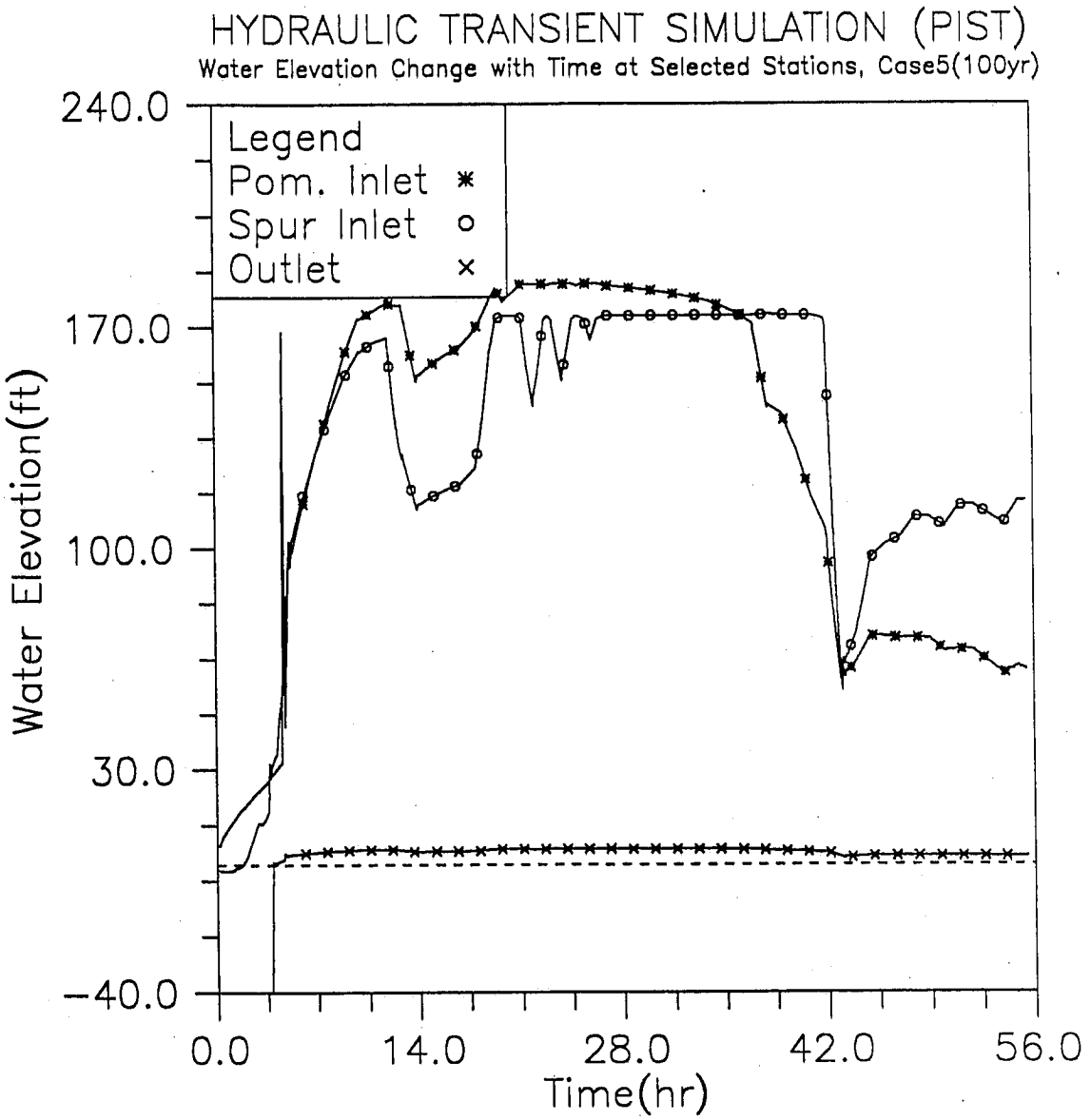

Fig. II–17 Time variation of water elevation at Pompton inlet, Spur inlet and downstream end during the simulated time period; modeling case: 100yr storm, 0.0 sea level, and high upstream level (testing run: Case5)

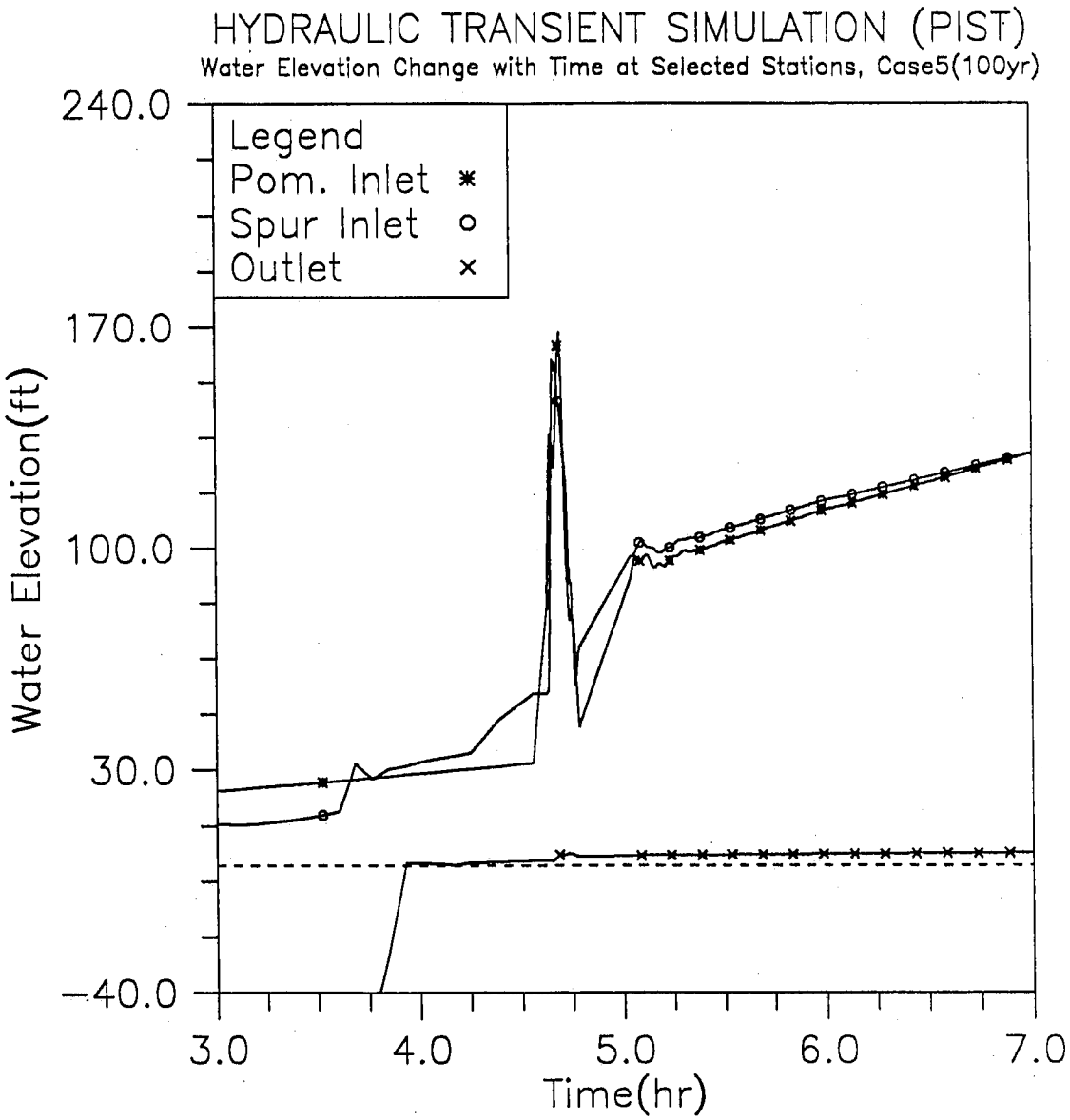

Fig. II–18 More detailed time variation of water elevation at Pompton inlet, Spur inlet and downstream end during the early surging period; modeling case: 100yr storm, 0.0 sea level, and high upstream level (testing run: Case5)

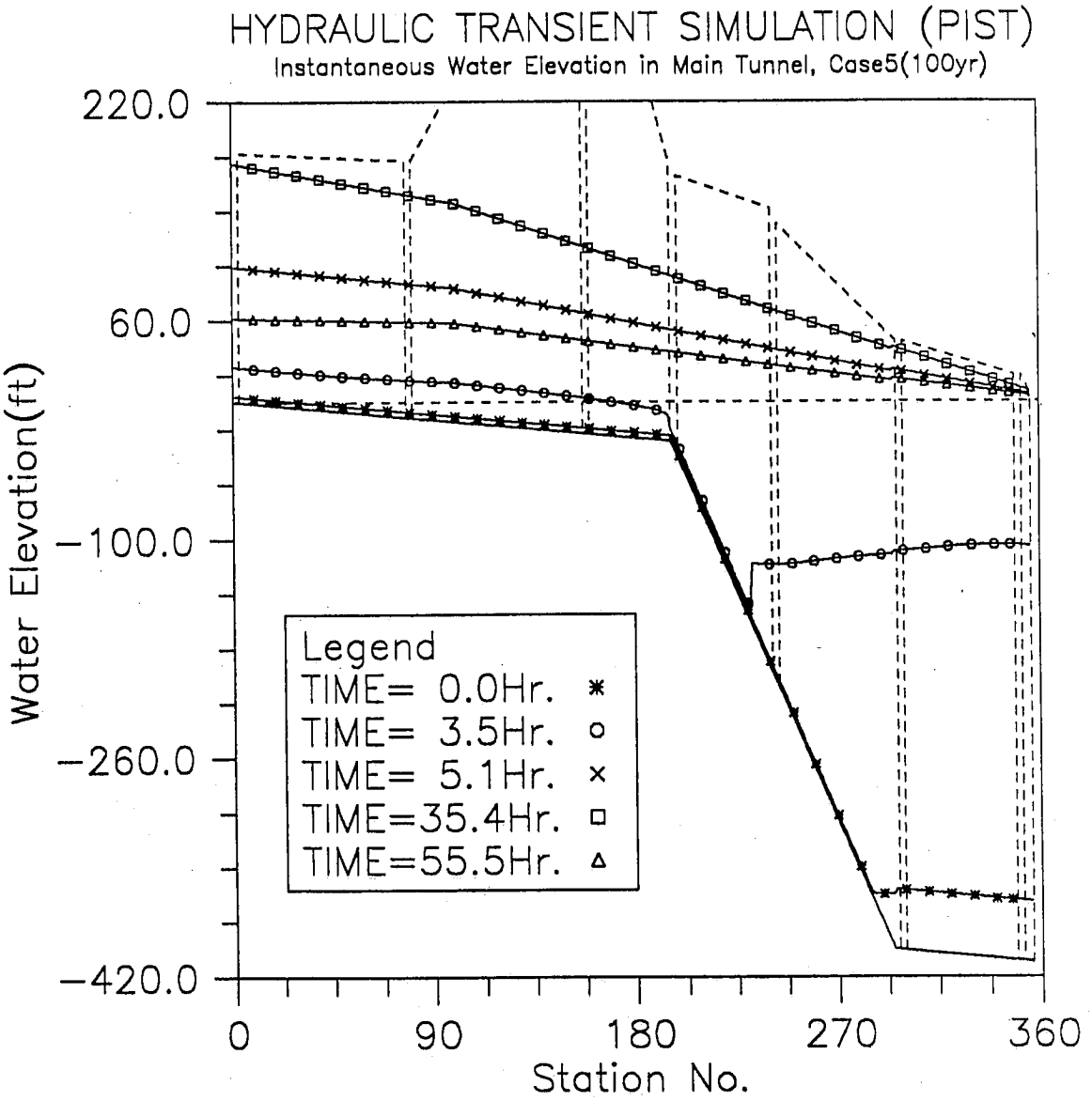

Fig. II–19 Instantaneous hydraulic gradelines along the main tunnel; modeling case: 100yr storm, 0.0 sea level, and high upstream level (testing run: Case5)

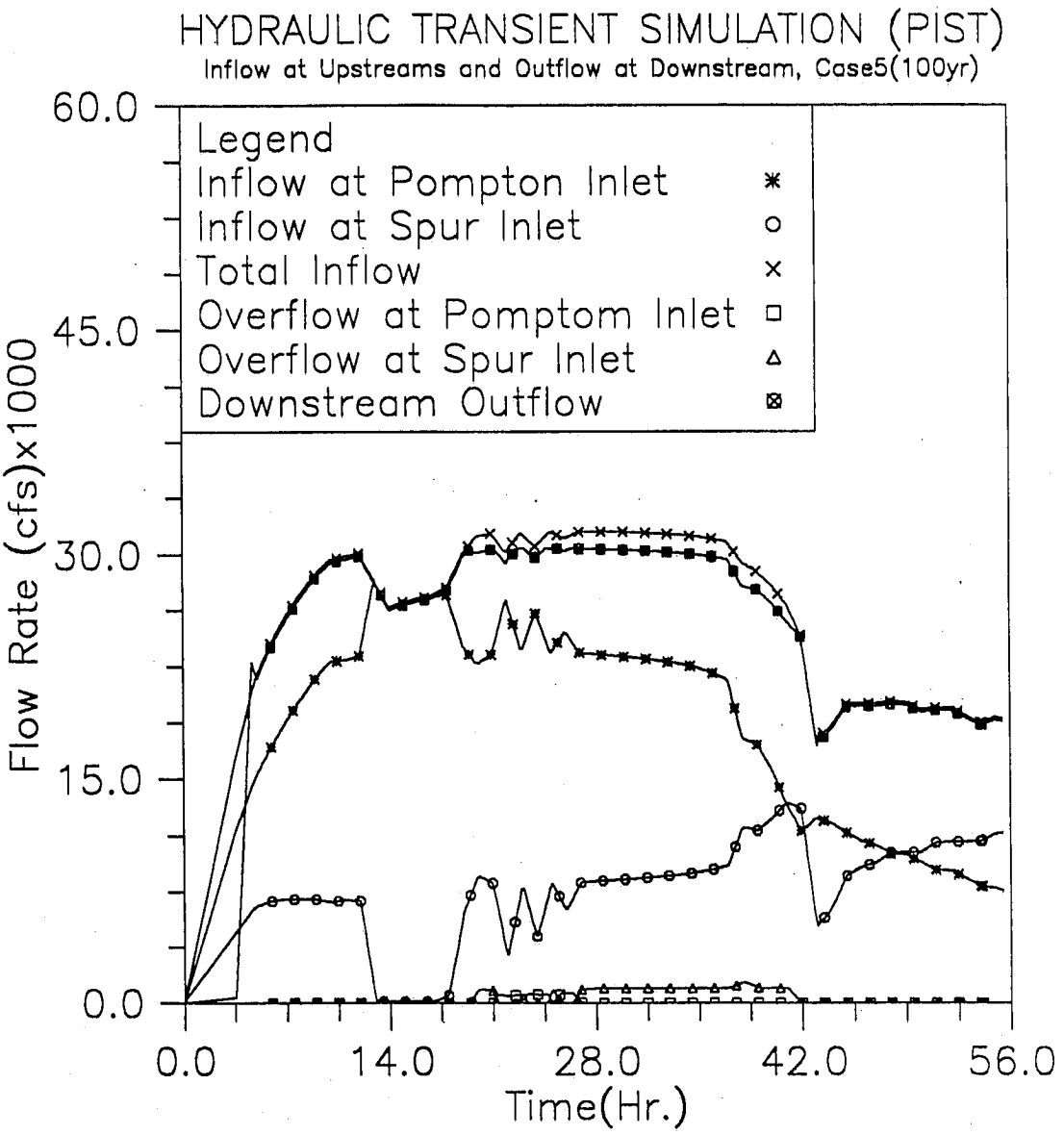

Fig. II–20 Inflow and overflow hydrographs at Pompton and Spur inlets, and outflow hydrograph at the downstream; modeling case: 100yr storm, 0.0 sea level, and high upstream level (testing run: Case5)

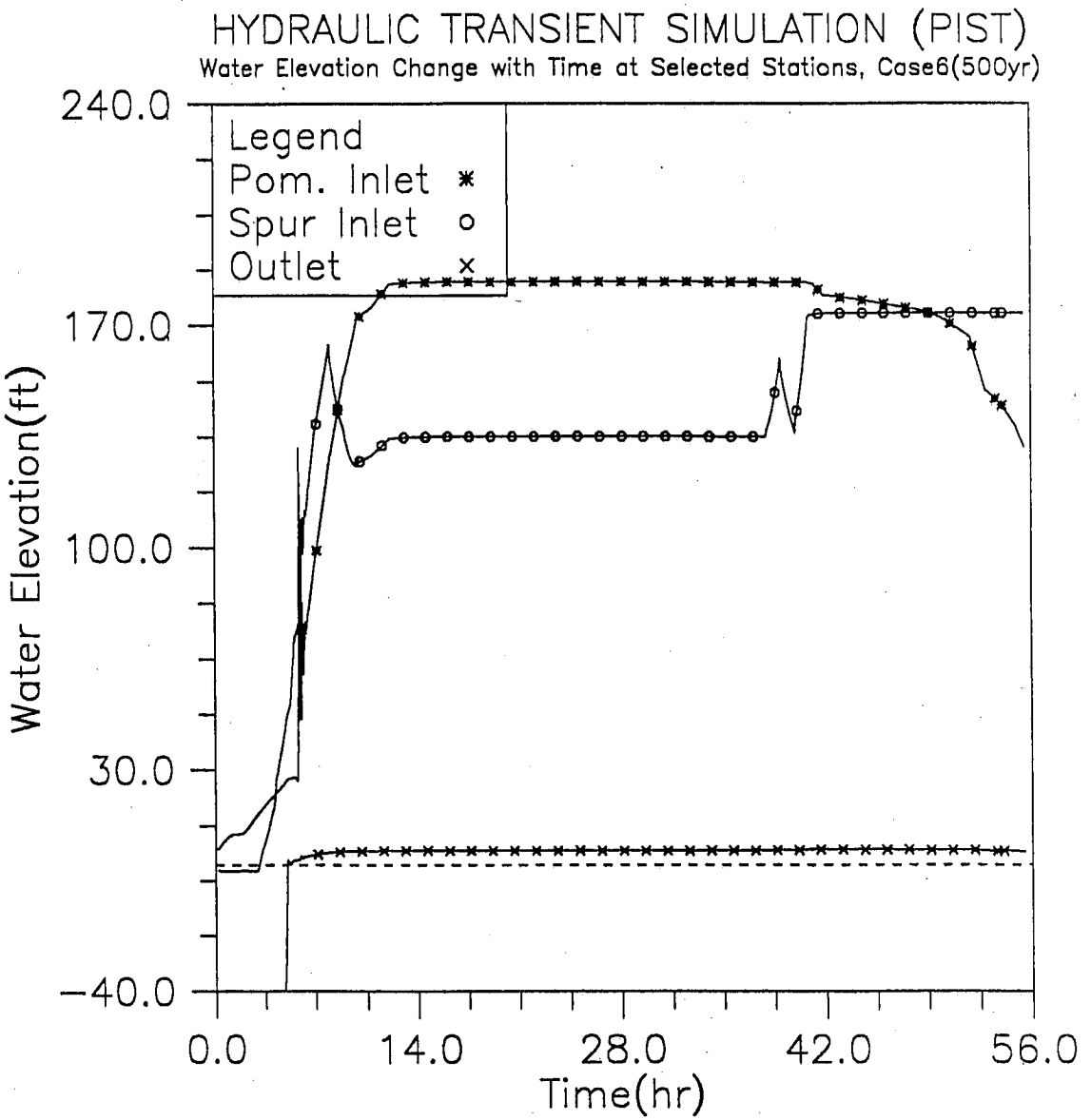

Fig. II–21 Time variation of water elevation at Pompton inlet, Spur inlet and downstream end during the simulated time period; modeling case: 500yr storm, 0.0 sea level, and high upstream level (testing run: Case6)

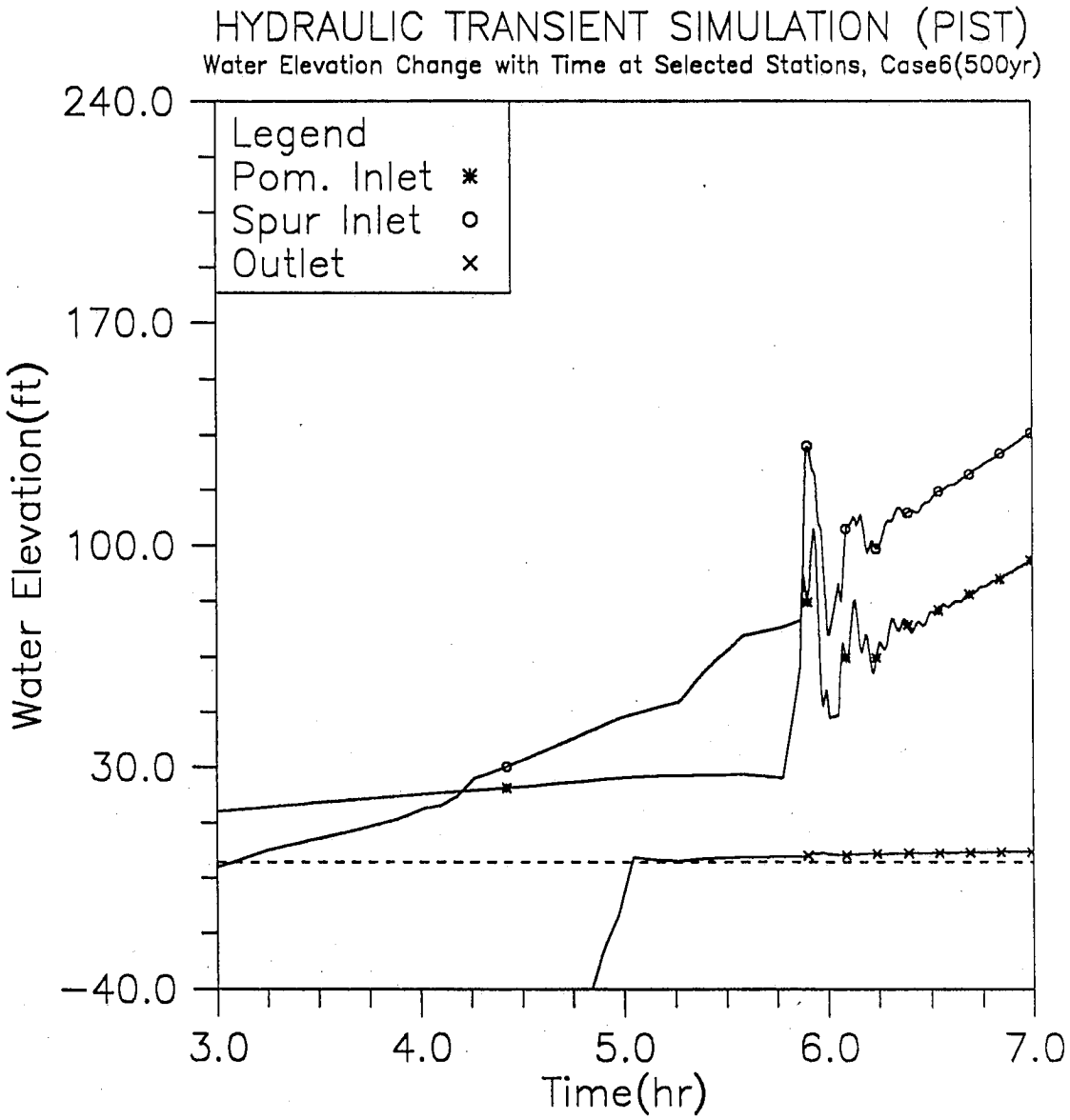

Fig. II–22 More detailed time variation of water elevation at Pompton inlet, Spur inlet and downstream end during the early surging period; modeling case: 500yr storm, 0.0 sea level, and high upstream level (testing run: Case6)

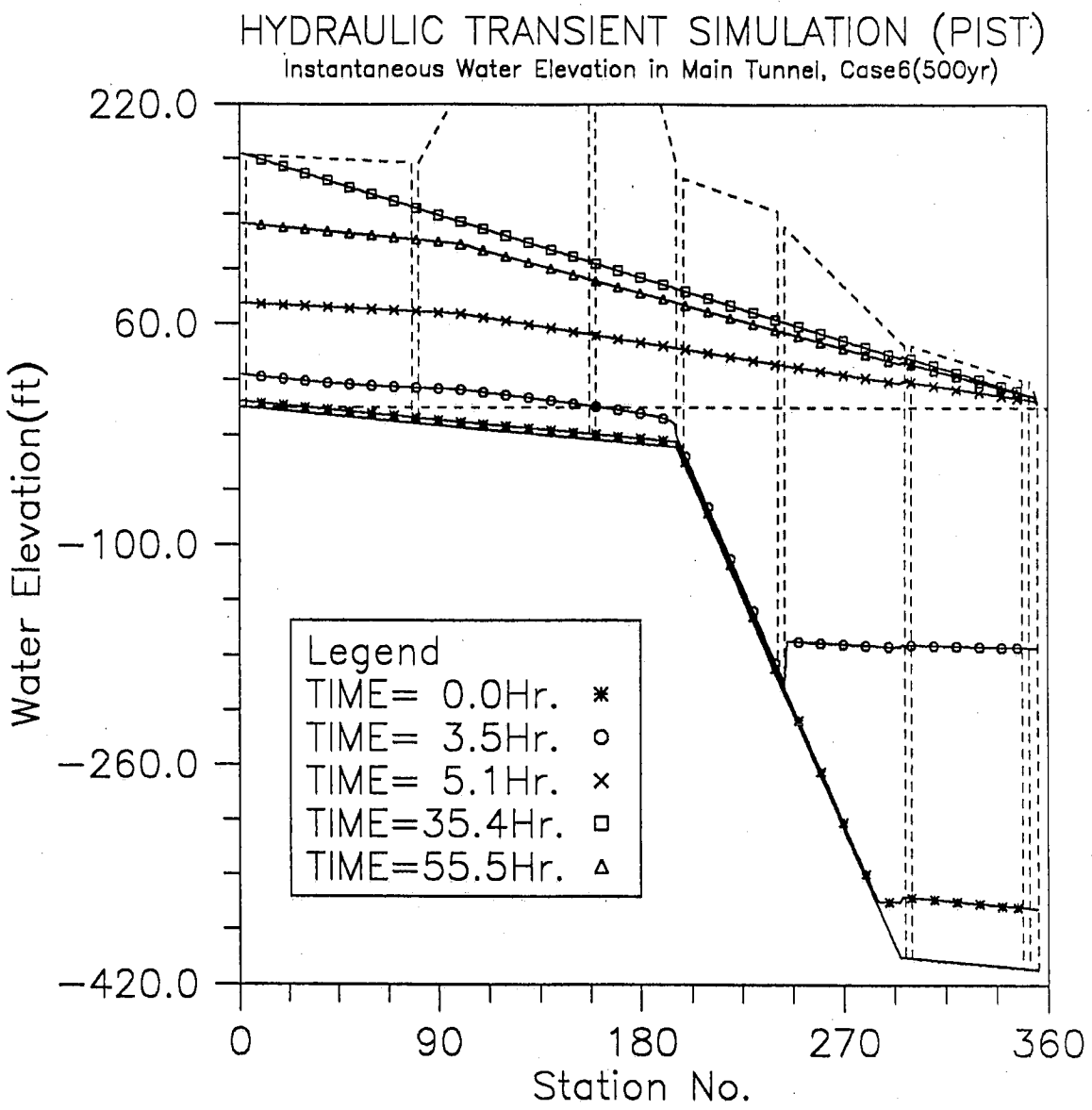

Fig. II–23 Instantaneous hydraulic gradelines along the main tunnel; modeling case: 500yr storm, 0.0 sea level, and high upstream level (testing run: Case6)

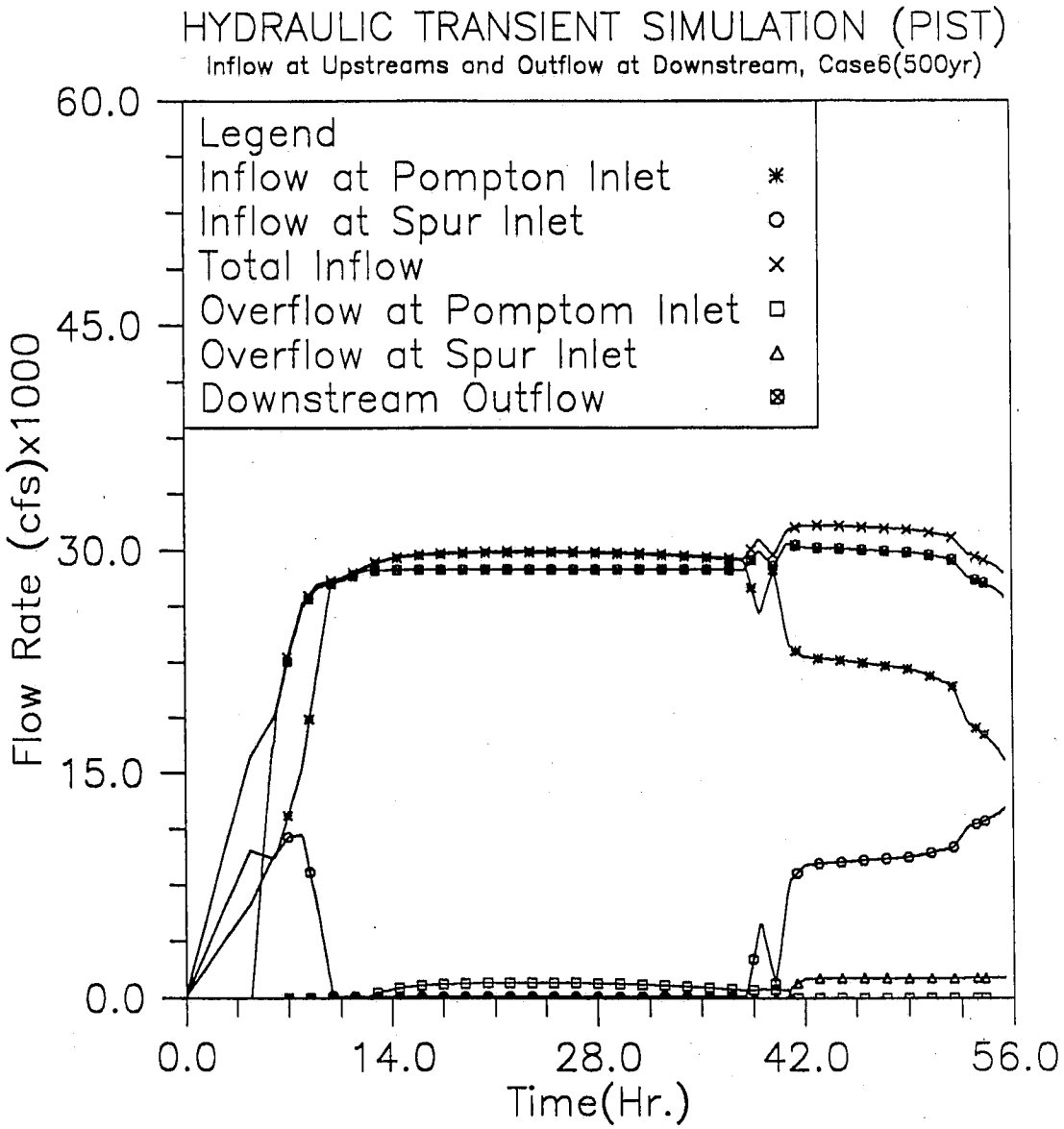

Fig. II–24 Inflow and overflow hydrographs at Pompton and Spur inlets, and outflow hydrograph at the downstream; modeling case: 500yr storm, 0.0 sea level, and high upstream level (testing run: Case6)

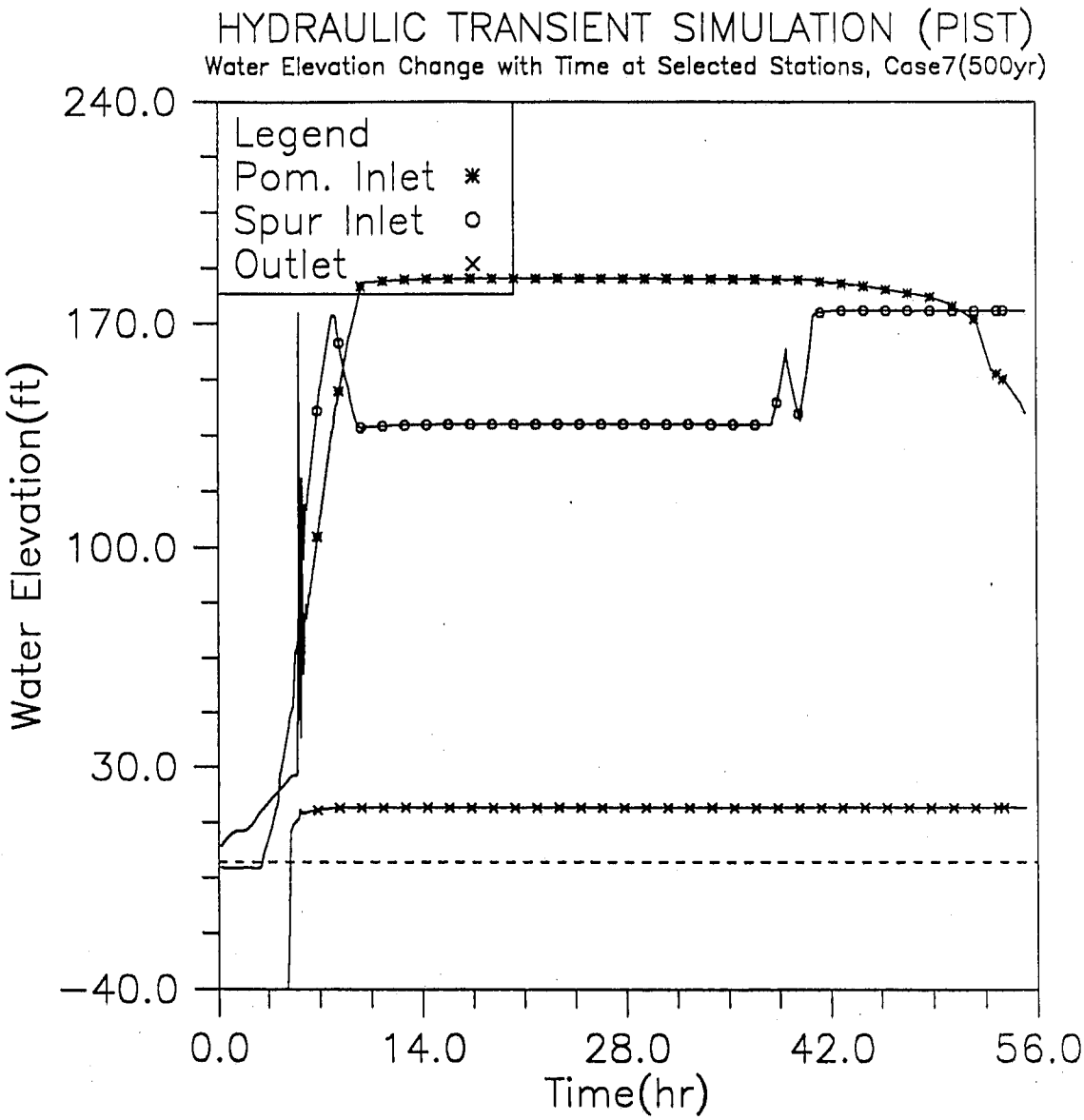

Fig. II–25 Time variation of water elevation at Pompton inlet, Spur inlet and downstream end during the simulated time period; modeling case: 500yr storm, 6.2 sea level, and high upstream level (testing run: Case7)

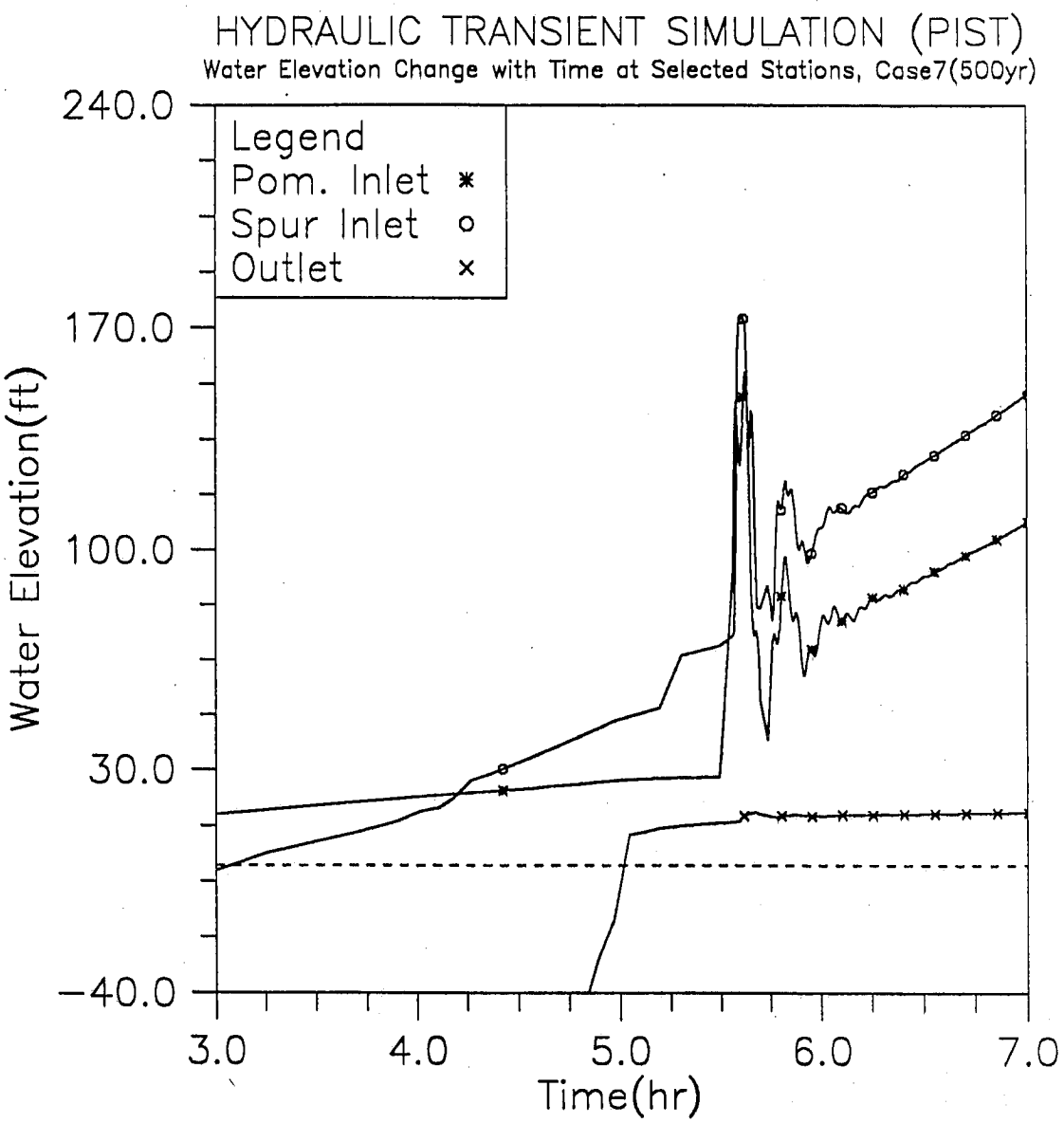

Fig. II–26 More detailed time variation of water elevation at Pompton inlet, Spur inlet and downstream end during the early surging period; modeling case: 500yr storm, 6.2 sea level, and high upstream level (testing run: Case7)

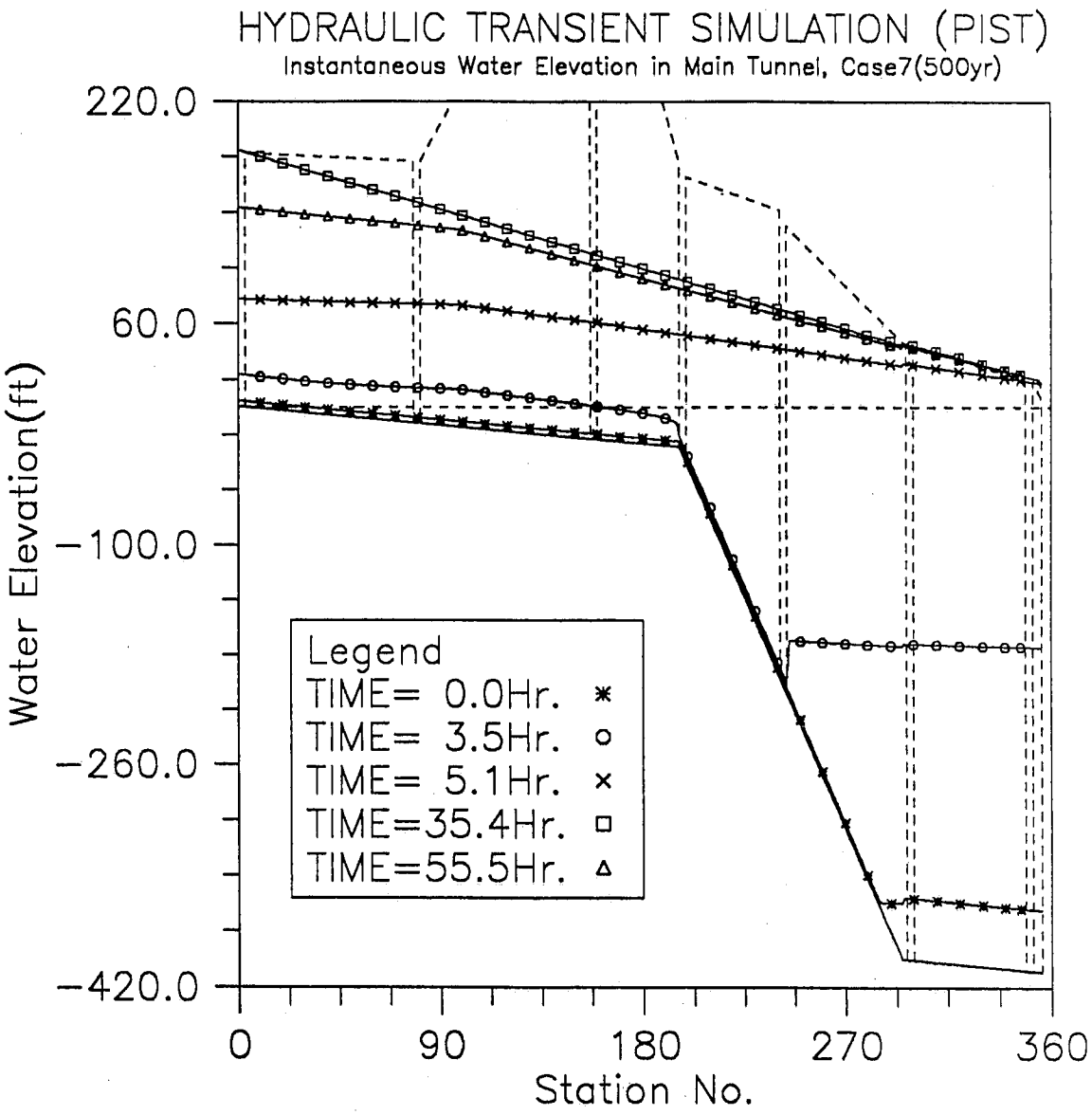

Fig. II–27 Instantaneous hydraulic gradelines along the main tunnel; modeling case: 500yr storm, 6.2 sea level, and high upstream level (testing run: Case7)

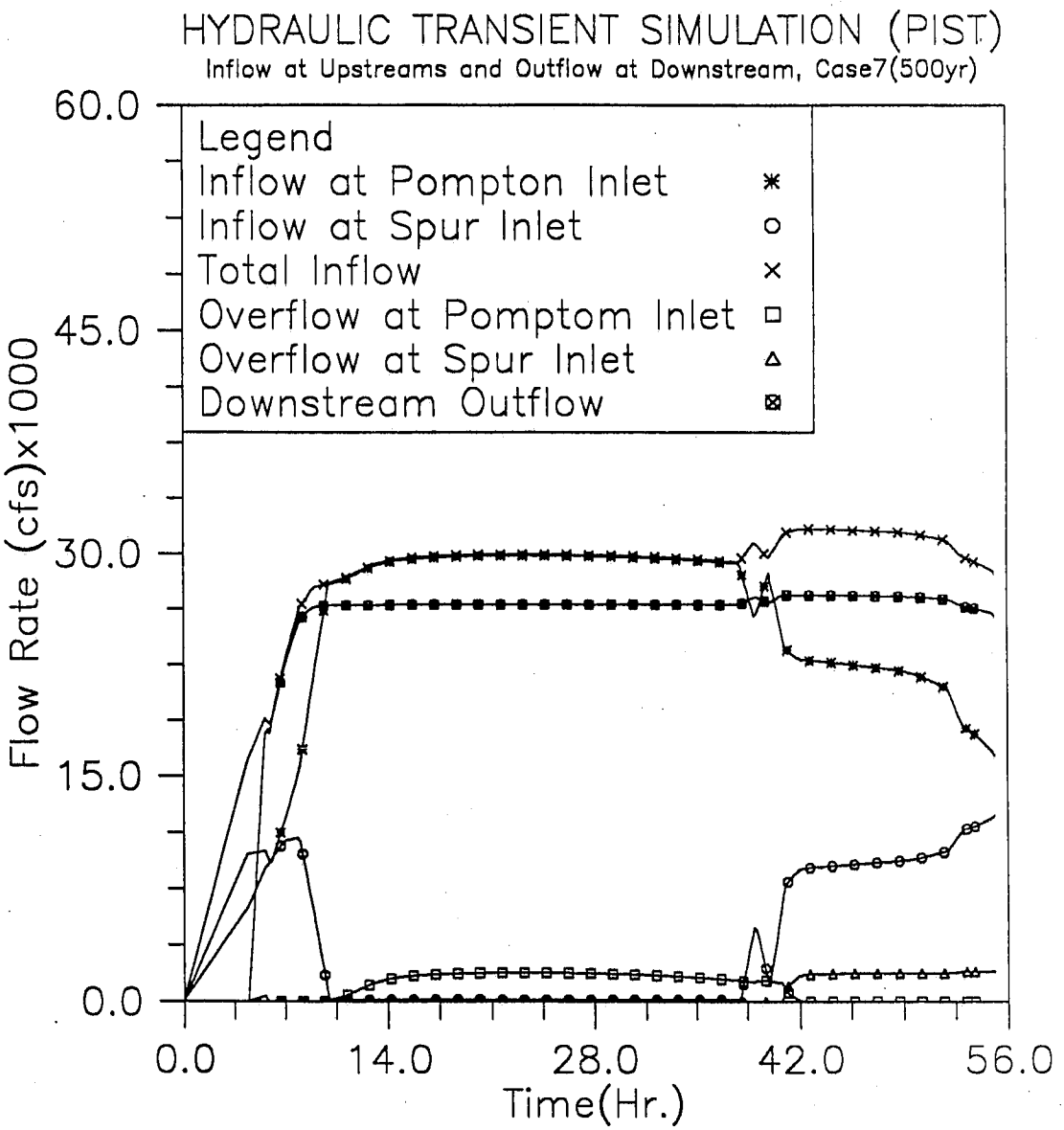

Fig. II–28 Inflow and overflow hydrographs at Pompton and Spur inlets, and outflow hydrograph at the downstream; modeling case: 500yr storm, 6.2 sea level, and high upstream level (testing run: Case7)

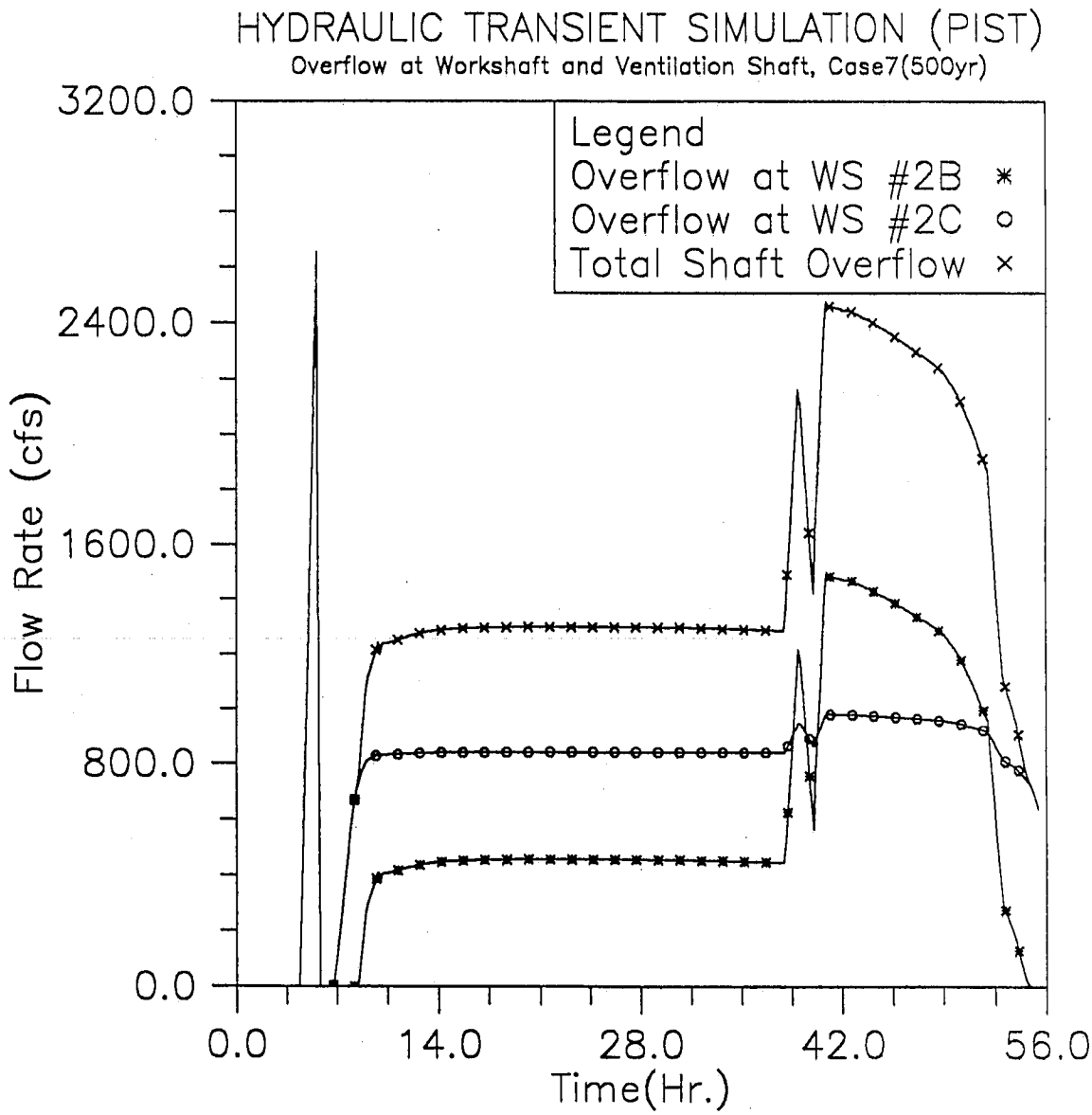

Fig. II–29 Overflow hydrographs at Workshafts #2B and #2C; modeling case: 500yr storm, 6.2 sea level, and high upstream level (testing run: Case7)